

**Functional Studies and X-Ray Structure Analysis of
Human Interleukin-5 Receptor Alpha and Human
Interleukin-5 Complex**

Dissertation zur Erlangung des
naturwissenschaftlichen Doktorgrades
der Bayerischen Julius-Maximilians-Universität Würzburg

vorgelegt von
Edwin Patiño Gonzalez
aus Medellín-Colombia

Würzburg, 2007

Eingereicht am: _____

Mitglieder der Promotionskommission:

Vorsitzender: Prof. Dr.

1. Gutachter: Prof. Dr. Walter Sebald

2. Gutachter: Prof. Dr. Roland Benz

Tag des Promotionskolloquiums: _____

Doktorurkunde ausgehändigt am: _____

*"Imagination
is more important than knowledge. Knowledge is limited;
imagination encircles the world."*

Albert Einstein

CONTENT

1.	INTRODUCTION.....	1
1.1	Overview.....	1
1.2	Diseases.....	2
1.2.1	Parasitic Infection.....	2
1.2.2	Asthma.....	2
1.2.3	Hypereosinophilic Syndrome.....	4
1.3	Haematopoietic Cytokine Family.....	5
1.4	Identification of Components of the Interleukin-5 System.....	7
1.4.1	Interleukin-5 (IL-5).....	7
1.4.2	Interleukin-5 Receptor (IL-5R).....	11
1.5	Interaction of IL-5 and IL-5 receptor.....	13
1.6	Intracellular Signaling Cascades of IL-5 Receptor.....	17
1.7	Structural Studies of IL-5 System.....	19
1.8	Therapeutic Approaches in Asthma and Hypereosinophilic Syndrome Treatment.....	23
2	AIMS.....	25
3	MATERIALS AND METHODS.....	26
3.1	Reagents.....	26
3.2	Kits.....	26
3.3	Sterilization.....	26
3.4	Bacteria Strains.....	26
3.5	Expression Vectors.....	27
3.6	Oligonucleotides.....	27
3.7	Site Directed Mutagenesis.....	28
3.7.1	Single mutation by Cyclic PCR.....	28
3.7.2	Two Step PCR.....	29
3.7.3	Truncation by PCR.....	30
3.8	Cloning.....	31
3.8.1	DNA digestion.....	31
3.8.2	DNA ligation.....	31
3.9	Preparation of Competent Cells (RbCl ₂ Method).....	31
3.10	Transformation of <i>E. coli</i>	32
3.11	<i>E. coli</i> Protein Expression.....	33

3.11.1	Native proteins.....	33
3.11.2	Selenomethionyl-proteins.....	34
3.12	Receptor.....	35
3.12.1	Inclusion bodies isolation.....	35
3.12.2	Renaturation.....	37
3.12.3	Purification.....	37
3.12.3.1	Anion Exchange chromatography I.....	37
3.12.3.2	Anion Exchange chromatography II.....	38
3.12.3.3	Size exclusion chromatography.....	38
3.12.3.4	Affinity chromatography.....	38
3.13	Ligand.....	40
3.13.1	Inclusion bodies isolation (Human).....	40
3.13.2	Inclusion bodies isolation (Mouse).....	41
3.13.3	Ligand renaturation.....	42
3.13.4	Ligand purification.....	42
3.13.4.1	Size exclusion chromatography I.....	42
3.13.4.2	Size exclusion chromatography II.....	43
3.14	Protein Analysis Methods.....	43
3.14.1	RP-HPLC.....	43
3.14.2	SDS-polyacrylamide gel electrophoresis (SDS-PAGE).....	44
3.14.3	Mass spectrometry analysis.....	46
3.14.4	Circular dichroism (CD).....	47
3.14.5	Biomolecular interaction analysis (BIAcore).....	47
3.14.6	TF-1 cells proliferation assay.....	48
3.15	Limited Proteolysis of protein.....	48
3.16	Crystallization.....	49
3.16.1	Complex crystallization.....	49
3.16.2	Ligand crystallization (Mouse).....	50
3.17	X-ray Data Analysis.....	51
4	RESULTS.....	52
4.1	Structural studies of the human IL-5R α /IL-5 complex.....	52
4.1.1	Expression, refolding and purification of wild type human IL-5R α and human IL-5R α variants.....	52

4.1.2	Analytical Methods.....	59
4.1.3	Expression, refolding and purification of the human IL-5.....	63
4.1.4	Biomolecular interaction analysis (BIAcore).....	64
4.1.5	Limited proteolysis approaches.....	67
4.1.6	Crystallization.....	68
4.1.7	X-ray analysis and complex structure.....	77
4.2	Structural studies of mouse interleukin-5.....	83
4.2.1	Expression, refolding and purification of mouse IL-5....	83
4.2.2	Biological activity assay.....	89
4.2.3	Crystallization of mL-5 ^{nullMet} variant.....	91
4.2.4	Structure of mL-5 ^{nullMet} variant.....	92
5.	DISCUSSION.....	96
5.1	Production of recombinant mouse IL-5 in <i>E. coli</i>	96
5.2	Structural studies of the mouse IL-5.....	98
5.3	Human IL-5R α /IL-5 complex structure.....	102
5.4	Cytokine recognition by human IL-5R α	106
5.5	Stoichiometrical interaction of human IL-5R α and human IL-5.....	110
6	ABSTRACT.....	114
7	ZUSAMMENFASSUNG.....	116
8	REFERENCES.....	119
9	APPENDIX.....	132

INDEX OF FIGURES AND TABLES

Figure 1-1. Eosinophil activation.....3

Figure 1-2. Haematopoietic related cytokines.....5

Figure 1-3. Cartoon representation of the haematopoietic cytokine
receptors.....7

Figure 1-4. Sequence alignment of human and mouse IL-5.....10

Figure 1-5. Residues in human IL-5 important for binding.....15

Figure 1-6. Up-regulation and down-regulation pathways of the IL-5
receptor.....18

Figure 1-7 Structure of the human IL-5.....21

Figure 1-8. Structure of the human β_c22

Figure 4-1. Schematic representation of the expression vector.....53

Figure 4-2. Expression of wild type hIL-5R α in *E.coli* Rosetta cells.....54

Figure 4-3. Purification of hIL-5R α mutants.....56

Figure 4-4. Analysis of hIL-5R α mutants.....57

Figure 4-5. Purification of hIL-5R α Del 1 variant.....58

Figure 4-6. Analysis of Interleukin-5 receptor alpha.....60

Figure 4-7. Circular dichroism spectrum of wild type hIL-5R α and variants..61

Figure 4-8. Expression and purification of hIL-5.....64

Figure 4-9. BIAcore analysis of human hIL-5R α variants.....66

Figure 4-10. Complex proteolysis.....68

Figure 4-11. Gelfiltration chromatography and SDS-PAGE analysis of the wt-
hIL-5R α /hIL-5 complex.....70

Figure 4-12. Concentrated complex analyzed by Fast Protein Liquid-
Chromatography (FPLC).....71

Figure 4-13. Optimization of crystallization conditions for the complex hIL-
5R α /hIL-5.....74

Figure 4-14. Optimization of the crystallization of the hIL-5R α C66A/hIL-5 by
detergent use.....76

Figure 4-15. hIL-5R α /hIL-5 crystal content analysis78

Figure 4-16. Electron density map of the hIL-5R α /hIL-5 complex.....80

Figure 4-17. Schematic representation of the hIL-5R α C66A/hIL-5
complex.....81

Figure 4-18. Stoichiometry of the hIL-5R α /hIL-5 complex.....	83
Figure 4-19. Sequence alignment of IL-5 from six different species.....	85
Figure 4-20. Schematic representation of the pET-31b/mIL-5 ^{nullMet} vector....	86
Figure 4-21. Expression of mouse IL-5 ^{nullMet} in <i>E. coli</i> Rosetta cells.....	87
Figure 4-22. Purification of mIL-5 ^{nullMet} E13Q.....	88
Figure 4-23. Proliferation of the TF-1 cells by IL-5.....	90
Figure 4-24. Analysis of human IL-5 E13Q on TF-1 cells.....	91
Figure 4-25. Crystals from mIL-5 ^{nullMet} or hIL-5.....	92
Figure 4-26. Structure of the mIL-5 ^{nullMet}	94
Figure 5-1. Alignment of mouse IL-5 ^{nullMet} structure with human IL-5 structure.....	100
Figure 5-2. Structure of the human IL-5R α /IL-5 binary complex	104
Figure 5-3. Representative structures of the class I cytokine family complexes.....	105
Figure 5-4. Schematic representation of the crucial hIL-5R α residues involved in IL-5 binding.....	107
Figure 5-5. Comparison of the structures of class I complexes.....	109
Figure 5-6. Regions involved in the interaction between hIL-5R α and hIL-5.....	110
Figure 5-7. Stoichiometry of the IL-5R α and IL-5 complex.....	111
Figure 5-8. Model of the biologically active hIL-5 receptor complex	112
Figure 5-9. Differences between class I and class II cytokine complexes..	113
Table 1-1. Amino acid sequences forming the secondary structure elements of hIL-5.....	21
Table 4-1. Production of non-labeled wild type hIL-5R α	55
Table 4-2. Description of wild type hIL-5R α and hIL-5R α variants.....	59
Table 4-3. Mass spectrometry of hIL-5R α proteins.....	62
Table 4-4. Biomolecular interaction analysis of hIL-5R α and hIL-5.....	65
Table 4-5. Analysis of peptides by mass spectrometry.....	68
Table 4-6. Crystallization buffers.....	72
Table 4-7. Data collection of hIL-5R α _{C66A} /hIL-5 complex.....	79
Table 4-8. Data processing and refinement statistics for mIL-5 ^{nullMet} ...	95
Table 5-1. Alignment of α -helix sequences of hIL-5 and mIL-5 ^{nullMet}	99

1. INTRODUCTION

1.1 Overview

The term eosinophilia refers to a condition in which abnormally high amounts of eosinophils are found either in the blood or in body tissues. The commonest causes of eosinophilia in industrialized countries are allergic diseases, whereas worldwide the main cause is the presence of parasitic infection. Increased numbers of eosinophils are beneficial to cope with parasitic helminth infections, but they are detrimental in the case of allergic diseases like asthma or hypereosinophilic syndrome, where eosinophils accumulate in tissues and cause damage. Damage of the lung airways is typical for eosinophilia in the course of asthma. The pathology of asthma is thought to represent an aberration in the immune response to fight parasitic helminth infection. The prevalence of asthma is increasing worldwide affecting at least 300 million people. Because of this dramatic increase in prevalence, particularly in children, the World Health Organization considers the fight on asthma as a priority target (www.who.int/topics/asthma/en).

Eosinophils were described by Paul Ehrlich in 1879. Eosinophils arise from CD34⁺ haematopoietic progenitor cells within the bone marrow and represent 1–3% of circulating leukocytes. Eosinophils predominately reside in the gastro-intestinal tract under healthy conditions and are thought to have evolved as part of the innate immune response against parasitic helminths. These granulocytes possess secondary granules containing four primary cationic proteins namely major basic protein (MBP), eosinophil cationic protein (ECP), eosinophil-derived neurotoxin (EDN), and eosinophil peroxidase (EPO), all of which are important for killing extracellular pathogens.

The diversity of secretory products of the eosinophils, together with the wide range of receptors expressed on the eosinophil surface, reflect their broad range of functions beyond the role of a basic granulocyte. Eosinophils are able to modulate immune mechanisms that contribute to inflammation and are important in the pathology of asthma. Due to the central role of eosinophils in the development of asthma, blocking their function is considered to be a useful therapeutic approach in asthma therapy.

Cytokines play an important role in eosinophil activation. This activation is a dynamic process triggered by specific interaction of the cytokine molecule with their

corresponding cytokine receptor. Therefore, structure/function studies of the cytokine-receptor complex responsible for eosinophil activation may facilitate the design of molecules conferring antagonistic effects on the receptor activation that will be useful for the development of novel therapeutic strategies in eosinophilic diseases.

1.2 Diseases

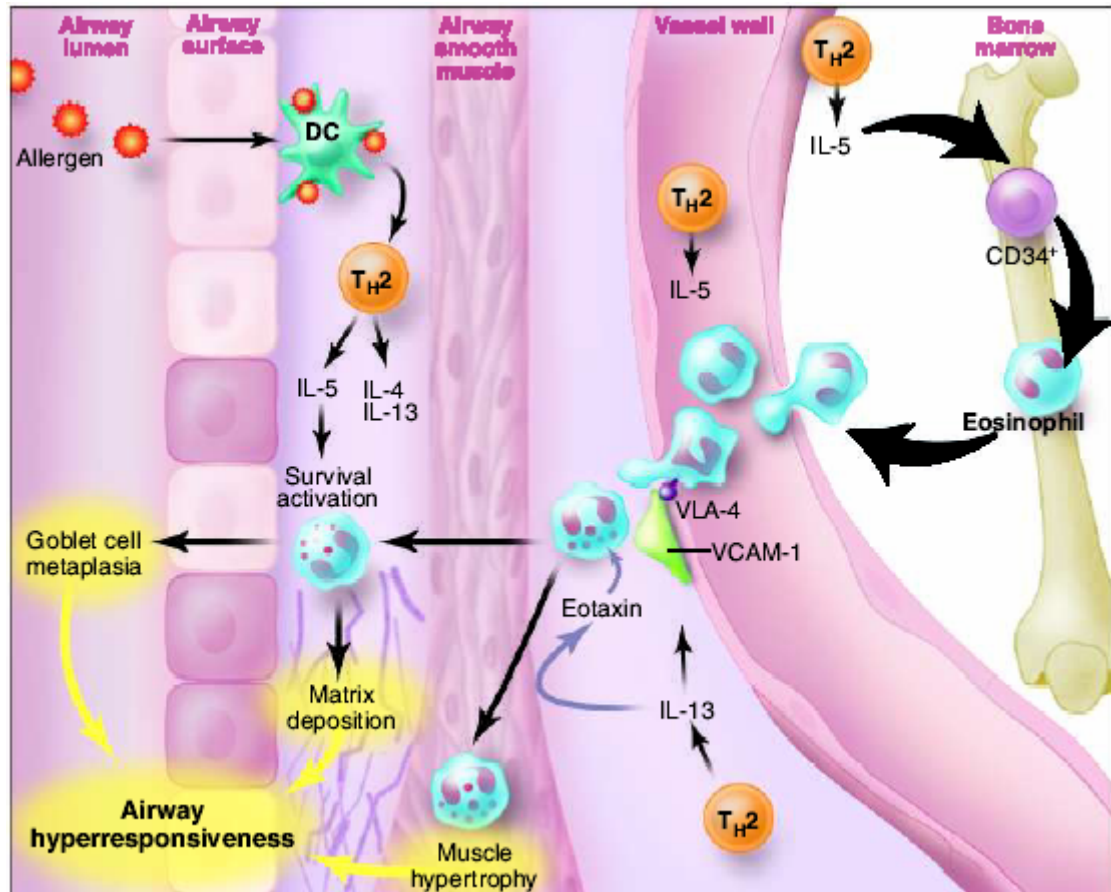
1.2.1 Parasitic Infection

Eosinophils are considered a fundamental diagnostic tool for the presence of parasitic helminth infections. Diseases caused by these extracellular pathogens are characterized by a sharp rise in eosinophil numbers in peripheral blood and high levels of circulating interleukin-5 (IL-5). The importance of IL-5 for this disease condition has been confirmed in e.g. helminth-infected IL-5-deficient knock out-mice, where eosinophilia fails to develop. Interestingly these mice show normal antibody and cytotoxic T cell responses, suggesting that IL-5 does not affect these immunological responses (Kopf et al., 1996). In parasitic infections, eosinophils and IL-5 are required for the induction of a protective immune response and eosinophils are crucial for larval killing and the production of protective antibodies. These observations led to the conclusion that IL-5 plays a key role in innate and adaptive immunity against parasites (Herbert et al., 2000).

1.2.2 Asthma

Asthma is a chronic disease with several traits such as elevated concentrations of serum immunoglobulin-E (IgE), airway mucus production, airway hyperresponsiveness (AHR), and airway inflammation. The specific cause of this allergic disease is not completely understood. The risk factors for developing asthma include any antigen (allergen) or conditions that cause inflammation in the airways. The structural changes that take place in the airways are known as airway remodeling (Figure 1-1). A possible cause of this remodeling is an imbalance in tissue repair and airway injury that results in deposition of extracellular matrix (ECM) proteins in the lungs. Remodeling is possibly caused by differentiation of the eosinophil, that may cause damage to the airway by exocytosis of their cytotoxic

granule proteins onto the bronchial mucosa (Kay, 2005; Wills-Karp and Karp, 2004). These granules contain cytotoxic proteins such as major basic protein (MBP), eosinophil cationic protein (ECP) and eosinophil peroxidase (EP) that are responsible for the tissue damage. A large body of evidence exists showing a strong correlation between the number of airway eosinophils (Eosinophilia) in allergic asthma and disease severity (Enokihara et al., 1990; Magnan and Vervloet, 1998).



Adapted from Wills, Karp 2004

Figure 1-1. Eosinophil activation. The allergen is phagocytosed, processed and presented to Th₂ cells by dendritic cells (DC). Th₂ cells produce different cytokines (IL-5, IL-4, IL-13) leading to activation of several cell types. The IL-5 promotes differentiation of CD34⁺ progenitor eosinophil cells in the bone marrow. Differentiated eosinophils migrate to swelling areas using vascular cell adhesion molecules-1 (VCAM-1) and vascular ligand adhesion-4 (VLA-4).

In asthmatic individuals, allergen presentation by dendritic cells (DC) stimulates Th₂-cell differentiation and Th₂-cytokine production e.g., IL-4, IL-5 and

IL-13 (Figure 1-1). It is well known that these Th2-cytokines orchestrate the immunopathogenesis of asthma. For example, IL-4 and IL-13 maintain the Th2 phenotype and promote isotype switching to IgE. IL-5 participates in airway remodeling, increase hypertrophy of muscle cells and proliferation of goblet cells (Wills-Karp and Karp, 2004).

Constriction of the airways is a consequence of the hypertrophy of muscle cells and metaplasia of goblet cells in the lung. In addition, IL-5 influences the development of eosinophil from CD34⁺ progenitor cells at the bone marrow level, resulting in an increased number of mature eosinophils that migrate to area of inflammation (Kay, 2005; Wills-Karp and Karp, 2004). The action of IL-5 is specific for eosinophils in humans due to the restricted expression of the IL-5 receptor alpha (IL-5R α) on the eosinophil surface (Yamada et al., 1998).

Transgenic knock out-mice (Humbles et al., 2004; Lee et al., 2004) and/or the use of monoclonal antibodies (Garrett et al., 2004) constitute major advances in our understanding of the biological functions of eosinophils and IL-5 in asthma. Different strategies to ablate the eosinophil populations have shown that these cells constitute an integral part of experimental allergic asthma (Humbles et al., 2004; Lee et al., 2004). In their seminal report, Humbles and colleagues demonstrated in eosinophil-deficient mice a decrease in the fibrotic area, due to less collagen deposition and increase smooth muscle (Humbles et al., 2004). In an another experimental approach, mice specifically devoid of eosinophils did not display mucus accumulation on the airway (Lee et al., 2004). These observations suggest that the eosinophil and IL-5 system may represent an alternative target for specific drug design as part of a novel asthma therapy.

1.2.3 Hypereosinophilic Syndrome

Hypereosinophilic syndrome (HES) is defined as a group of disorders characterized by the accumulation of large numbers of eosinophils in peripheral blood and organ tissues. These disorders are rare and multisystemic. The peripheral blood of patients contains more than 800 - 1500 eosinophils/mm³. Eosinophils cause inflammation and organ tissue damage. In some patients the eosinophilia correlates with an overproduction of IL-5 due to the activation of Th2 lymphocytes (Owen et al., 1989; Straumann et al., 2001).

1.3 Haematopoietic Cytokine Family

The IL-5, IL-3, and granulocytes macrophage colony stimulator factor (GM-CSF) cytokines belong to the haematopoietic cytokine family or class I cytokines and have multiple biological functions through their interaction with cell surface receptors. These three cytokines (IL5, IL-3, and GM-CSF) do not share significant amino acid homology. However, they appear closely related with respect to their genetic localization. Genetic linkage analysis has shown that the IL-5, IL-3, and GM-CSF genes are all found on the long arm of the chromosome 5 (van Leeuwen et al., 1989).

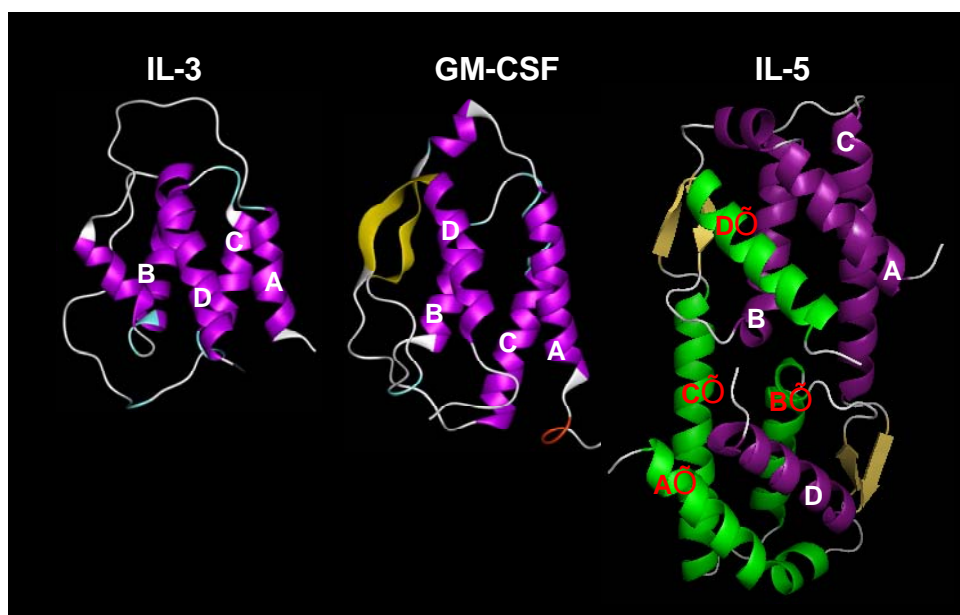


Figure 1-2. Haematopoietic related cytokines. IL-5, IL-3 and GM-CSF are mainly comprised of α -helices designated A-D, and A'-D' for the second IL-5 monomer. IL-5, IL-3 and GM-CSF are short-chain cytokines with an up-up-down-down topology.

In addition, these cytokines share a similar protein-folding motif consisting of four helices bundle architecture with two β -strands (Figure 1-2). These structural elements in IL-3 (Feng et al., 1996) and GM-CSF (Walter et al., 1992) fold in a single polypeptide chain, whereas IL-5 folds in a homodimer conformation (Milburn et al., 1993) (Figure 1-2).

The cellular receptors of IL-5, IL-3 and GM-CSF consist of two different chains called α and β chains (Tavernier et al., 1991). All three cytokines have a cytokine specific α -chain for ligand binding called IL-5R α , IL-3R α , and GM-CSFR α , respectively (Figure 1-3). The three different α -chains IL-5R α , IL-3R α , and

GM-CSFR α , and β_c chain belong to the haematopoietic receptor family and they share common features.

The haematopoietic receptor family is characterized by the presence of a so-called cytokine recognition motif (CRM) within the extracellular portion, which is usually involved in cytokine binding (Figure 1-3). This CRM is formed by two domains each one containing approximately 100 amino acids that are classified as fibronectin III like domains (Fn-III like) (Bazan, 1990). Each Fn-III like domain contains seven β strands folded into anti-parallel β sandwiches. Known X-ray structures of complexes from some haematopoietic receptor family members show that these two Fn-III like domains fold in an L shape, and the cytokine binds in an elbow region (de Vos et al., 1992; Wells and de Vos, 1996). In contrast to the structure of the growth hormone receptor (GHR), the IL-5, IL-3, and GM-CSF receptor alpha chain contains an additional Fn-III like domain (Figure 1-3), whereas β_c can be distinguished from each one of these receptor alpha external domains by the presence of two CRMs (Martinez-Moczygemba and Huston, 2001; Wells and de Vos, 1996). For IL-5, IL-3, and GM-CSF receptors, the N-terminal of the CRM contains four strictly conserved cysteine residues (Figure 1-3). These cysteine residues are buried in the core of the molecule and form two disulphide bridges (Bazan, 1990; Martinez-Moczygemba and Huston, 2003; Wells and de Vos, 1996). A membrane proximal Trp-Ser-X-Trp-Ser (WSXWS) motif is found in the C-terminal part of the CRM (Figure 1-3) (Bazan, 1990; Martinez-Moczygemba and Huston, 2003; Wells and de Vos, 1996). All these features have been found in the human as well as in the mouse system (Martinez-Moczygemba and Huston, 2003; Wells and de Vos, 1996).

In terms of biological activity IL5, IL-3, and GM-CSF have synergistic actions concerning differentiation and function of myeloid cells. However, the role of these cytokines in the immune response (IR) is clearly determined by the expression of tissue-specific receptors. For example, the IL-5 receptor is mainly expressed in eosinophils, while the IL-3 receptor is present on early haematopoietic cells. The GM-CSF receptor is expressed on myeloid progenitors, mature monocytes, eosinophils and basophils (Guthridge et al., 1998).

In line with the cell receptor expression pattern, GM-CSF and IL-3 activate immature myelomonocytic cells of the haematopoietic system and promote differentiation into granulocyte and macrophage cells. On the other hand, IL-5

mainly acts on eosinophil, triggering maturation and survival of these cells (Woodcock et al., 1997).

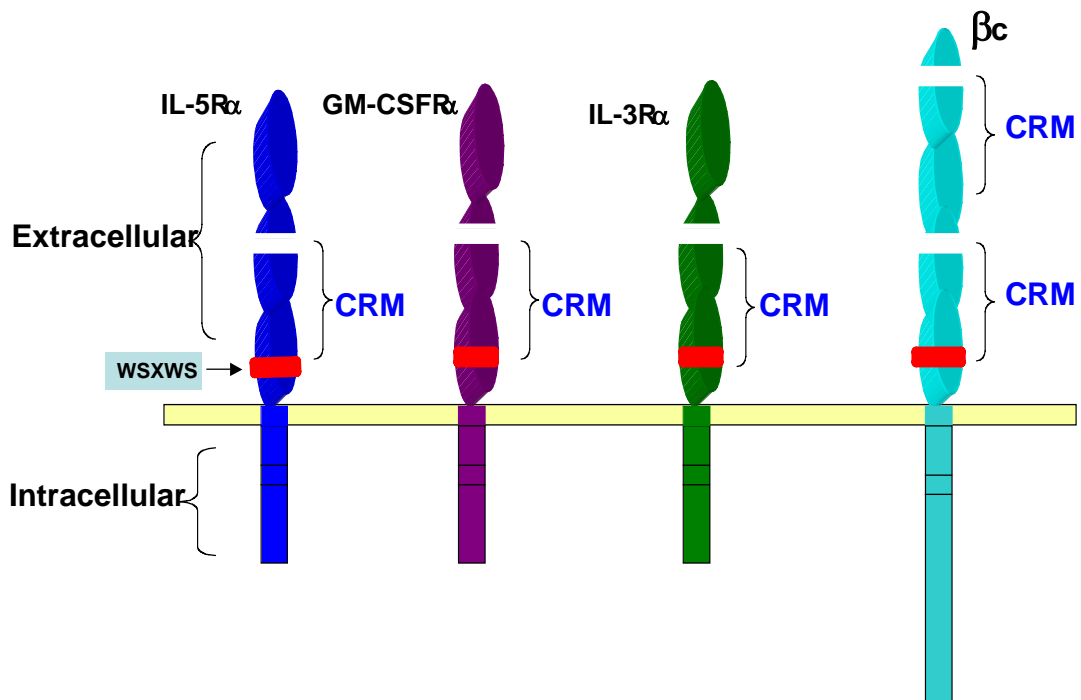


Figure 1-3. Cartoon representation of the haematopoietic cytokine receptors. The IL-5R α , IL-3R α , and GM-CSFR α and β_c subunit are presented with their modular architecture. Three Fn-III-like domains form the extracellular parts of the alpha-receptors; in contrast, the same part in β receptor consists of four Fn-III-like domains. The white lines represent the conserved cysteine residues. The WSXWS motif is shown in red. The putative cytokine binding region is called cytokine recognition motif (CRM).

1.4 Identification of Components of the Interleukin-5 System

1.4.1 Interleukin-5 (IL-5)

Activated T-cells produce soluble lymphokines that act on B-cells as growth factors (BCGF) or as B-cell differentiation factors (BCDF). BCGF induces B-cell proliferation in contrast to BCDF, which triggers maturation of B-cells into immunoglobulin secreting cells. The T-cell replacing factor (TRF) is a BCDF that can be constitutively produced by a murine T-cell hybridoma B151K12. TRF induces differentiation of pre-activated B-cells and the B leukemia cell line (BCL₁)

into antibody secreting cells (Takatsu et al., 1980). In addition, a factor derived from thymoma and/or hybridoma cells, identified as BCGF-II, induces B-cells differentiation (Swain et al., 1983). Activated T-cells also produce another cytokine, called eosinophil differentiation factor (EDF) (Sanderson et al., 1985). EDF induces eosinophil differentiation from mouse bone marrow cells *in vitro* and prolongs the survival of eosinophils. In addition, EDF stimulates the B-cell tumor (BCL₁) cell line proliferation.

Attempts to discriminate between the TRF and BCGF-II activity using different purification procedures such as ammonium sulphate precipitation, DEAE-cellulose chromatography or hydroxyl apatite chromatography were unsuccessful due to the tendency of both proteins to co-elute together. This suggests that these two cytokines may represent the same molecule. In addition, the activity of TRF and BCGF-II were found in the same fractions eluted from reverse phase-HPLC (RP-HPLC).

BCGF-II as well as TRF active material was incubated with BCL₁ cells and the resulting supernatant was assayed for residual BCGF-II and TRF activity using new BCL₁ cells. The absorption of TRF and BCGF-II with BCL₁ cells abolished not only the TRF activity but also the activity of BCGF-II. In addition, the monoclonal antibody 9TI that preferentially blocks the TRF activity in plaque-forming cell assay also blocks BCGF-II activity (Harada et al., 1985). Taking together these results it can be assumed that a single cytokine could be responsible for all the observed effects (Kinashi et al., 1986; Sanderson et al., 1986).

The activities of TRF, EDF or BCGF-II are different from the function of already known cytokines such as IL-1, IL-2, IL-3 and IFN- γ in cell assays. This led to the assumption that the activity of TRF or EDF or BCGF-II on B-cells and eosinophils possibly corresponds to a novel cytokine (Harada et al., 1985; Kinashi et al., 1986; Sanderson et al., 1986). In 1986 Kinashi, Harada et al. proposed the new term IL-5 replacing the term TRF. Subsequent studies on continuation confirmed later that TRF or EDF or BCGF-II were indeed the same molecule, now called IL-5 (Takatsu et al., 1987).

The mouse IL-5 gene was initially cloned by Kinashi and collaborators using a murine complementary DNA (cDNA) library from T-cell messenger RNA (mRNA). The murine cDNA encodes a protein of 133 residues). Twenty amino acids at the amino terminal end (N-terminus) constitute the signal peptide (Figure 1-4).

The protein has three putative glycosylation sites (Kinashi et al., 1986). Without glycosylation, the polypeptide exhibits a theoretical molecular weight (MW) of 12300 Da. The glycosylated protein has a MW that ranges between 32000-46000 Da. Additionally; mouse IL-5 cDNA contains three cysteine residues that may play a role in oligomer formation (Figure 1-4).

On continuation, the human homologue of the IL-5 gene was cloned by several groups using Southern blot hybridization techniques with a mouse IL-5 cDNA as a probe. The cDNA libraries were generated from different cell sources like human T cell leukaemia lines (Azuma et al., 1986), human liver DNA (Campbell et al., 1987), human fetal liver DNA, human placental DNA or human myeloma cell line 266B1 (Tanabe et al., 1987).

The human cDNA encodes for a protein that consists of 134 residues. Nineteen residues in the N-terminus constitute the signal peptide. Of three glycosylation sites and three cysteine residues in the mouse IL-5, only two glycosylation sites and two cysteine residues were conserved in the human IL-5 homologue (Azuma et al., 1986). Comparison of the cDNA- and amino acid sequences of murine IL-5 with those of the human IL-5 homologue (Figure 1-4) reveals 77% sequence homology at the nucleotide level and 70% at the protein level (Azuma et al., 1986). Human and mouse mature proteins have 115 and 113 amino acids, respectively (Figure 1-4).

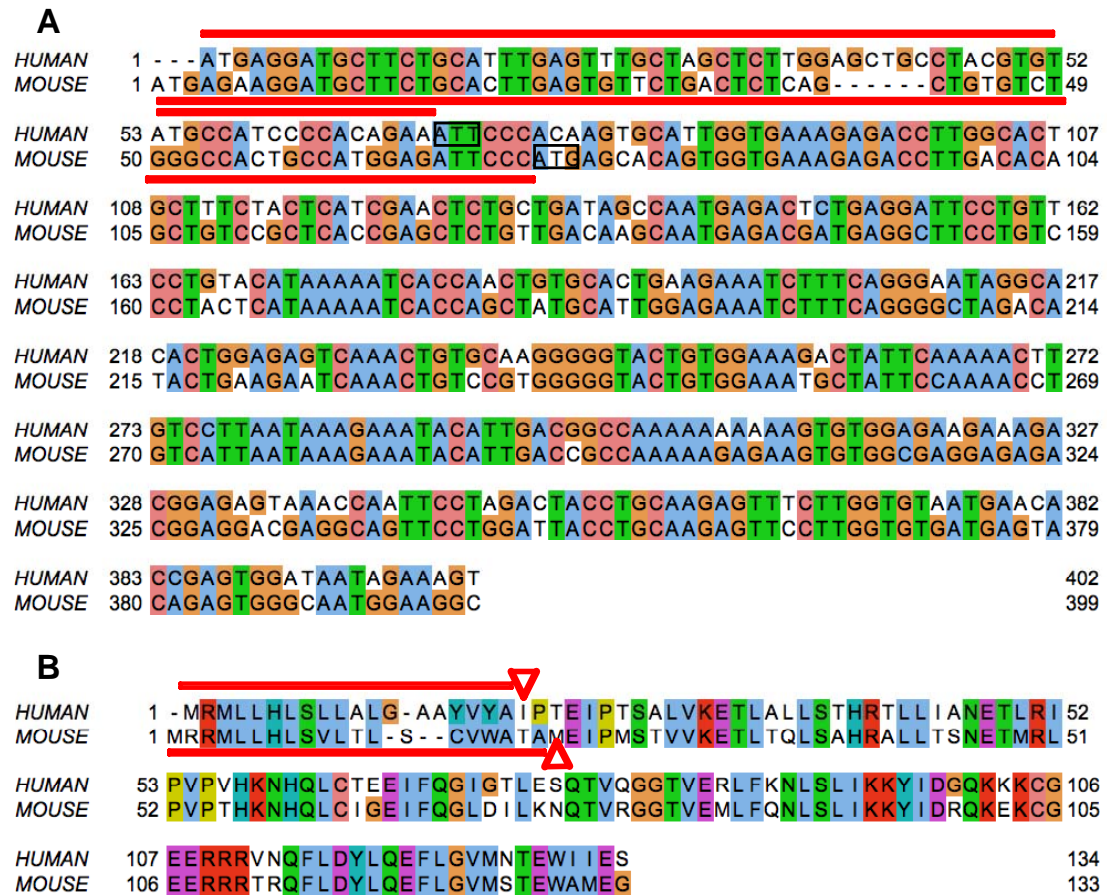


Figure 1-4. Sequence alignment of human and mouse IL-5. (A) Nucleotide sequence and (B) amino acid sequences of hIL-5 and mIL-5 show 77% and 70% identity between the two cytokines. Red lines show the signal peptide (nucleotides or amino acids) of the two cytokines. Black squares show the codon of the first amino acid of the mature proteins. Red arrowheads point to the first residue of the mature protein. Matched nucleotides or residues are shown with the same color. Mismatched nucleotides or residues are not shown in color. Gaps are shown by hyphens. The alignments were done with the Jalview program using Clustal W analysis (Clamp et al., 2004).

The biological activity of both, human and mouse IL-5, requires configuration of a homodimer protein, linked together by disulphide bridges (Tavernier et al., 1989). IL-5 is an important mediator of several biological processes, such as 1. induction of expression of the IL-2 receptor on activated B-cells (Loughnan et al., 1987; Nakanishi et al., 1988), 2. activation of B-cell proliferation and differentiation into antibody-secreting cells (Harada et al., 1985; Kinashi et al., 1986; Sanderson et al., 1986; Takatsu et al., 1980). and 3. induction of

expression of the activation-induced cytidine deaminase (Aid) and B lymphocyte-induced maturation protein-1 (Blimp-1) (Horikawa and Takatsu, 2006).

Both, mouse IL-5 and human IL-5, have been expressed in eukaryotic expression systems such as *Xenopus laevis* oocytes, NIH-3T3, *sf9*, and *Saccharomyces cerevisiae* cells (Ingley et al., 1991; Tavernier et al., 1989). In the prokaryotic expression system as *E. coli*, only human IL-5 could be expressed and purified so far (Proudfoot et al., 1990). The human IL-5 recombinant protein generated in bacteria shows high specific activity in biological assays *in vitro*. These results demonstrated that the carbohydrate moiety of the human IL-5 is not required for biological activity or IL-5 dimer formation (Proudfoot et al., 1990).

1.4.2 Interleukin-5 Receptor (IL-5R)

The knowledge of the biological functions of IL-5 on B-cells, eosinophil precursors and mature eosinophil has prompted the scientific community to extend the studies to the cellular receptor responsible for transmitting the specific signal into these cells.

Analysis of the specific binding of mouse IL-5 to its receptor in cell assays demonstrated that IL-5 binds to B-cells with two different affinities. The affinity constant (K_D) for the high affinity binding site was determined to be 66 pM, and for the low affinity binding sites to be 12 nM (Mita et al., 1988). Additionally, crosslinking experiments identified two crosslinked complexes with mouse IL-5. The first complex was shown to have a MW of 92.500 Da and the second complex a MW of 210.000 Da (Mita et al., 1988). The MWs of the mouse IL-5 crosslinked proteins in the first and second complexes were close to 46.500 Da and 114.000 Da, respectively. These result also suggests that the 46.500 MW component represents the complex with mouse IL-5 with the low affinity receptor subunit, while the high affinity receptor consists of this complex and one additional protein (receptor) with a MW of 114.000 (Mita et al., 1989).

The low affinity receptor and the additional protein (receptor) constitute a complex of highly glycosylated proteins. Due to the glycosylation moiety, their MWs likely range between 46.500-60.000 and 114.000-130.000 Da, respectively. In 1991 Mita and colleagues proposed to designate the low affinity receptor (46.500-60.000 Da) and the additional peptide receptor chain (114.000-130.000 Da) as the alpha and the beta chains of the IL-5 receptor, respectively (Mita et al., 1991). The

alpha subunit (mIL-5R α) can bind to mouse IL-5 on its own, while the beta subunit (mIL-5R β) does not (Takaki et al., 1990). Similar results were obtained during characterization of the human IL-5 receptor (hIL-5R) in the pro-myelocytic cells HL60 (Plaetinck et al., 1990), suggesting that the IL-5R/IL-5 system is highly conserved in mice and human.

The gene structure of the IL-5R α chain was first described in the murine system using a cDNA library derived from IL-5 dependent B-cells (Takaki et al., 1990). For the human IL-5R α , the cDNA was isolated from cDNA libraries of human eosinophils using a murine IL-5R α cDNA as a probe (Murata et al., 1992). Both, human IL-5R α and mouse IL-5R α , share a 70% homology on amino acid (aa) sequence level (Murata et al., 1992). The mRNA of IL-5R α undergoes alternative splicing (Takaki et al., 1990; Tavernier et al., 1992). Transcripts found in HL-60 cells encode both, secreted and anchored forms, of IL-5R α . The secreted form exhibits antagonist properties in an eosinophil differentiation assay (Tavernier et al., 1991).

Amino acid sequence analysis of mouse IL-5R α demonstrated that the receptor is a glycoprotein of 415 residues with a MW of 45284 Da, including a N-terminal hydrophobic region (17 aa), which is the signal peptide, an extracellular domain (322 aa), a single transmembrane segment (22 aa), and a cytoplasmic tail (54 aa). Similarly, the cDNA human IL-5R α encodes a glycoprotein of 420 amino acids with a MW of 47670, that consists of an N-terminal (signal peptide) hydrophobic region (20 aa), an extracellular domain (324 aa), a single transmembrane domain (21 aa), and a short cytoplasmic domain of 55 amino acids (Murata et al., 1992).

The mouse beta chain (mIL-5R β or β_c) gene structure was initially characterized by Gorman and colleagues, and it was called AIC2B (Gorman et al., 1990). They used a monoclonal antibody (anti-Aic2) against mIL-3 to characterize a cDNA library from the mouse mast cell line M/C9 cloned into COS-7 cells. The isolated cDNA was called AIC2B, due to its homology to the previously characterized cDNA for IL-3R that had been named AIC2A. AIC2B encodes for a glycoprotein of 874 amino acids with a MW of 96681 Da, that consists of a 22 amino acid signal peptide, an extracellular domain of 419 amino acids, a single transmembrane domain of 22 residues, and a cytoplasmic domain of 433 residues (*Swiss-Prot: IL-3R β -Mouse P26955*). Binding assays with IL-3, IL-4, or GM-CSF

have shown that AIC2B does not bind to cytokines on its own (Gorman et al., 1990) confirming the previous results showed by Mita and colleagues (Mita et al., 1991)

The human IL-5R β homologue (hIL-5R β) was subsequently identified using an AIC2B cDNA as probe. The homologous gene was identified in a cDNA library of TF-1 cells. The new gene reveals 56% amino acid sequence identity with AIC2B. The protein encoded by this cDNA has a MW of 120 kDa and showed no cytokine binding capability (Hayashida et al., 1990).

Further experiments have demonstrated that the murine- and human IL-5-, IL-3-, and granulocyte-macrophage colony-stimulator factor-receptor (GM-CSFR) share a beta chain (Kitamura et al., 1991; Takaki et al., 1991; Tavernier et al., 1991). In contrast to the human receptor, the mouse receptor has two different but related β chain genes, AIC2A and AIC2B. The former is specific for the mouse IL-3 (Hara and Miyajima, 1992) and the latter is shared between GM-CSF, IL-3 and IL-5, now known as the common beta chain (β_c).

1.5 Interaction of IL-5 and IL-5 receptor

Several studies aimed at elucidating the molecular basis of the IL-5/IL-5R α interaction led to important findings on epitope usage. Initial results showed that the chemical proteolysis of human IL-5 with cyanogen bromide (CNBr) led to the cleavage of eight residues on the C-terminus of human IL-5 resulting in the complete loss of biological activity (Kodama et al., 1991). Furthermore, several cell assays showed that mouse IL-5 activates human responsive cells as effectively as human IL-5. However, human IL-5 is a weaker inducer of mouse responsive cells to IL-5. In IL-5 human/mouse protein chimeras, it has been shown that replacement of the last 36 residues at the carboxyl terminal end (C-terminus) in human IL-5 with the last 36 residues of mouse IL-5 produces a hybrid molecule with biological activity comparable to mIL-5. In this C-terminal, eight amino acids are not conserved between humans and mice. Replacing these eight amino acids in the C-terminal region of human IL-5 by those of mouse IL-5 resulted in the hybrid human IL-5/mouse IL-5 exhibiting comparable activity in mouse responsive cells (McKenzie et al., 1991a). In addition, the substitution of Lys 84 and Asn 108 in human IL-5 by their respective murine counterpart residue Glu 84 and Ser 108 yielded molecules with the same activity of murine IL-5 (Cornelis et al., 1995). These results imply that the amino acid replacement did not disturb the overall-structure of the protein and

confirm the crucial role of the C-terminal residues of IL-5 for its receptor binding activity (Kodama et al., 1991; McKenzie et al., 1991a).

However, the biological activity of IL-5 does not only depend on C-terminal residues as demonstrated by Shanafelt and colleagues (Shanafelt et al., 1991). Experiments using site-directed mutagenesis revealed that several key residues in the N-terminal α -helix of IL-5 also govern the recognition binding with IL-5R β , although the responsible residues were not identified (Shanafelt et al., 1991).

The dimeric form of IL-5 was shown to be essential for bioactivity. Native human IL-5 monomers produced by site directed mutagenesis of cysteine residues to threonine (C44T or C86T) did not exhibit any biological activity neither on the murine eosinophils nor on an IL-5-dependent B-cell line (McKenzie et al., 1991b). In contrast, human IL-5 monomers obtained by protein engineering showed the same biological activity as native IL-5. Although these IL-5 monomers bind to its receptor with 30-40-fold lower affinity than wild type IL-5 dimeric protein, the monomers interact with the IL-5R α with the same stoichiometry as wild type IL-5 dimeric protein (Dickason et al., 1996a; Dickason et al., 1996b; Edgerton et al., 1997; Li et al., 1997). The latter results suggest that the role of IL-5 disulphide bonds is related to the structural maintenance of the functional domains.

The residues in human IL-5, which are important for the molecular interaction with human IL-5R α were found to be mainly charged residues (Figure 1-5). Different human IL5 mutants such as H38A, K39A, H41A, E89A, R91A, and E110A showed a strong reduction in the activation of cell proliferation or binding to IL-5R α compared with the wild type IL-5 (Graber et al., 1995; Tavernier et al., 1995b). The human E13Q mutation was completely inactive and failed to induce proliferation in TF-1 cells, although crosslinking experiments demonstrated the interaction with the receptor (Tavernier et al., 1995b). Further mutation analysis on the human IL-5 Glu13 position confirmed the important role that this residue plays in receptor activation due to β_c recruitment. Mutation which removed the charge (E13A) or led to charge reversal (E13K) were also shown to decrease cell proliferation activities (Graber et al., 1995; McKinnon et al., 1997).

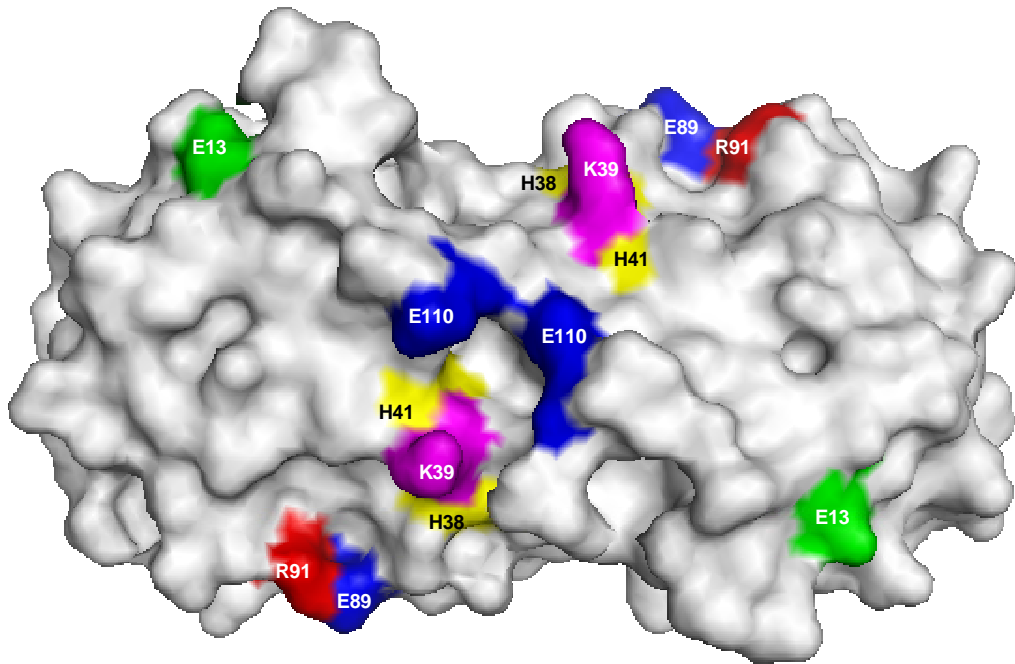


Figure 1-5. Residues in human IL-5 important for binding. The residues involved in binding to the alpha chain of the receptor (IL-5R α) are colored in red (Arg91), yellow (His38 and His41), magenta (Lys39) and blue (Glu89 and Glu110). The residue involved in binding to the beta chain of the receptor (IL-5R β) is colored in green (Glu13).

On the other hand, site-directed mutagenesis studies of IL-5R α provided further clues that the IL-5 binding properties are highly dependent on the amino acids at the first domain (N-terminal). Subsequent analysis defined as crucial the Asp55, Asp56, and Glu58 residues (Cornelis et al., 1995). Additionally, an alignment between the second and third Fn-III-like domains of the IL-5R α and growth hormone receptor (GHR) was done to identify crucial residues in the cytokine recognition motif (CRM) of the IL-5R α . The alignment reveals five residues that align with five known residues to contact the growth hormone ligand (GH). Afterwards, Arg188 in IL-5R α corresponding to residue Trp104 in GH receptor (GHR) proved to be important for ligand interaction. Mutations at this position in IL-5R α (R188A) showed strongly reduced human IL-5 binding affinity (Cornelis et al., 1995). These results demonstrated the importance of residues of the second Fn-III like for the ligand interaction.

More recent data suggest that the IL-5/IL-5R α system adopts a complex and unique binding topology in which the cytokine is recognized by a combination of residues in the first (Asp55, Asp56 and Glu58), second (Lys186 and Arg188) and third (Arg297) Fn-III-like domains, forming a new type of cytokine recognition interface (Ishino et al., 2004).

On the other hand, the Asp 56, Glu 58 and Arg 188 residues of the human IL-5R α seem to govern the species-specific interaction between human and mouse IL-5 (Glu 56, D58 and Phe 188), since they are not conserved in the mouse IL-5R α (Cornelis et al., 1995). With other words, the β_c (IL-5R β) interacts with both cytokines of either human and mouse origin. The species-specific role of IL-5R α in ligand interaction was demonstrated by Takaki and colleagues in 1994 (Takaki and Takatsu, 1994). By cell transfection, they succeeded in expressing human- and mouse IL-5R α cDNA in the IL-3-dependent mouse cell line FDC-P1 producing the mouse β_c constitutively. The transfected cells become responsive to stimulation with human and mouse IL-5 (Takaki and Takatsu, 1994).

Furthermore, site directed mutagenesis, ligand binding and cell proliferation assays have demonstrated the critical role of Tyr 15, Phe 79 and Tyr 421 of the β_c (IL-5R β) in high affinity binding, complex formation and receptor activation (Figure 1-8) (Murphy et al., 2003; Woodcock et al., 1996). The way in which the β_c interacts with IL-5R α /IL-5 complex in the respective active complex is yet poorly understood.

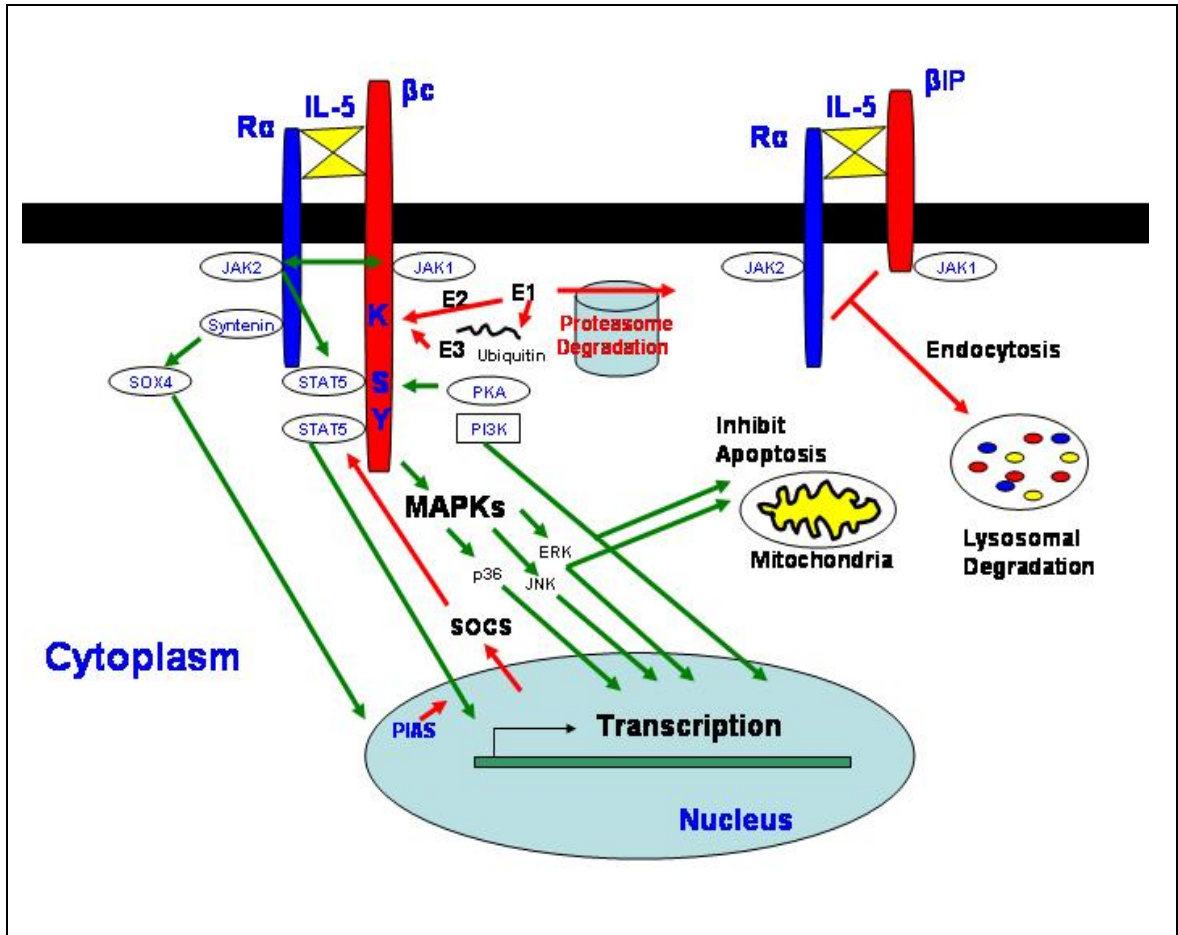
Although several key binding determinants between IL-5 and IL-5R are now known, a closer insight into the three dimensional structure of the complex is required to confirm the mechanism of the molecular interaction between IL-5 and IL-5R. So far, different experiments such as cross-linking, gelfiltration, ultracentrifugation, and titration microcalorimetry have shown a 1:1 stoichiometry for the interaction between IL-5 with IL-5R α at the cellular level as well as *in vitro* (Devos et al., 1993; Johanson et al., 1995). In addition, the exact stoichiometry of the trimeric complex (IL-5/IL-5R α / IL-5R β) was assumed to consist of one copy of each IL-5/IL-5R α / IL-5R β in a 1:1:1 stoichiometry (Li et al., 1996). With the three-dimensional structure of IL-5R α /IL-5 complex the binding stoichiometry would be confirmed if they interact in a 1:1 relationship, since the dimeric conformation of the IL-5 suggest a potential accommodation of two IL-5R α molecules, that denotes a binding stoichiometry of 1:2.

1.6 Intracellular Signaling Cascades of IL-5 Receptor

Binding of IL-5 to its receptor occurs by a sequential mechanism. The IL-5 triggers its cellular responses by first binding the IL-5R α (Johanson et al., 1995; Mita et al., 1988; Mita et al., 1989; Takaki et al., 1990; Tavernier et al., 1991). The IL-5/IL-5R α complex recruits the β_c chain (Johanson et al., 1995; Mita et al., 1988; Mita et al., 1989; Takaki et al., 1990; Tavernier et al., 1991), which leads to heteromeric receptor assembly and triggers intracellular signaling (Figure 1-6).

The cytoplasmic domain of IL-5R lacks an intrinsic kinase activity. However, these cytoplasmic regions of the IL-5R α and IL-5R β (β_c) are critical in mediating signal transduction by the activation of intracellular protein kinases and transcription factors. The cytoplasmic domains of IL-5R α and β_c are associated with the Janus kinases (JAK) JAK2 and JAK1, respectively (Figure 1-6) (Kouro et al., 1996; Ogata et al., 1998). The trans-phosphorylation between JAK2 and JAK1 occurs after IL-5 binding to IL-5R α and recruiting of the β_c chain into the complex

The activated JAKs subsequently phosphorylate the β_c in different tyrosine residues; six of them are conserved between mouse and human receptors (Tyr 577, Tyr 612, Tyr 695, Tyr 750, Tyr 806 and Tyr 866). The phosphorylation of the β_c on Tyr 577 induces the activation of the ERK pathway (Guthridge et al., 1998; Martinez-Moczygamba and Huston, 2003), whereas tyrosine phosphorylation of Tyr 577 and Tyr 612 is important for activation of the growth factor receptor-bound adaptor protein (Grb2). The ERK pathway is involved in the prevention of apoptosis, by increasing the levels of two anti-apoptotic proteins bcl-2 and bcl-x (Figure 1-6). Activated Grb2 activates downstream partners of the mitogen-activated protein kinase (MAPK) pathway (de Groot et al., 1998; Guthridge et al., 1998; Martinez-Moczygamba and Huston, 2003).



Adapted from Martinez-Moczygemba, 2003

Figure 1-6. Up-regulation and down-regulation pathways of the IL-5 receptor. IL-5 binds to the IL-5R α and this dimeric complex recruits a second member of the receptor system β_c . Simultaneously, pathways as MAPK, PI3K and syntenin-SOX4 are activated (green arrows). Ubiquitination, proteasome degradation, PIAS and SOCS appear as a down regulation mechanism (red arrows).

JAK activation also results in tyrosine phosphorylation of the signal transducer and activator of transcription (STAT) STAT5. Activated STAT5 translocates into the nucleus and regulates the transcription of genes encoding for proteins such as cytokine-inducible SH2-containing proteins (CIS), and the related suppressor of cytokine signaling proteins (SOCS). These are involved in the negative feedback, thus leading to down-regulation of JAK activity (Figure 1-6). NF- κ B is also activated after phosphorylation of STAT5 as it was shown in murine Ba/F3 cells upon IL-5 activation (Nakamura et al., 2002).

There are different sequence motifs (box) in the cytoplasmic domain of the β_c related with cell proliferation, differentiation, and survival. For instance, the box 1 is a region formed by approximately 35 residues found proximal to the inner leaflet

membrane. Deletion of the box 1 was shown to interfere with cell proliferation. A second motif found downstream of box 1, called box 2, enhances the proliferation signals of box 1. The cell survival depends on a region that encompasses the residues 544-763. This entire domain is required for cell survival in absence of serum (Guthridge et al., 1998; Martinez-Moczygemba and Huston, 2003).

As well as the β_c , the IL-5R α cytoplasmic C-terminal domain also participates in mediating growth signal transduction and activation of JAK kinases and STAT5. The membrane proximal sequence (Pro 352-Pro353-X-Pro355) of the cytoplasmic domain of the IL-5R α is required for cell proliferation and JAK/STAT activation (Kouro et al., 1996). In addition, the cytoplasmic tail of IL-5R α is associated with the protein syntenin. Syntenin was found to directly interact with the transcription factor Sox4 which is important in B-cell development (Geijsen et al., 2001). The down-regulation of the IL-5 signaling pathway is mediated by ubiquitination of the cytoplasmic domain of the β_c (Figure 1-6). Ubiquitinated intracellular domain of the β_c suffers proteasome degradation resulting in the generation of β_c intracytoplasmic proteolysis (β IP). After that, the β IP/IL-5/IL-5R α complex is endocytosed and degraded in the lysosomes (Figure 1-6) (Martinez-Moczygemba and Huston, 2001).

In addition, the suppressor of cytokine signaling (SOCS) and protein inhibitors of activated STAT (PIAs) proteins participate in the down-regulation of signaling, and thereby inhibit JAK and STAT pathways (Martinez-Moczygemba and Huston, 2003). Recently it was shown that the regulation of the IL-5 signaling pathway is a result of Dynamin-2 GTPase protein activation that is associated with alpha subunit of the IL-5 receptor. The specific role of Dynamin is the termination of the ERK1/2 signaling pathways. Dynamin also is required for the receptor endocytosis (Gorska et al., 2006).

1.7 Structural Studies of IL-5 System

Structure/function studies of the IL-5 complex are focused on understanding the molecular assembly of the protein molecules and how they interact to form an active complex. The first studies to determine the human IL-5/IL-5R α complex X-ray crystal structure were performed by Johanson and colleagues in 1995 (Johanson et al., 1995). They deglycosylated human IL-5 using PNGaseF enzyme. After deglycosylation of the ligand, they co-crystallized the human IL-5/IL-5R α complex

by hanging drop diffusion method. Only needle crystals were obtained from the complex crystals and the crystal structure of human IL-5/IL-5R α complex could not be determined successfully (Johanson et al., 1995). The structure determination of IL-5/IL-5R α / β_c has also not been successful yet; instead of a complex X-ray crystallography structure picture, only the structure of individual components of the IL-5 system such as human IL-5 (Milburn et al., 1993) or human β_c (Carr et al., 2001) has been determined so far.

The first structure of the IL-5 system published was hIL-5. This structure of human IL-5 purified from *E. coli* was determined using X-ray crystallographic analysis (1-7). In 1992, Hassel and collaborators published the crystallization and preliminary X-ray diffraction studies of the recombinant hIL-5. They obtained crystals that belong to the space group C2 with cell unit constant of $a = 122.1 \text{ \AA}$, $b = 36.1 \text{ \AA}$, $c = 56.4$ and $\beta = 98.6^\circ$ (Hassell et al., 1993). On continuation, the human IL-5 protein structure was determined by Milburn and colleagues in 1993 (Milburn et al., 1993).

The human IL-5 structure consists of two left-handed bundles of four helices (A-D) all positioned end to end, and two short β -sheets on opposite sides of the molecule (Figure 1-7). The two β -sheets are located between the helices A and B, and C and D. The helix bundle is formed by three helices A, B, and C from one monomer. Each one has a different length (Table 1-1); a fourth helix D (17 residues) is derived from the other monomer (Figure 1-7).

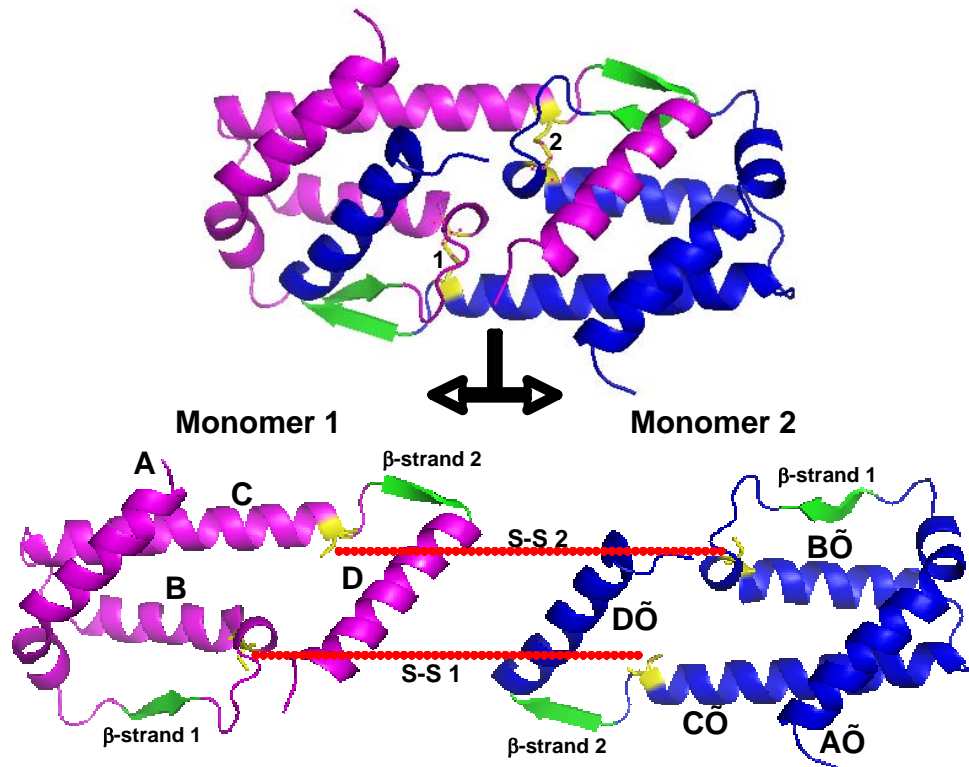


Figure 1-7. Structure of the human IL-5. The figure (ribbon) shows the complete molecule (upper) and each monomer (lower). Alpha helices of each monomer named A-D or A'-D'. β -strands (green) and disulphide bonds (yellow) are designed 1 and 2. The structure was generated using PyMOL.

Table 1.1 Amino acid sequences forming the secondary structure elements of hIL-5.

Motif	Start	End	Secondary structure	Sequence
A	Thr 7	Ile 26	α	TSALVKETLALLSTRLLI
B	Hist 41	Glu 56	α	HQLCTEEIFQGIGTLE
C	Val 65	Lys 84	α	VERLFKNLSLIKKYIDGQKK
D	Val 93	Thr 109	α	VNQFLDYLDQEFLGVMNT
Strand₁	Arg 32	Val 35	β	RIPV
Strand₂	Glu 89	Arg 92	β	ERRR

The structure also reveals that the human IL-5 dimer is stabilized by two inter-chain disulfide bridges between Cys 44 and Cys 86 (Milburn et al., 1993).

The secondary structure of the IL-5 system published was the human IL-5R β (β_c). The crystal structure of the extracellular domain of β_c was determined by X-ray crystallography (Carr et al., 2001; Gustin et al., 2001). This extracellular part of the human β_c forms a stable intertwined dimer. The β_c dimer is stabilized due to five disulfide bridges. The β_c dimer has also been confirmed in chemical cross-linking experiments (Muto et al., 1996).

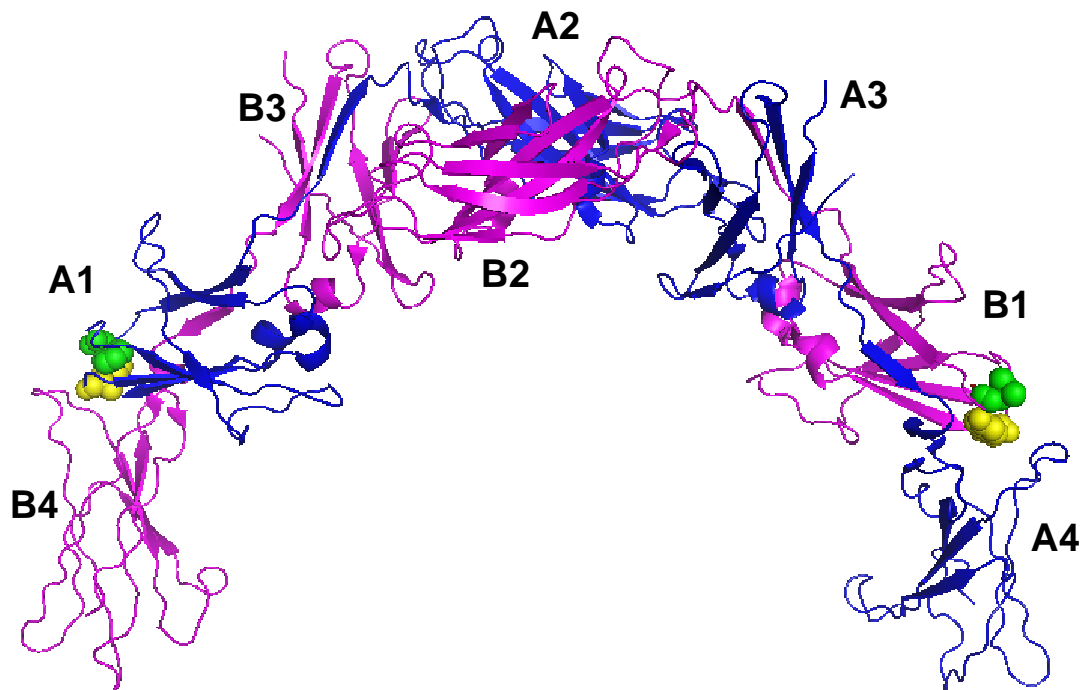


Figure 1-8. Structure of the human β_c . Monomer A is colored blue and monomer B is colored magenta. Each monomer has four Fn-III-like domain designed A1-A4 or B1-B4. The residues involved in binding to the IL-5R α /IL-5 complex are colored in yellow (Tyr15) and green (Phe79).

Each human β_c monomer consists of four domains with a Fn-III like topology (Figure 1-8). The WSXWS motif is found in domain four which is similar to those in other class I cytokine receptors (Carr et al., 2001).

The elucidation of the crystallography structure of the IL-5R/hIL-5 complex represents an important breakthrough towards the design of antagonist molecules

that may affect the interaction of IL-5R α with human IL-5. This complex may become the most promising target for rational drug design.

1.8 Therapeutic Approaches in Asthma and Hypereosinophilic Syndrome Treatment

Some therapeutic strategies have been developed to counteract eosinophil activation by IL-5 inhibition in asthma or hypereosinophilic syndrome. In this way, an anti-IL-5 antibody (Mepolizumab) was used in eosinophils dermatitis patients. Mepolizumad effectively controlled the symptoms in these patients. Eosinophils counts and serum levels of eosinophil cationic proteins were normal 24 and 48 hours after initial treatment, respectively. Other symptoms (pruriginous, eczematous and urticarial skin lesions) diminished after the first infusion (Plotz et al., 2003).

In another clinical setting, mepolizumab was administered to four men (10 mg/kg, maximum 750 mg) with hypereosinophilic syndrome (HES) defined by peripheral blood and/or tissue eosinophilia. The patients showed a ten-fold reduction in tissue-eosinophil levels. Furthermore, the treatment improved the clinical symptoms and quality of life. The number of peripheral blood eosinophils had significantly decreased three months after the last dose (Garrett et al., 2004). Contradictory results were recently reported by Oldhoff and colleagues (Oldhoff et al., 2006); they showed that mepolizumad did not exhibit any effect on the atopic path test in atopic dermatitis. The atopic path test is an *in vivo* model used to study the induction of eczema by inhaled allergens in atopic dermatitis patients. Mepolizumab could not prevent the eczematous reactions or lower the number of eosinophils in the tissue. However, peripheral blood eosinophils were decreased by antibody therapy (Oldhoff et al., 2006). These discrepancies suggest that there is a possible redundancy in the cytokines, which participate in this biological phenomenon.

Accordingly, anti-IL-5 humanized antibodies like mepolizumab have been used in several clinical tests. Different trials carried out in 2003 in asthmatic individuals showed that the anti-IL-5 (mepolizumab) therapy arrested the eosinophil maturation and decreased the number of eosinophil progenitors (Menzies-Gow et al., 2003). The mepolizumab treatment also reduced the levels of extracellular matrix proteins such as tenascin, lumican and procollagen III (Flood-Page et al., 2003a).

However, the anti-IL-5 therapy did only partially reduce, but did not completely deplete the eosinophils in the airway (Flood-Page et al., 2003b).

On the other hand, peptides with antagonist action to IL-5 have been developed as new therapies (England et al., 2000; Ishino et al., 2005; Ruchala et al., 2004). The peptides evaluated so far seem to employ the same contact residues of IL-5 and in this way, they might block the interaction of the IL-5 with the receptor alpha chain. These *in vitro* results showed competition between IL-5 and the antagonist peptide for binding to IL-5R α , and these antagonist peptide displayed the same affinity as IL-5 (England et al., 2000). More recently, by using cyclic peptides as therapeutic agents it could be demonstrated that they effectively mimic the CD turn recognition epitope for alpha-receptor. Additionally, the peptide could exhibit a similar interaction mechanism to that of IL-5. Also, biological experiments showed peptide inhibition of IL-5 activity (Ishino et al., 2005; Ruchala et al., 2004). Further experiments were performed using site-directed mutagenesis on the peptides, which were then examined for the type of IL-5R α interaction. In order to interact with the receptor, the peptide must undergo a conformational rearrangement during binding. The studies also demonstrated that this peptides use two amino acids (Arg 6 at the N-terminal and His 11 at the C-terminal) to stabilize the final complex (Ishino et al., 2006). Most importantly, this peptide was able to deactivate the IL-5 receptor function. Taken together these results it can be hypothesized that such peptides may have good potential to act as antagonist molecules for modern asthma therapy.

In order to improve the current strategies of asthma therapy, it would be highly beneficial to increase our understanding of the molecular IL-5 receptor and IL-5 agonist interaction. The knowledge of the three dimensional structure of this complex will provide new insights in this crucial step of asthma pathogenesis. Ultimately, this may create new options to design specific antagonist molecules, which may result in a breakthrough of our current arsenal of targeted pharmacological options to relieve this disease condition of increasing importance.

2 AIMS

Interleukin-5 (IL-5) belongs to the family of haematopoietic cytokines and plays a key role during development of Th₂ immune responses. IL-5 contributes to the differentiation and function of eosinophils, which are implicated in the pathophysiology of asthma disease as well as the hypereosinophilic syndrome. Both diseases are characterized by tissue damage due to eosinophil activation as a result of the interaction of IL-5 and the extracellular membrane IL-5 receptor. The IL-5 and its IL-5R represent a promising target for the development of new therapeutic strategies that can block the pathophysiological eosinophil activation. Structural aspects of the IL-5R/IL-5 complex should be clues towards the understanding of the mechanism of their interaction. Additionally, the structural features of the mouse IL-5 system can be used to study the species-specific interaction. Thus, the receptor ectodomain of human IL-5R α (IL-5R α_{ECD}) in complex with human IL-5 (hIL-5) and mouse IL-5 (mIL-5) X-ray structure should be examined in this work.

The principal objective of this thesis was to resolve the three-dimensional structure of the extracellular domain of the receptor-specific binding chain of the IL-5 (hIL-5R α_{ECD}) in complex with hIL-5, which is essential to recruit the second receptor chain, in order to trigger intracellular signaling. In addition, the elucidation of the three-dimensional structure of the mIL-5 was also a primary goal of this work. The first step towards deciphering the complex and the mIL-5 structure was to achieve the expression of the proteins in an *E.coli* expression system that would allow the production of large amounts of protein. Another important task to be accomplished was to find the specific crystallization conditions of the hIL-5R α_{ECD} /hIL-5 complex and of the mIL-5. A further objective was to resolve the three-dimensional structures of mIL-5 and to compare it with the hIL-5, in order to determine the molecular basis for the species-specific receptor binding properties. Last but not least, the specific binding topology of the hIL-5R α_{ECD} /hIL-5 complex should be analyzed and compared to other receptors of the same family.

3 MATERIALS AND METHODS

3.1 Reagents

The basic chemicals were obtained from Applichem, Merck, Roth and Sigma-Aldrich. The enzymes were purchased from New England Biolab and Fermentas. Crystallization buffers were from Hampton research and Jena Bioscience.

The proteins were dialyzed in Spectra/por 3 (132720) regenerated cellulose membranes from Roth. The Spectra/por 3 has a Molecular Weight Cutoff (MWCO) of 3500, a diameter of 11.5 mm, and a capacity of volume/length of 1 ml/cm. Proteins were concentrated by ultra-filtration membranes regenerated cellulose YM3 membranes with 3000 MWCO. Amicon ultra-4 with 5000 MWCO (UFC 800524) were from Millipore. Viva flow 200 system with 5000 MWCO membranes was used to concentrate proteins in large volume.

For bacteria and mammalian culture medium, distilled and standard deionized water were used, respectively. For the preparations of stock solutions for crystallization, Milli Q quality water [18.2 M Ω cm] was used.

3.2 Kits

The sequencing kit “DTCS Quick Start” was purchased Beckman Coulter. Kits for PCR product purification (QIAquick PCR), plasmid purification (QIAfilter plasmid), and DNA agarose cleaning (QIAquick Gel Extraction) were obtained from QIAGEN. The sensor chips CM5, and the amine coupling kit with the N-ethyl-N’-(3-diethylaminopropyl) carbodiimide, N-hydroxysuccinimide and ethanolamine hydrochloride were from Pharmacia (Pharmacia, BIAcore).

3.3 Sterilization

Buffers and media were autoclaved for 20 min at 121°C, 1.1 bar. Crystallization stocks solutions were sterile filtered through Millipore 0.22 μ m filters.

3.4 Bacterial Strains

E. coli Rosetta-gami (DE3)pLysS (Novagen)

Genotype: $\Delta(ara-leu)$ 7697 $\Delta lacX74$ $\Delta phoA$ P_{vull} $phoR$ $araD139$ $ahpC$ $gale$ $galK$ $rpsL$ (DE3) $F'[lac^+ lacI^q pro]$ $gor522::Tn 10$ $trxB$ pLysSRARE (Cam^R, Kan^R, Str^R, Tet^R).

***E. coli* AD494 (DE3)** (Novagen)

Genotype: $\Delta(ara-leu)$ 7967 $\Delta lacX74$ $\Delta phoA$ P_{vull} $phoR$ $\Delta maIF3$ $F'[lac^+ lacI^q pro]$ $trx::kan$

3.5 Expression Vectors

pET expression vectors: pET-3d, pET-31b, pET-32a, pET-44a (Novagen)

3.6 Oligonucleotides

Mutation (hIL-5R α)

C66A: 5'-ACTGAAAGCAAAGCTGTAACCATCCTC-3'

D55E: 5'-GCTCCAAAAGAAGAAGACTATGAAACC-3'

Y57F: 5'-AAAGAAGATGACTTTGAAACCAGAATC-3'

F182A: 5'-TTTCCCAGGACTGCTATCCTCAGCAAAG-3'

I183A: 5'-CCAGGACTTTTGCCCTCAGCAAAGGGC-3'

R188K: 5'-CTCAGCAAAGGGAAAGACTGGCTTGCG-3'

L72M Forward 5'-ACCATCCTCCACATGGGCTTTTCAGCA-3'

L138M Forward 5'-CACTGCACCTGGATGGTTGGCACAGAT-3'

L167M Forward 5'-CAAGAATACAGCATGGACACACTGGGG-3'

L234M Forward 5'-GAAGGAACTCGTATGTCTATCCAATGG-3'

Mutation (hIL-5)

E13Q Forward: 5'-GCATTGGTGAAACAGACCTTGGCACTG-3'

Mutation (mIL-5)

M5T Forward: 5'-GGAGATTCCCACCAGCACAGTGGTG-3'

M29L Forward: 5'-GCAATGAGACGCTTAGGCTTCCTGTC-3'

M65R Forward: 5'-GGTACCGTGGAAGACTATTCCAAAAC-3'

M105L Forward: 5'-TTCCTTGGTGTGCTTAGTACAGAGTGG-3'

M111I Forward: 5'-ACAGAGTGGGCAATTGAAAGGCTAAGGA-3'

E13Q Forward: 5'-ACAGTGGTGAAACAGACCTTGACACAG-3'

Truncation (hIL-5R α)

10aaRaForward: 5'-TTACCATGGCAATTTCACTTCTCCACCTG-3'

20aaRaForward: 5'-TTACCATGGCAAAAGTTACTGGTTTGGCTCAAG-3'

Reverse BamH I: 5'-TTTTTTGGATCCTATCTTGAGAACCC-3'

Del2 Forward: 5'-TTTTTTTCCATGGCAGACTTACTTCTTG-3'

Del2Reverse: 5'-TTTTGGATCCTCAATTTATTTGATCAATGGCGTGA-3'

Del3 Forward: 5'-TTTTTTTCCATGGCAGACTTACTTCTTG-3'

Del3Reverse: 5'-TTTTGGATCCTCAGGCATGAAGTTCAGCAGAAG-3'

Cloning (mIL-5)

Forw NcoI: 5'-TTTTTTTTTCCCATGGAGATTCCCATGAGCAC-3'

Reve BamH I: 5'-TTTTTTGGATCCTTAGCCTTCCATTGCCCA-3'

Forw AlwN I: 5'-CAGATGCTGGAGATTCCCACCAGCACAGTG-3'

Reve Xho I: 5'-CTCGAGTTAGCCTTCAATTGCCCACTC-3'

Sequencing

T7 Promoter: 5'-TAATACGACTCACTATAGGG-3'

T7 Terminator: 5'-GCTAGTTATTGCTCAGCGG-3'

3.7 Site Directed Mutagenesis**3.7.1 Single mutation by Cyclic PCR**

Master mix	2.5 μ l 10X pfu buffer (200 mM Tris-HCl, pH 8.8, 100 mM (NH ₄) ₂ SO ₄ , 100 mM KCl, 1 % (v/v) Triton X-100, 1 mg ml ⁻¹ BSA)
	5.0 μ l plasmid DNA [5 ng/ μ l]
	2.0 μ l dNTP (2.5 mM)
	1.0 μ l Forward primer (10 pmol/ μ l)
	1.0 μ l Reverse primer (10 pmol/ μ l)
	1.0 μ l pfu Polymerase (prepared by Dr. Joachim Nickel)
	12.5 μ l water

Mutations were introduced into the DNA template with two complementary mutagenesis oligonucleotide primers (3.6). The PCR was performed in a reaction volume of 25 μ l (Maxter mix). For PCR mutagenesis a total of 25 cycles were run with 2 min denaturation at 94°C, 2 min annealing at 60°C; and 6 min extension at 72°C; with a last extension time of 10 min at 72°C. The parental Dam-methylated plasmid was digested with 10 U Dpn I restriction enzyme at 37°C for 1 hour, and the *E. coli* cells were transformed with the newly synthesized, nonmethylated and thus Dpn I resistant plasmid.

3.7.2 Two Step PCR

First PCR	Reaction I
Master mix	2.5 μ l 10X pfu buffer
	1.0 μ l plasmid DNA [2 ng/ μ l]
	2.0 μ l dNTP (2.5 mM)
	1.0 μ l T7 Promoter primer (10 pmol/ μ l)
	1.0 μ l Reverse primer of the specific mutation (10 pmol/ μ l)
	1.0 μ l pfu Polymerase (prepared by Dr. Joachim Nickel)
	16.5 μ l water
	Reaction II
Master mixes	2.5 μ l 10X pfu buffer
	1.0 μ l plasmid DNA [2 ng/ μ l]
	2.0 μ l dNTP (2.5 mM)
	1.0 μ l Forward primer of the specific mutation (10 pmol/ μ l)
	1.0 μ l T7 Terminator primer (10 pmol/ μ l)
	1.0 μ l pfu Polymerase (prepared by Dr. Joachim Nickel)
	16.5 μ l water
Technical device	Thermocycler (Master cycler personal, Eppendorf)
Second PCR	
Master mixes	2.5 μ l 10X pfu buffer
	2.0 μ l DNA from <u>Reaction I</u>
	2.0 μ l DNA from <u>Reaction II</u>

2.0 μ l dNTP (2.5 mM)
1.0 μ l T7 Promoter primer (10 pmol/ μ l)
1.0 μ l T7 terminator primer (10 pmol/ μ l)
1.0 μ l pfu Polymerase (prepared by Dr. Joachim Nickel)
13.5 μ l water

Mutations were introduced into template DNA with two complementary mutagenesis and two sequencing oligonucleotide primers (3.6). The two PCR reactions were carried out in a reaction volume of 25 μ l. The PCR reactions (I and II) were performed for 25 cycles of 45 sec at 94°C (denaturation), 45 sec at 60°C (annealing), and 45 sec extension at 72°C, followed by the final extension step of 10 min at 72°C. The PCR reaction I employs a 5' sense primer annealing to the T7 promoter region and a 3' antisense primer harboring the mutation. The reaction II employs a 5' sense primer encoding the mutation and a 3' antisense primer, which is complementary to the T7 terminator region in the expression vector. After the first PCR, the two PCR products matched in 24 nucleotides and the mismatched (mutation) is found in the middle of the matched region.

Afterwards, a second PCR reaction was done with 2 μ l of Reaction I and 2 μ l of Reaction II following the same cycling parameters (First PCR). The PCR products were analyzed by agarose gel stained with EtBr to verify the molecular size.

3.7.3 Truncation by PCR

Master mixes 2.5 μ l 10X pfu buffer
 1.0 μ l plasmid DNA [2 ng/ μ l]
 2.0 μ l dNTP (2.5 mM)
 1.0 μ l Forward primer (10 pmol/ μ l)
 1.0 μ l Reverse primer (10 pmol/ μ l)
 1.0 μ l pfu Polymerase (prepared by Dr. Joachim Nickel)
 16.5 μ l water

Mutations were introduced by simultaneous annealing of two oligonucleotide primers to one strand of the denatured double strand plasmid DNA (3.6). One primer introduces the desired mutation. The PCR was performed for 25 cycles which were

run for 45 sec denaturation at 94°C, 45 sec annealing at 60°C; and 45 sec extension at 72°C; with a last extension time of 10 min at 72°C.

All mutations were verified by DNA sequencing (DTCS Quick start kit, Beckman Coulter # 608120)

3.8 Cloning

3.8.1 DNA digestion

Digestion reaction 1.0 µl restriction enzymes (s) (10 or 20 U)
2.5 µl 10 X specific buffer (see catalog)
2.0 µl plasmid DNA or PCR products (0.5-1.0 µg/µl)
19.5 µl dH₂O

Technical Device Thermo Block (TDB-120, Biosan)

The digestion reaction was incubated for 3 hours at 37°C. Restriction enzyme activity was stopped by incubating 20 minutes at 65°C. The digestion products were visualized on 1.2% agarose gels stained with EtBr. The different digestion products were purified by QIAquick Gel purification kit (QUIAGEN) before ligation reaction.

3.8.2 DNA ligation

Set up 1.0 µl T4 DNA ligase (40 U)
1.0 µl 10 X T4 DNA ligase buffer
50-100 ng digested PCR product (2.0 µl)
25-50 ng digested Vector (1.0 µl)
5.0 µl dH₂O

Technical device Thermocycler (Master cycler personal, Eppendorf)

Digested plasmid and PCR products were purified by QIAquick Gel purification kit (3.8.1). The ligation reaction was set up with a ratio of 1:2 (vector:insert) and it was incubated at RT for 2 hours, or at 16°C ON. The ligated DNA was transformed in competent *E. coli* cells (Nova Blue) to amplify the DNA.

3.9 Preparation of Competent Cells (RbCl₂ Method)

Buffer I, pH 5.8	30 mM Potassium acetate 100 mM RbCl ₂ 10 mM CaCl ₂ 50 mM MnCl ₂ 15 % Glycerin (v/v) Adjust pH with Acetic acid
Buffer II, pH 6.5	10 mM MOPS 10 mM RbCl ₂ 75 mM CaCl ₂ 15 % Glycerin (v/v) Adjust pH with NaOH

One colony from transformed *E.coli* cells was picked and transferred into 2 ml LB with a specific antibiotic. The culture was incubated at 37°C with shaking at 130 rpm overnight. This 2 ml culture was used to inoculate a flask containing 100 ml LB medium with respective antibiotics and the culture was incubated at the same conditions. The cells were incubated until the OD₆₀₀ 0.4-0.6 was reached. The cells were transferred to 50 ml centrifuge tubes and pelleted by centrifuge at 3000 rpm at 4°C for 5 min. After that, the cells were dissolved into 40 ml of cold buffer I and incubated in ice for 15 min. New centrifugation was performed at 3000 rpm at 4°C for 5 min. The last pellet was re-dissolved in 10 ml cold buffer II and the cells suspension was stored in ice for 15 min. After that, the cell suspension was split in 100 µl aliquot and immediately frozen in liquid nitrogen. The aliquots were stored at -74°C.

3.10 Transformation of *E. coli*

LB-agar plates Add 10 g agar powder (Applichem) to 250 ml dH₂O
Add 500 µl 2 M NaOH
Sterilized by autoclaving
Add antibiotic (s) at 45°C

LB-broth Add the following to 800 ml of dH₂O
10 g Bacto-tryptone, 10 g NaCl and 5 g Bacto-yeast
Adjust to pH 7.4 with NaOH

Adjust volume to 1 liter with dH₂O
Sterilize by autoclaving

One aliquot of competent *E. coli* cells was thawed on ice and 10-20 ng of plasmid DNA or 2.0-4.0 µl of a ligation reaction was added and mixed with the cells by stirring gently with a pipette tip. The vial was incubated on ice for 30 min. Afterwards, incubate the cells for 60 sec at 42°C (heat shock) block heater. Remove the cells from the block and place them on ice for 2 min. The volume of solution was increased by adding 250 ml of LB medium without antibiotics and the cells were incubated at 37°C for 1 hour with shaking. Transformed cells were spread on agar plate containing the specific antibiotic. Cells without plasmid DNA was seeded on a new agar plate as negative control. The plates were incubated at 37°C for 24 hours.

3.11 *E. coli* Protein Expression

3.11.1 Native proteins

TB-broth Add the following to 800 ml of dH₂O
13.4 g Bacto-tryptone, 26.6 g Bacto-yeast and 4.4 ml glycerin
Adjust volume to 1 liter with dH₂O
Sterilize by autoclaving

Pi Buffer (10X) Add the following to 800 ml of dH₂O
23.1 g KH₂PO₄ (0.17 M) and 25.4 g K₂HPO₄ (0.72 M)
Adjust volume to 1 liter with dH₂O
Sterilize by autoclaving

Working medium: Use 9 volumes of TB with 1 volume Pi

LB-broth Add the following to 800 ml of dH₂O
10 g Bacto-tryptone, 10 g NaCl and 5 g Bacto-yeast
Adjust to pH 7.4 with NaOH
Adjust volume to 1 liter with dH₂O
Sterilize by autoclaving

Technical devices: Incubator shaker (Multitronic INFORS), centrifuge HERAUS Suprafuge 22 (12.500 rotor), Ultraspect 3000 (Pharmacia Biotech).

One colony from transformed *E.coli* cells was picked from an agar plate (3.10) and transferred into 500 ml *E.coli* culture medium with the respective antibiotic (s) and incubated at 37°C with shaking at 130 rpm ON. Next day, a 40 ml aliquot were used to inoculate twelve 2-L Erlenmeyer flasks containing 800 ml (1:20) fresh medium. The flasks were incubated at 37°C with shaking until an optical density of 0.6 O.D_{600nm} was reached. At this point, IPTG was added to a final concentration of 1 mM to induce protein expression. Then, the culture was incubated for additional 3 hours. Cells were harvested by centrifugation at 6500 rpm (Heraeus, 12.500 rotor) for 20 min at 4°C. The cell pellet was resuspended in 10-15 volumes of lysis buffer (TBSE, STE or TE).

3.11.2 Selenomethionyl-proteins

M9-media (10X)

Add the following to 800 ml of dH₂O
60g Na₂HPO₄, 30g KH₂PO₄, 5g NaCl, 10g NH₄Cl,
Adjust pH to 7.2-7.4 with NaOH
Sterilize by autoclaving

Trace Metals (100X)

Add the following to 800 ml of dH₂O
5 g EDTA, 0.8 g FeCl₃, 0.05 g ZnCl₂, 0.01 g CuSO₄,
0.01 g CoCl₂, 0.01 g H₃BO₃, 1.6 g MnCl₂, 0.01 g
Na₂WO₄
Sterilize by Filtration
Adjust to 1 L with water

Complete M9 medium

Add the following to 800 ml of dH₂O
100 ml of M9 (10X)
Add 1 ml MgSO₄ (1.0 M)
100 µl CaCl₂ (1.0 M)
10 ml Trace metals
40 ml 20 % (w/v) glucose
100 mg Thiamine

Adjust to 1 L with water

Amino acids: Add 100 mg L-Lysine, 100 mg L-Phenylalanine, 100 mg L-Threonine, 50 mg L-Leucine, 50 mg L-Isoleucine, 50 mg L-Valine and 50 mg L-SelenoMet.

Cells from a fresh transformation were transferred from an 16-24 hours old plate into 2.0 ml LB with specific antibiotic (s) and incubated at 37°C with shaking at 130 rpm over day. Then, the 2.0 ml cultured cells were centrifuged at 4°C for 5 min at 4000 rpm and the pellet was resuspended to inoculate 400 ml of complete M9-media without L-amino acids, and incubated at 37°C with shaking ON. Next day, a 40 ml aliquot of the culture was added into an Erlenmeyer flask containing 800 ml M9 medium freshly without L-amino acids. The culture cells was incubated at 37°C with shaking until an optical density of 0.6 O.D was reached. At this point, L-amino acids were added and after 30 min further incubation, IPTG was added to a final concentration of 1 mM to induce protein expression. The culture was incubated for additional 18 hours at 37°C with shaking. Cells were processed as it was described above.

3.12 Receptor

3.12.1 Inclusion bodies isolation

Buffers

6M or 8M GuHCl 50 mM NaAc, pH 5.0
6M or 8M GuHCl

TBSE 10 mM Tris-HCl, pH 8.0
150 mM NaCl
1mM EDTA
0.001 % (v/v) β -ME

TE 10 mM Tris-HCl, pH 8.0
1 mM EDTA

Size exclusion chromatography with GuHCl (SEC-GuHCl)

SEC-GuHCl Buffer	50 mM NaAc pH 5.0 6M GuHCl 1 mM EDTA
Column	Superdex 200 (preparative grade 16/60, Pharmacia)
Column volume	120 ml

Technical devices

Sonifier (KLM system 585), centrifuge Sorvall RC5C (GSA rotor), centrifuge HERAUS Suprafuge 22 (22.50 rotor), Ultrospect 3000 (Pharmacia Biotech), Chromatography system (Äkta prime plus, Pharmacia) and magnetic stirrer.

The cells in TBSE (native 3.11.1 or Se-protein 3.11.2) were supplemented with 20 μ l of a protease inhibitor cocktail (Calbiochem). To isolate the inclusion bodies (IB), the cell suspension was disrupted by sonication. Sonication was carried out for 5 min at 300 watts on ice and the suspension was centrifuged at 11500 rpm (Sorvall, GSA rotor) for 30 min at 4°C. The pellet was resuspended with 200 ml of TBSE buffer and the cell lysis was repeated as it was described above. The pellet (IB) was washed twice with 200 ml TBSE buffer; each wash was followed by centrifugation at 11500 rpm for 20 min. The pellet was resuspended in 30 volumes TBSE (w/v) and 10 volumes 8 M GuHCl (w/v), and shaken for 30 min at RT. Then, IB were precipitated by centrifugation at 11500 rpm for 30 min at 4°C. The protein was then extracted by resuspension of the pellet into 4 volumes TE (w/v), 5 volumes 8 M GuHCl (w/v) and 100 μ l β -ME (v/v). The solution was incubated at room temperature with mild shaking ON. Next day, the suspension was centrifuged for 90 min to 16000 rpm at 4°C (HERAUS, 22.50 rotor) to clarify the supernatant. Afterwards, the supernatant was filtered with paper filters by flow gravity. The protein concentration was determined by optical density (OD) spectrum at 280 nm using the Ultrospect 3000 (Pharmacia Biotech). Protein concentration was adjusted to 40 mg ml⁻¹ using an Amicon system. To eliminate bacterial DNA in the protein preparation, 200 mg of protein were loaded into the equilibrated column. The column was pre-equilibrated with 2 volumes of buffer 6M GuHCl at a flow rate of 1.5 ml min⁻¹ before the protein

was loaded. 7 ml protein fractions were collected. Protein concentration was adjusted to 20 mg ml⁻¹.

3.12.2 Renaturation

Protein renaturation was carried out as follows: approximately 100 mg of denatured protein (3.12.1) were diluted into one liter of refolding buffer (50 mM Tris-HCl pH 9.5, 7.5 M Urea, and 0.1 mM reduced cysteine). The solution was then incubated for 2 hours at RT with mild shaking. Afterwards, the solution was dialyzed in 10-fold volume of dialysis buffer (50 mM Tris-HCl pH 9.5, 3 M Urea, and 100 µg/L CuSO₄) for one day at 4°C. After that, the urea concentration was reduced by 50 % in dialysis buffer by replacing 50% with fresh 50 mM Tris-HCl pH 9.5 buffer, until 0.75 M urea concentration was reached. After, the protein was changed to 50 mM Tris-HCl pH 9.5 buffer, for 24 hours and finally, the protein was dialyzed in 50 mM Tris-HCl pH 8.1 buffer, for 24 hours. The protein was concentrated to a final volume of 100 ml with a protein concentration of approximately 1 mg ml⁻¹.

3.12.3 Purification

3.12.3.1 Anion Exchange chromatography I

Pre-equilibration buffer	50 mM Tris-HCl, pH 8.1
Wash buffer	50 mM Tris-HCl, pH 8.1 150 mM NaCl
Elution buffer	50 mM Tris-HCl, pH 8.1 0.5 M NaCl
Column	HighLoad 16/10 Q-sepharose
Column volume	20 ml
Chromatography system	Akta prime plus (Pharmacia)

100 ml of refolded protein (3.12.2) were applied to Q-sepharose column equilibrated with 10 volumes of pre-equilibration buffer at a flow rate of 1.5 ml min⁻¹ and then washed with 10 volumes. A linear gradient leading to a final concentration of 0.5 M

NaCl was used to elute bound material. 5 ml protein fractions were collected and analyzed by SDS-PAGE.

3.12.3.2 Anion Exchange chromatography II

Buffer A1	40 mM TAPS
Buffer A2	40 mM Sodium TAPS
Buffer B1	Water
Buffer B2	2 M Sodium Chloride
Column	UNO Q1 column (Bio-Rad)
Chromatography system	Biologic Duo Flow (Bio-Rad)
Software	Biologic Duo Flow software (Bio-Rad) Scouting program (Bio-Rad)

Refolded protein from Anion exchange chromatography I was purified by an UNO Q1 column. The column was pre-equilibrated with 10 volumes of 40 mM TAPS buffer at a flow rate of 1.5 ml min⁻¹. After that, the protein was loaded on the column at a flow rate of 1.5 ml min⁻¹. Then, the column was washed with 5 volumes of buffer A at a flow rate of 2.0 ml min⁻¹. The bound protein was eluted with a gradient between 0 % - 100 % buffer B2, at constant pH (7.8), and at a flow rate of 3.0 ml min⁻¹. The gradient profile utilized for solvent B2 was 0% for 6.5 min and 0 to 100% for 12 min. 1 ml protein fractions were collected and analyzed by SDS-PAGE.

3.12.3.3 Size exclusion chromatography

Buffer	50 mM Tris-HCl, pH 8.1
Column	HiLoad 16/60 Superdex 200 (Pharmacia)
Column volume	120 ml
Chromatography system	Akta prime plus (Pharmacia)

The column was previously pre-equilibrated with 2 volumes of buffer at a flow rate of 1.5 ml min⁻¹ before loading protein (3.12.3.1). 5 ml protein fractions were collected and analyzed by SDS-PAGE.

3.12.3.4 Affinity chromatography

Matrix	CNBr-activated sepharose 4 fast flow
Conjugate protein	hIL-5 (6.0 mg ml ⁻¹)
Dialysis buffer	0.1M NaHCO ₃ pH 8.3 0.5mM NaCl
Acid solution	1mM HCL
Coupling buffer	0.1M NaHCO ₃ pH 8,3 0.5M NaCl
Store buffer	0,1M Tris-HCl pH 8.0
Centrifuge	Eppendorf 5702

The protein was previously dialyzed overnight at 4°C into dialysis buffer. Add 3 g of matrix into 40 ml of 1mM HCl; mix gently but thoroughly by inverting 5 min. After that, the suspension was centrifuged at 4000 rpm at 4°C for 5 min. Then, the matrix was washed with 200 ml coupling buffer. The protein was immediately immobilized onto activated matrix by adding aliquots of 5 mg one by one until 30 mg. The solution was incubated for 60 min at 4°C with rotation. To remove the unbound protein the centrifugation was carried out at 1000 rpm for 5 min at 4°C. The matrix was resuspended in 25 ml of 0,1M Tris-HCl, pH 8.0 and packed into a Biorad yellow column.

Chromatography

Pre-equilibration buffer	50 mM Tris-HCl, pH 8.1
Elution buffer	4M MgCl ₂
Column	Immobilized hIL-5 in CNBr-activated sepharose 4B (Amersham pharmacia biotech)
Pump	Peristaltic-pump LKB
Detector	2238 UVICORD SII (LKB)

The affinity column was pre-equilibrated for 60 min at 4°C with pre-equilibration buffer. The refolded protein (3.12.2) was loaded at a flow rate of 1.0 ml min⁻¹. Then, the column was washed for 60 min with pre-equilibration buffer to eliminate the unbound protein. The bound protein was eluted with 4 M MgCl₂ at a flow rate of 1.0 ml min⁻¹. 5 ml protein fractions were collected and they were immediately dialyzed in cold (4°C) pre-equilibration buffer.

3.13 Ligand

3.13.1 Inclusion bodies isolation (Human)

Buffers

6 M and 8 M GuHCl 50 mM NaAc, pH 5.0
6 M or 8 M GuHCl

STE (lysis buffer) 50 mM Tris-HCl, pH 8.0
0.375 M Sucrose
1mM EDTA

NaAc 50 mM Sodium acetate, pH 5.0

EDTA 250 mM, pH 8.0

Size exclusion chromatography with GuHCl (SEC-GuHCl)

SEC-GuHCl Buffer 50 mM NaAc pH 5.0
6M GuHCl
1mM EDTA
1mM DTT

Cells were lysed by sonication (300 watts for 5 min at 4°C) and the centrifugation was carried out at the same condition mentioned before (3.12.1). Pellet was dissolved in 8 volumes NaAc (w/v), 1 volume 6 M GuHCl (w/v), and 1 mM EDTA; shaking the solution for 30 min at RT. The inclusion bodies (IB) were precipitated by centrifugation at 11500 rpm for 30 min at 4°C. The last pellet was weighted and resuspended in 1.5 volumes NaAc (w/v), 7.5 volumes 8 M GuHCl (w/v) and 100 µl β-ME (v/v). The solution was incubated overnight at room temperature with mild shaking. Next day, the suspension was centrifuged for 90 min at 16000 rpm at 4°C (HERAUS, 22.50 rotor) to remove cellular debris. Afterwards, the supernatant was filtered with paper filters by flow gravity. The protein concentration was determined by optical density (OD) spectrum at 280 nm using the Ultrospect 3000 (Pharmacia Biotech). Protein was purified by size exclusion chromatography as it was described before (3.13.1).

3.13.2 Inclusion bodies isolation (Mouse)

Buffers

6 M or 8 M GuHCl 50 mM NaAc, pH 5.0
 6 M GuHCl

TE 20 mM Tris-HCl, pH 7.8
 0.5 mM EDTA

Washing buffer 20 mM Tris, pH 7.8
 0.5 mM EDTA
 2 % (v/v) Triton X-100

Dissolving buffer 50 mM Tris, pH 7.8
 2 % (v/v) β -ME
 2 % (w/v) SDS

Acetone Pure Acetone

Acid Formic Acid

The cell pellet was resuspended in TE buffer (3.11.1). Sonication and centrifugation were carried out at the same conditions as mentioned before. Then, the pellet (IB) was washed one time in washing buffer; followed by centrifugation at 11500 rpm for 20 min (Sorvall). The pellet was resuspended in 100 ml of dissolved buffer and incubated at 37°C with shaking for 60 min. To clarify the supernatant, the suspension was centrifuged at 16500 rpm, for 30 min at 4°C (Heraeus, rotor 22.50) and the pellet was discarded. Two volumes of cold acetone were added to supernatant and incubated on ice for 20 min. After that, the solution was centrifuged at 11500 rpm for 60 min at 4°C (Sorvall, GSA rotor). The pellet was dissolved in 40 ml 80% formic acid and centrifuged at 16000 rpm for 60 min at 4°C. The supernatant was used to CNBr digestion. Fusion protein was digested by 100 μ l of β -ME and 125 mM final concentration of cyanogen bromide (CNBr). The reaction was incubated overnight at room temperature with shaking. Next day, the formic acid concentration was reduced to 40 % with one volume of water, and the protein was

dialyzed (2-3 liters) in 6 M GuHCl pH 6.5 for two days by changing the buffer each 24 hours. To avoid a possible reaction of sulfhydryl group with other thiols or irreversible oxidation of sulfhydryl groups the protein was subjected to sulphonation treatment. The protein was incubated for 5 hours at 37°C with 2 g of Na₂SO₃ and 0.5 g of Na₂S₄O₆ (Hoppe et al., 1989; Hoppe et al., 1990). To eliminate insoluble material, the solution was centrifuged to 16000 rpm for 60 min at 4°C and the supernatant filtered. Protein was purified by size exclusion chromatography as it was described above (3.13.1).

3.13.3 Ligand renaturation

Refolding buffer	100 mM Tris-HCl pH 8.5 2.0 M Urea 1 mM Oxidized glutathione (GSSH) 0.1 mM Reduced glutathione (GSH)
Dialysis buffer I	100 mM Tris-HCl pH 8.5 2.0 M Urea 0.1 mM Oxidized glutathione (GSSH) 0.01 mM Reduced glutathione (GSH)
Dialysis buffer II	100 mM Tris-HCl pH 8.5 0.1 mM Oxidized glutathione (GSSH) 0.01 mM Reduced glutathione (GSH)

50 mg of the denatured protein (3.13.1 and 3.13.2) were dissolved in refolding buffer at 4°C overnight with mild shaking. Afterwards, the protein solution was dialyzed at 4°C for two days in different buffers. The first day the dialysis was performed in buffer I, and the second day the buffer II was used. After the dialysis, the IL-5 was concentrated at a final volume of 5 ml.

3.13.4 Ligand purification

3.13.4.1 Size exclusion chromatography I

Buffer	100 mM Tris-HCl, pH 8.5
---------------	-------------------------

Column	HiLoad 16/60 Superdex 200 (Pharmacia)
Column volume	120 ml
Chromatography system	Akta prime plus (Pharmacia)
Pressure	0.35 bar

The column was previously pre-equilibrated with 2 volumes of buffer at a flow rate of 1.5 ml min⁻¹ before loading protein. 5 ml protein fractions were collected and analyzed by SDS-PAGE.

3.13.4.2 Size exclusion chromatography II

Buffer	100 mM Tris-HCl, pH 8.5
Column	Analytical Superdex 75 (Pharmacia)
Column volume	30 ml
Chromatography system	DuoFlow (Biorad)
Pressure	300 psi

The column was previously pre-equilibrated with 2 volumes of buffer at a flow rate of 0.5 ml min⁻¹ before loading protein. Protein was purified with a flow rate of 0.25 ml/min. 1 ml protein fractions were collected and analyzed by SDS-PAGE.

3.14 Protein Analysis Methods

3.14.1 RP-HPLC

Buffer A	0.1% TFA
Buffer B	Acetonitril with 0.1% TFA
Column	VYDAC 214TP1010 C4
Chromatography system	Biologic Duo Flow (Bio-Rad)
Software	Biologic Duo Flow software (Bio-Rad)

Protein purity was analyzed by reversed-phase high-performance liquid chromatography (RP-HPLC). The column was pre-equilibrated during 30 min with buffer A. After that, the protein was loaded at a flow rate of 1.5 ml min⁻¹; the separation was conducted via gradient elution of two solvents: TFA 0.1% buffer A and ACN/0.1% TFA buffer B at a flow rate of 1.5 ml min⁻¹. The gradient profile

utilized for solvent B was as it follows: 0% for 9 min, 0 to 100% 37 min, 100% for 2 min, 100 to 0% in 2 min, and 0% for 4 min, with a total run time of 54 min at RT. The fractions were collected into 2 ml tubes and each fraction was analyzed with SDS-PAGE.

3.14.2 SDS-polyacrylamide gel electrophoresis (SDS-PAGE)

Stacking gel buffer (4X)	504 mM Tris 10 % SDS (w/v) pH 6.7
Running gel buffer (4X)	1.5 M Tris 10 % SDS (w/v) pH 8.8
Sample Buffer	125 mM Tris pH 6.8 20 % glycerol (v/v) 4 % SDS (w/v) 10 μ M bromophenol blue
Electrophoresis buffer (10X)	50 mM Tris-HCL 196 mM glycine 0.1 % SDS
Polyacrylamide solution	40 %, 29:1 solution (Roth #A515.1)
Stacking Gel preparation	0.625 ml stacking buffer 4X 0.25 ml polyacrylamide 1.6 ml ddH ₂ O 9 μ l 40% Ammonium persulfate (APS) 9 μ l TEMED
Running gel preparation	1.25 ml running buffer 4X 1.5 ml polyacrylamide 1 ml glycerin 87% 1.25 ml ddH ₂ O 10 μ l 40% Ammonium persulfate (APS)

	10 μ l TEMED
Protein marker	Low molecular weight (Pharmacia)

Equal amounts of all purified proteins were suspended in 100 μ l of 1X sample buffer and the solution was boiled for 5 min. Afterwards, samples (5-15 μ l) were loaded onto a 12 % SDS-PAGE gel and separated at 320 V for 30 min. The proteins were revealed by coomassie blue or silver stained procedures.

Coomassie blue staining buffer	2.5 g coomassie blue
	40 % Methanol (v/v)
	10 % acetic acid (v/v)
	50 % dH ₂ O to 1L

Destaining buffer	10 % methanol (v/v)
	10 % acetic acid (v/v)
	80 % water

After the SDS-PAGE, the electrophoresis system was disassembled and the gel was recovered. The gel was put in a glass box and incubated with staining solution for 30 min at room temperature with agitation. Then, the staining solution was removed and the gel was washed with water. Afterwards, the gel was put for 60 min with destaining buffer. Alternatively, the glass box was sealed with alum paper and left overnight with shaking at RT.

Silver stain

Stock solution 1	50 % (v/v) Acetone in water
Stock solution 2	50 % (w/v) TCA in water (stored in glass container)
Stock solution 3	20 % (w/v) Silver Nitrate in water
Stock solution 4	10 % (w/v) Sodium thiosulfate pentahydrate
Stock solution 5	1 % (v/v) Glacial Acetic Acid
Stock solution 6	37 % Formaldehyde solution

The gel was put in a clean glass box and incubated with 60 ml acetone stock with 1.5 ml TCA stock and 25 μ l formaldehyde solution for 5 min with shaking. After three

washes with water, the gel was left with water for additional 5 min. After that, the gel was rinsed in water 15 sec. Then, the gel was immersed in acetone stock solution for 5 min. Afterwards 100 μ l sodium thiosulfate stock solution in 60 ml water was added for 1 min. The gel was washed with water and immersed in 0.8 ml silver nitrate stock solution and 0.6 ml formaldehyde solution in 60 ml water for 8 min. Proteins bands were developed with 1.2 g Na_2CO_3 , 25 μ l formaldehyde solution and 25 μ l sodium thiosulfate stock solution dissolved in 60 ml water for 30 sec. The reaction was stopped with 1% acetic acid.

Drying gel solution 30% methanol (v/v)
 5% glycerol (v/v)
 ddH₂O to 1L

Envelop Cellophane membrane

Frames Two

Developed gel by coomassie blue or silver stained was incubated with drying solution for 15 min at room temperature with shaking. Two cellophane sheets were soaked in water. One soaked cellophane membrane was spread out to cover one frame. The gel was placed on the cellophane membrane in the center. The second wet cellophane sheet was then carefully placed so that it covers the first cellophane sheet and the gel. The second frame is placed upon the first. Four clamps were used to press together the frames. The gel was maintained at room temperature at least one day.

3.14.3 Mass spectrometric analysis

All purified proteins were dialyzed in Milli Q water to remove salt content. The molecular weights of the proteins or peptides were determined using a mass spectrometer device (APEX-II FT ICR). The desalted oligopeptides were dissolved in a 1:1 solution of methanol and 2% acetic acid, at a final concentration of 5 μ M. The protein was then applied to the ion source with a flow rate of 2.0 μ l/min. The data were analyzed with the X-mass software (Bruker Daltonics, Bremen), which was supplied with the instrument.

3.14.4 Circular dichroism (CD)

The secondary structure of the protein was analyzed by circular dichroism method. For CD analysis, each protein was dialyzed against Milli Q water. A JASCO J-720 spectropolarimeter was used for all measurement and the spectra were recorded from 190 to 240 nm. Proteins (0.2-0.5 mg ml⁻¹) were measured in a 0.1 cm path length cells. Qualitative data analysis was carried out with JASCO Spectra Manager Analysis software.

3.14.5 Biomolecular interaction analysis (BIAcore)

Reagent required Sulfo-NHS-LC Biotin (Pierce) 4 mM stock solution in DMSO
0.5 M NaHCO₃, pH 8.5
CM5 chip

BIAcore analysis was performed to measure the binding of the interaction between hIL-5R α or hIL-5R α variants with hIL-5. The CM5 sensor chip surface was coated with streptavidin according to the protocol of the amide coupling method. Briefly, streptavidin was diluted in 10 mM sodium acetate buffer (pH 4,5) and perfused over a biosensor chip surface that had been pre-activated with N-hydroxysuccinimide and N-ethyl-N'(dimethylaminopropyl) carbodiimide, as described by the manufacturer. Typically, 2800-3000 resonance units (1RU = 1pg/mm²) were immobilized. The hIL-5 was biotinylated with EZ-Link sulfo-NHS-LC biotin (PIERSE) in a 1:1 molar reaction following the BIAcore handbook protocol. The biotinylated hIL-5 was immobilized onto the CM5 chip via interaction between biotin and streptavidin. The streptavidin coated flow cell 1 was used as a control for nonspecific binding and bulk face effects. However, hIL-5 was immobilized in flow cell 2-3-4 on the sensor chip with an average of 500 resonance units (RU). To further reduce bulk face effects, proteins were extensively dialyzed against running buffer (10 mM HEPES, pH 7,4, 150 mM NaCl, 3,4 mM EDTA and 0,005% (v/v) surfactant P20). All experiments were carried out at RT. The association rate was determined using six different protein concentrations from 20 nM to 180 nM at a flow rate of 10 μ l/min. For the dissociation rate analysis, the chip surface was perfused only with running buffer. Between each analyte binding experiment, injecting 4 M MgCl₂ regenerated the chip surface. The sensorgrams were evaluated using the software BIAevaluation version

2.0 assuming a 1:1 Langmuir association model. The association rate constant (k_{on}) and the dissociation rate constant (K_{off}) were obtained after analysis. In order to reduce mass transfer and rebinding effects only the last 10% of the association phase before reaching steady state were used to analyze the k_{on} , and the first 10% of the dissociation phase were used to analyze the k_{off} . Apparent dissociation constants, K_D , were calculated as $K_D = k_{off}/k_{on}$.

3.14.6 TF-1 cells proliferation assay

Media RPMI 1640 (Gibco BRL)

Supplement 10 % (v/v) Fetal calf serum
2 mM L-glutamine
100 U/ml penicillin
100 μ g/ml streptomycin

The biological activity of purified recombinant proteins were evaluated by measuring [3 H] thymidine incorporation into the human promyeloid cell line TF-1 (Kitamura et al., 1989). TF-1 culture cells were counted using a Neubauer counting chamber and a vital-dye (Trypan Blue) that was incorporated by death cells. Cells were cultured in RPMI medium supplemented with 10% FCS and 2ng ml⁻¹ recombinant GM-CSF. After that, the cells were washed twice with RPMI without GM-CSF. Cells were seeded at a density of 20000 cells/well in a 96 well plate in RPMI medium without GM-CSF to growth cells starve factor. Cells were grown in the presence of serial dilutions of purified recombinant proteins (log₃ dilutions starting at 1 μ g as the highest concentration) for 72 hours. Tritiated thymidine (Amersham, 0.25 μ Ci/well) was added to each well 24 h before the plates were harvested using a Skatron cell harvester (Skatron Inc., USA). Filters were counted in a β plate counter. Each experiment was performed in triplicate, and the concentration of half maximal response (EC₅₀) in TF-1 cells was plotted using the statistic program "Origin".

3.15 Limited proteolysis of protein

The protein (3.16) was dialyzed in 100 mM Tris, pH 8.5 for 24 hours at 4°C. Trypsin protease was prepared following the manufacturers recommendation. The digestion

reaction was carried out with 50 µg of protein and 0.25 µg of trypsin in a ratio of 200:1 (protein : trypsin) at 37°C. Eight reactions were set up in a 1.5 ml eppendorf tube and each 5 min one reaction was stopped. Control digestion was carried out without trypsin. Each reaction was stopped with 10 µl 10 % (v/v) trifluoroacetic acid (TFA). Afterwards, samples taken from each reaction were mixed and boiled with sample buffer, and loaded on a 12% SDS-PAGE. After electrophoresis, the gel was stained with coomassie blue buffer.

3.16 Crystallization

3.16.1 Complex crystallization

Buffer	10 mM Tris-HCl, pH 8.1 150 mM NaCl
Column	HiLoad 16/60 Superdex 200 (Pharmacia)
Column volume	120 ml
Chromatography system	Akta prime plus (Pharmacia)
Pressure	0.35 bar
Sparse matrix screens:	Crystal screen I (Hampton Research) Crystal screen II (Hampton Research) PEG/Ion screen (Hampton Research) Index Screen (Hampton Research) Malonat Screen (Hampton Research) JBS screen 4 (Jena Bioscience) JBS screen 5 (Jena Bioscience)
Plates for sitting drop	Crystal Quick (96 wells)
Cover	Plastic film
Plates for hanging drop	Linbro plates (24 wells)
For hanging drop	Siliconized glass circle cover slides (Ø 22) Silicon fat

Purified proteins (3.12.4 and 3.13.3) were used for complex formation. The complex was formed using the molar ratio of 1:1.1 of the receptor to ligand. To remove unbound components the complex was purified by gelfiltration chromatography with

a S200 column equilibrated with 10 mM Tris-HCl pH 8.1 and 150 mM NaCl buffer, with a flow rate of 1.5 ml/min as it was described above. Protein fractions were analyzed by SDS-PAGE. The protein fractions, which were present bands with similar amount of receptor and hIL-5 were pooled. Amicon system with 5000 MWCO membrane was used to concentrate the complex up to 10 mg/ml. Initial crystallization experiments were carried out by the sitting drop or hanging drop vapor diffusion method (Cudney et al., 1994) at room temperature. Each sitting-drop was prepared by mixing 1 μ l each of the complex (10 mg ml⁻¹) and 1 μ l reservoir solution. It was placed with 100 μ l of the of the reservoir solution in each well of the 96 well plate. After that, the plate was capped with plastic film.

The initial conditions yielding crystals were submitted to a fine-tuning screen procedure using the hanging drop method. Briefly, the optimization of the these conditions were carried out as follows: (i) complex was concentrated at presence of 0.3% (w/v) CHAPS (3-[(3-Cholamidopropyl) dimethylammonio]-1-propanesulfonate), to avoid protein aggregation and increase protein stability (Chen et al., 2000; Gall et al., 2003; Garman et al., 2000; Itou et al., 2002); (ii) crystallization was performed in 0.1 M MOPS buffer, pH 6.5; (iii) the buffer was supplemented with 20% glucose (w/v) as a cryoprotectant for X-ray analysis; (iv) the buffer was also supplemented with 2.5 % (v/v) of MPD (2-methyl-2,4-pentandiol). Finally, hanging drop was prepared by mixing complex with reservoir buffer at ratio of 1:2 (1 μ l of the complex 7.8 mg ml⁻¹ and 2 μ l of reservoir solution) and it was placed over 500 μ l reservoir solution. To evaluate the components of the crystal, the crystal was removed from the X-ray machine goniometer. Crystal was washed three times with 10 μ l reservoir solution and dissolved in SDS sample buffer. The protein was loaded on SDS-PAGE gel and revealed by silver staining (3.14.2).

3.16.2 Ligand crystallization (Mouse)

Initial screening for crystallization of mIL-5 (3.13.4) was carried out by sitting and hanging drop using 8 mg ml⁻¹ of mIL-5. The screening and the optimization experiments were performed at room temperature. Suitable crystals for analysis were obtained using hanging-drop vapor diffusion technique with a final reservoir solution contained 26 % PEG 4000, 0.1 M Tris, pH 8.5, 0.21 M Sodium acetate. Each drop was formed by mixing 1 μ l of the mIL-5^{nullMet} (6 mg ml⁻¹) and 1 μ l of reservoir solution at 291° K. The drop was placed over 500 μ l of the of the reservoir solution.

3.17 X-ray data analysis

Datasets were collected from single crystals at the beam line of the home source (Biocentrum-Wuerzburg University (Rigaku, MSC, USA)). Crystals were mounted in a nylon loop and flash-frozen in liquid nitrogen without further soaking. Crystal-to-detector distance can be set to 130 mm. The X-ray wavelength is 1.54 Å and data collection was performed at 100 K. For high-resolution data, datasets were collected from single crystals at the Cyclotron beam line (SLS, Switzerland); the crystal was rotated through a total of 170°, with a 0.5° oscillation per frame and a different exposure time per frame. Data processing was performed using the software “Crystalclear 1.3.6” (Rigaku, MSC, USA), and for high resolution data were used the software HKL and SHELX.

4 RESULTS

4.1 Structural studies of the human IL-5R α /IL-5 complex

4.1.1 Expression, refolding and purification of wild type human IL-5R α and human IL-5R α variants

The interleukin-5 receptor alpha (IL-5R α) is expressed as a transmembrane protein as well as a soluble protein. The soluble isoform is produced as a result of alternative splicing and it consists of the extracellular part of the receptor lacking the transmembrane and cytoplasmic regions (Shanafelt, Miyajima et al. 1991). Both isoforms are involved in the binding of IL-5 (Monahan et al., 1997; Shanafelt et al., 1991).

The cDNA that encodes the different extracellular domains of the wild type human IL-5R α (wt-hIL-5R α) (Swiss-Prot Q01344-2) was cloned into a pET-3d expression vector (Figure 4-1). A bacterial expression system was used for protein expression, as it is an efficient, widely used host for recombinant protein production due to its high transformation efficiency, cultivation simplicity, fast protein expression and low cost method. In addition, *E.coli* is the organism of choice for the expression of a wide variety of recombinant proteins used in structural studies, such as X-ray analysis, due to the fact that *E.coli* does not glycosylate proteins. Hence, the resulting proteins tend to be more homogeneous.

E.coli Rosetta cells were transformed with the pET-3d/wt-hIL-5R α vector (3.10) and grown in Terrific broth medium (TB) (3.11). The protein expression was induced with 1 mM IPTG during three hours (4-2). Afterwards, cells were harvested to produce 2,0 g of bacteria per liter culture medium.

The wt-hIL-5R α protein accumulated as insoluble protein in form of inclusion bodies. Samples of bacteria culture were analyzed by SDS-PAGE to verify protein expression (Fig 4-2, lane 3). Cells were disrupted by sonication to release the inclusion bodies. The inclusion bodies represented approximately 20-30% of the total bacterial weight. The inclusion bodies were washed (3.12) to remove remaining bacteria cell membranes (Fig 4-2, lane 5). After washing, 95% of inclusion bodies were recovered and solubilized overnight with guanidinium hydrochloride (GuHCl) at room temperature to extract the protein under denatured conditions (Fig 4-2, lane 6).

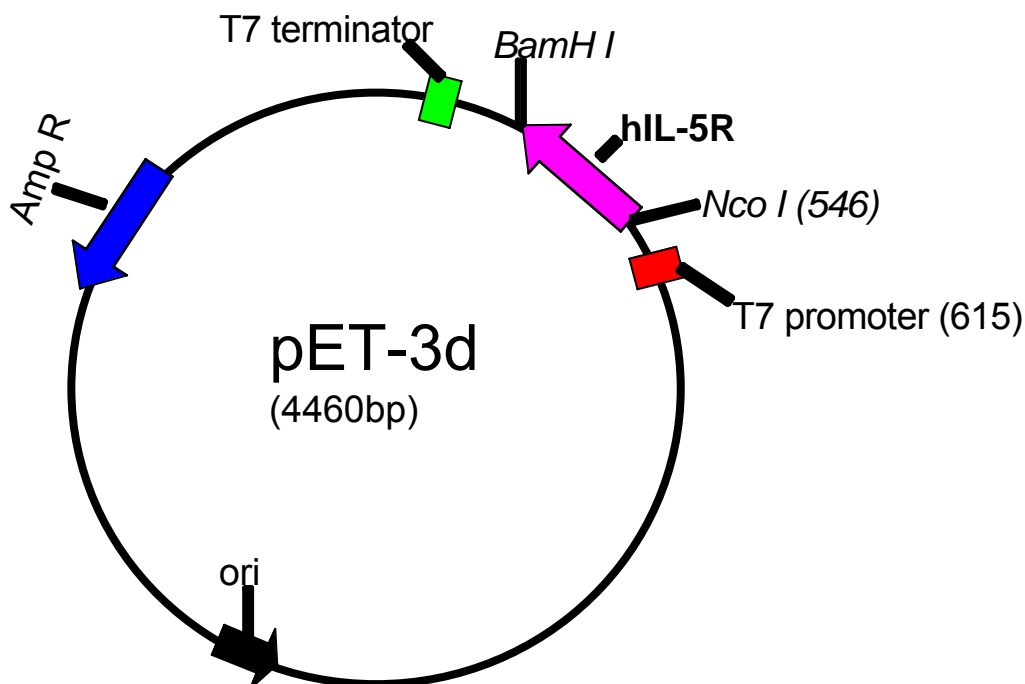


Figure 4-1. Schematic representation of the expression vector. The pET-3d vector contains the wt-hIL-5R α gene (magenta). The cDNA was cloned between Nco I and BamH I restriction sites. T7 promoter is used for hIL-5 transcription. pET-3d carries an Ampicillin resistance gene (Amp R).

Nucleic acids and host proteins can also contaminate the inclusion bodies during its solubilization and all of these components can induce aggregation during the refolding process. To avoid these difficulties the denatured protein was purified by size exclusion chromatography (3.12.1). The yield of denatured protein obtained after gel filtration was 70 mg of wt-hIL-5R α per liter of bacterial culture.

wt-hIL-5R α refolding was carried out by diluting 100 mg of protein in 1 liter of renaturation buffer containing high denaturant concentrations (3.12.2). Dialysis provides means to change the buffer solution from denaturing to non-denaturing conditions. The protein was dialyzed stepwise against buffers with decreasing urea concentration until the desired final buffer condition without urea. After protein refolding and concentration, the wt-hIL-5R α was bound to a Q-sepharose column (3.12.3.1). To remove protein aggregates the column was washed with Tris-HCl buffer and the bound wt-hIL-5R α was eluted by application of 0.0-0.5 M gradient of NaCl.

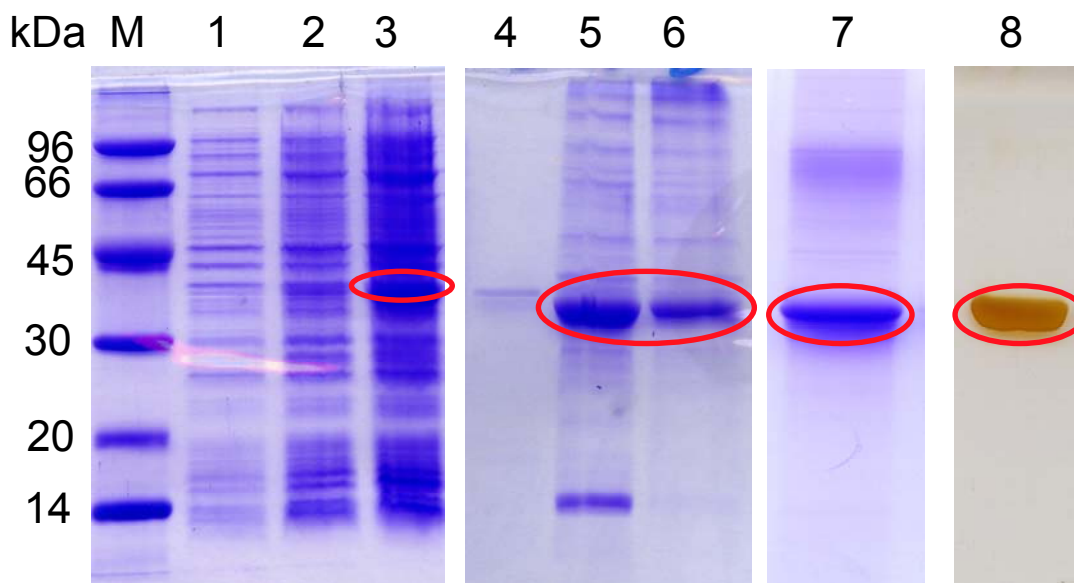


Figure 4-2. Expression of wild type hIL-5R α in *E.coli* Rosetta cells (red oval). Protein expression was induced with 1 mM IPTG for three hours. Protein was analyzed onto a 12% SDS-PAGE. The gel shows: lane M; the protein marker, lane 1; non-induced cells, lanes 2 and 3; IPTG induction after 1 and 3 hours, lane 4; supernatant after washing of inclusion bodies (IB), lane 5; the protein pre-extraction of IB, lane 6; protein main-extraction of IB, lane 7; hIL-5R α after Q-sepharose chromatography and lane 8; hIL-5R α after hIL-5 affinity column. Proteins were separated by reducing (lanes 1-6) and non-reducing (lanes 7 and 8) SDS-PAGE and stained with Coomassie Blue (lanes 1-7) or silver staining (lane 8).

Due to presence of some protein aggregates after anion exchange chromatography, the wt-hIL-5R α was further purified (Fig 4-2, lane 7). The active receptor was purified by affinity chromatography (3.12.3.4) making use of the specific binding interaction between IL-5 and IL-5R α (Fig 4-2, lane 8). The active wt-hIL-5R α was eluted with 4 M MgCl₂, yielding 2-3 mg of pure and active protein (Table 4-1).

The wt-hIL-5R α formed aggregates and precipitated after affinity column purification when it was concentrated above 5.0 mg ml⁻¹. Wild type hIL-5R α also aggregates and precipitates at room temperature at the extent of at least 50% in 12 hours.

Table 4-1. Production of non-labeled wild type hIL-5R α

Protein	wt-hIL-5Rα
Bacteria culture (g)	20
Inclusion Bodies (g)	4-6
Recover IB after wash (g)	3.8-5.7 (represents 95 %)
Refolded Protein (mg)	100
Yield active protein (mg)	2-3

Aggregation is a broad definition that includes several types of interaction. For instance, covalent aggregation takes place through the formation of a chemical bond between monomers. Unpaired free thiols on cysteines residues are the reason for covalent aggregation due to disulfide bond formation. With respect to wt-hIL-5R α , the extracellular part of this receptor contains 7 cysteine residues (Cys 66, Cys 114, Cys 135, Cys 162, Cys 176, Cys 249 and Cys 296). One cysteine residue is located in the first domain (Cys 66). Four of them are involved in the function of conserved disulfide bridges in the second domain (Cys 114, Cys 135, Cys 162 and Cys 176). The two remaining cysteine residues (Cys 249 and Cys 296) are found in the third domain linked through a disulfide bridge (Devos et al., 1994). Mutagenesis analysis in hIL-5R α of these two cysteine residues showed that Cys 249 or Cys 296 are necessary for the maintenance of the active biological conformation. However, the free Cys 66 mutation did not affect IL-5 binding (Devos et al., 1994).

Different groups have shown that mutation of the free cysteine residue increases protein stability (Amaki et al., 1994; Miyazaki et al., 1993). Therefore, Cys 66 in the wild type receptor might be responsible for receptor precipitation during protein concentration. To avoid receptor aggregation Cys 66 of wt-hIL-5R α was mutated to Ala. The resulting hIL-5R α C66A variant (3.7.1) was purified in the same way as it was described for wt-hIL-5R α . This receptor could be finally concentrated up to an amount of 6.0 mg per ml. Precipitation at room temperature was reduced by 60% after 24 hours.

On continuation, four point mutations (3.7.2) within the hIL-5R α C66A variant were generated (K72M, L138M, K167M and L234M) and the effects of these amino acid substitutions on selenium incorporation were determined by *E.coli* transformation and protein expression. Expression of Se-hIL-5R α C66A was

performed in complete M9 medium (3.11.2). No changes were observed in cell growth and protein expression. Inclusion body preparation of the Se-human IL-5R α resulted in proteins of the same quantity and quality as the wild type receptor. Renaturation of Se-hIL-5R α C66A required an increase in β -mercaptoethanol to a concentration of 0.1%. After renaturation the Se-hIL-5R α was purified by affinity column chromatography. Additional variants of human wt-IL-5R α such as D55E, Y57F, C66A, F182A, I183A, R188K (Figure 4-3), and truncated variants of IL-5R α C66A such as Δ 10R α , Δ 20R α , Del 1, Del 2, and Del 3 were generated by site-directed mutagenesis (3.7.1 and 3.7.3, respectively).

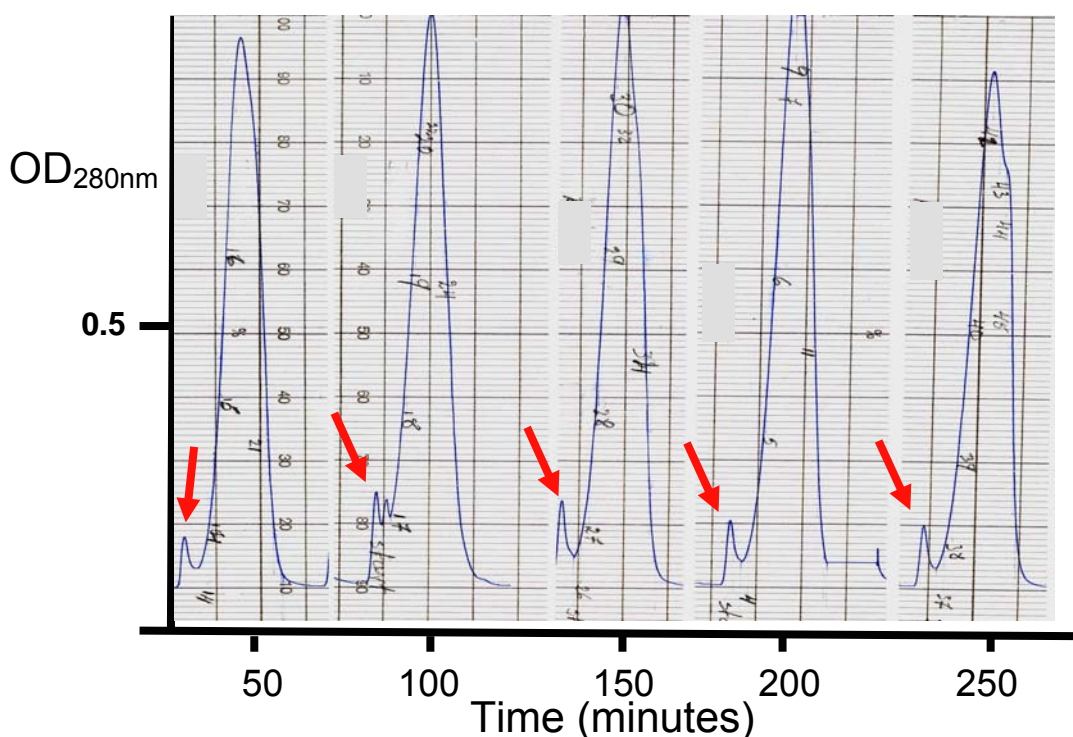


Figure 4-3. Purification of hIL-5R α mutants. hIL-5R α variants were purified employing S200 gelfiltration chromatography. High molecular weight protein aggregates eluted before the monomeric protein (red arrows). Chromatograms show (left to right) D55E, I183A, R188K, Y57F and F182A.

Protein expression, inclusion body purification and solubilization, as well as protein refolding, were performed under the same conditions as described for the wt-hIL-5R α . Similar to wt-hIL-5R α , these hIL-5R α variants were not totally pure after purification by anion exchange chromatography. The IL-5R α variants except hIL-5R α Del 1 were therefore further purified by S200 size exclusion chromatography

(3.12.3.2). As shown in figure 4-3, the different mutants showed the same elution profile. The yield for the mutant proteins was slightly different (Table 4-2), but in all cases, their purity was close to 95% as confirmed by non-reducing SDS-PAGE (Fig 4-4).

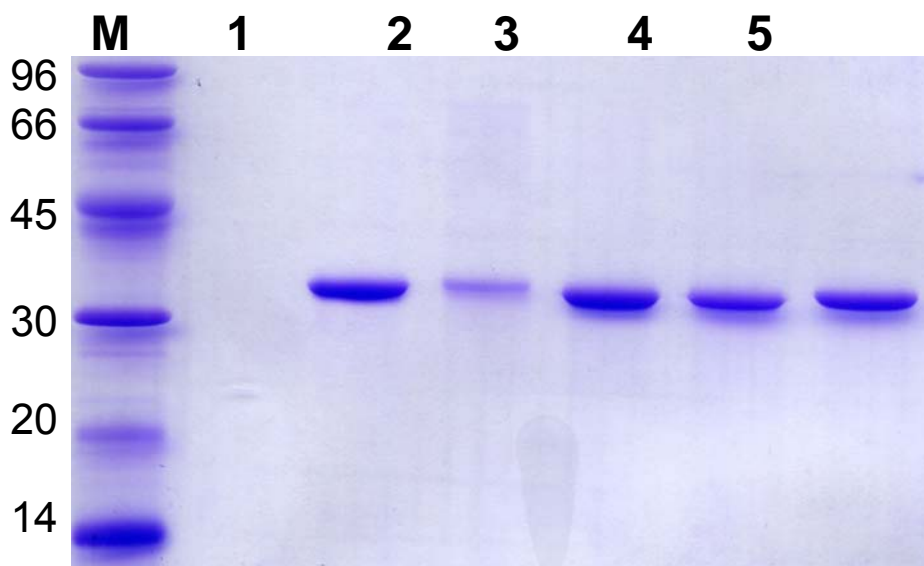


Figure 4-4. Analysis of hIL-5R α mutants. hIL-5R α variants were analyzed by SDS-PAGE under non-reducing conditions (Coomassie stained). The gel shows in lane 1, D55E; lane 2, I183A; lane 3, R188K; lane 4, Y57F and lane 5, F182A.

The hIL-5R α Del 1 variant could not be purified using these techniques. A second anion exchange chromatography (3.12.3.3) provided a suitable procedure to remove aggregates (Fig 4-5). The result indicated that at pH 7.8 with a gradient of 0-100% Na-TAPS buffer, the hIL-5R α Del 1 was eluted at 30-62 % of NaCl buffer (3.12.3.3) and its purity was confirmed by non-reducing SDS-PAGE (Fig 4-5 B).

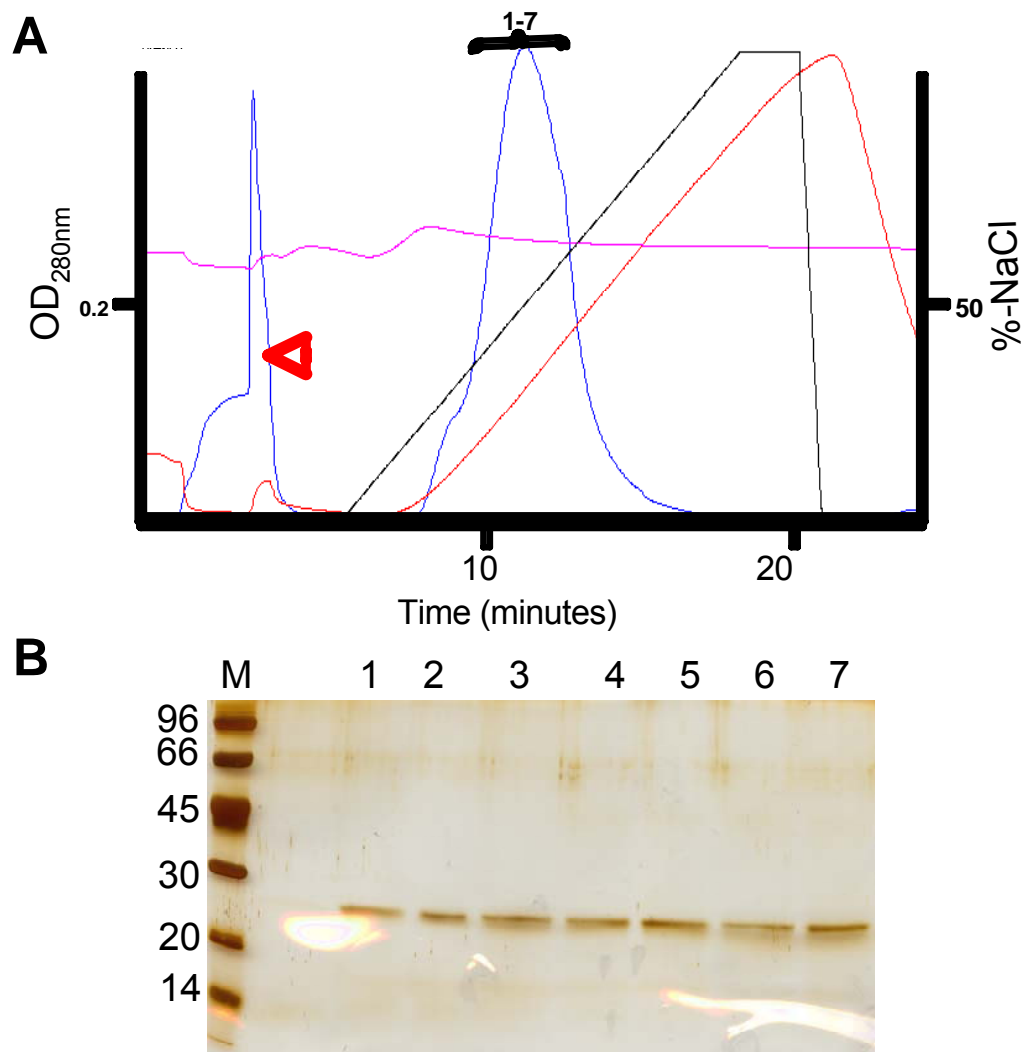


Figure 4-5. Purification of hIL-5R α Del 1 variant. (A) hIL-5R α Del 1 was purified employing (2.0 mg) anion exchange chromatography, aggregates eluted ahead of the gradient (head red arrow). (B) Several fractions (1-7) of hIL-5R α Del 1 were analyzed by SDS-PAGE (silver stained) under non-reducing conditions. All fractions 1-7 show a single band migrating at 25 kDa approximately.

All hIL-5R α proteins were stored at -20°C in 50 mM Tris buffer at pH 8.1. The table 4-2 summarizes the yields of all different mutants and describes the position of the mutation.

Table 4-2. Description of wild type hIL-5R α and hIL-5R α variants

Protein	Da	Domain containing mutation	Yield (mg/L culture)
WT	36011		2,5
D55E	36025	M1	1.4
Y57F	35995	M1	1.5
C66A	35903	M1	2,5
Δ 10R α	35358	M1	3.4
Δ 20R α	34195	M1	3.0
F182A	35935	M2	1.7
I183A	35970	M2	0.6
R188K	35984	M2	1.9
* Del 1	24487	Δ M1	2,5
* Del 2	11320	Δ M2 and Δ M3	8.0
* Del 3	25017	Δ M3	6.0

* Deletion with either domain designated M1, M2 or M3.

4.1.2 Analytical Methods

Analytical methods such as reverse-phase high performance liquid chromatography (RP-HPLC), circular dichroism (CD), electro-spray mass spectrometry (ESI) and SDS-PAGE were used to analyze the purified proteins with respect to purity, secondary structure and the molecular weight.

The wt-hIL-5R α purity and homogeneity were determined by RP-HPLC. By employing this technique, the protein impurities and protein aggregates can be detected, due to different polarity with the target protein. For the mobile phase, RP-HPLC was used with a linear gradient 0-100% of acetonitril. As shown in Fig 4-6, a single peak of the purified hIL-5R α was obtained. The wt-hIL-5R α eluted after 20 min at 40-44% of acetonitril. SDS-PAGE analysis of the fractions showed the wt-hIL-5R α as a single visible band (Fig 4-6).

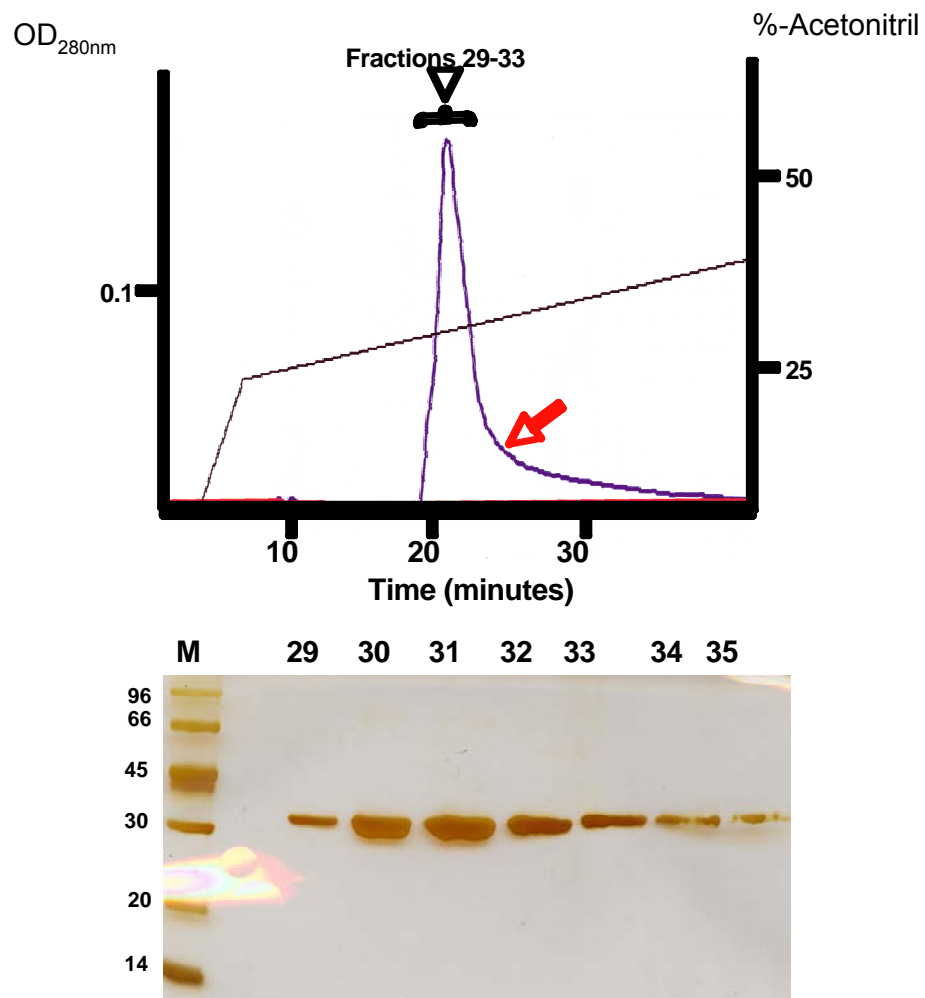


Figure 4-6. Analysis of interleukin-5 receptor alpha. 500 μg of wild type hIL-5R α were analyzed using C4 column. The RP-HPLC shows the chromatogram of wild type hIL-5R α (above). Gel analysis of fractions 34 and 35 from tail peak (red arrow) indicates that the peak appendage is performed by the HPLC column (red arrow).

Circular dichroism (CD) spectroscopy comprises a technique, which allows the analysis of protein secondary structures. The CD is the difference between the absorption of left and right-handed circularly polarized light. The conformation of the hIL-5R α variants was compared with the conformation of wt-hIL-5R α by circular dichroism (3.14.4). The results of the CD spectra analysis suggest that the secondary structures of variants D55A, D55N, and L184A are similar or almost identical to wt-hIL-5R α , confirming that these substitutions do not affect the hIL-5R α general protein folding pattern (Figure 4-7). However, the variant Y57A shows a marked difference in its CD spectrum compared to wt-hIL-5R α . These data provide

evidence that that Tyr57 plays a very important role in maintaining the folding pattern of hIL-5R α (Figure 4-7).

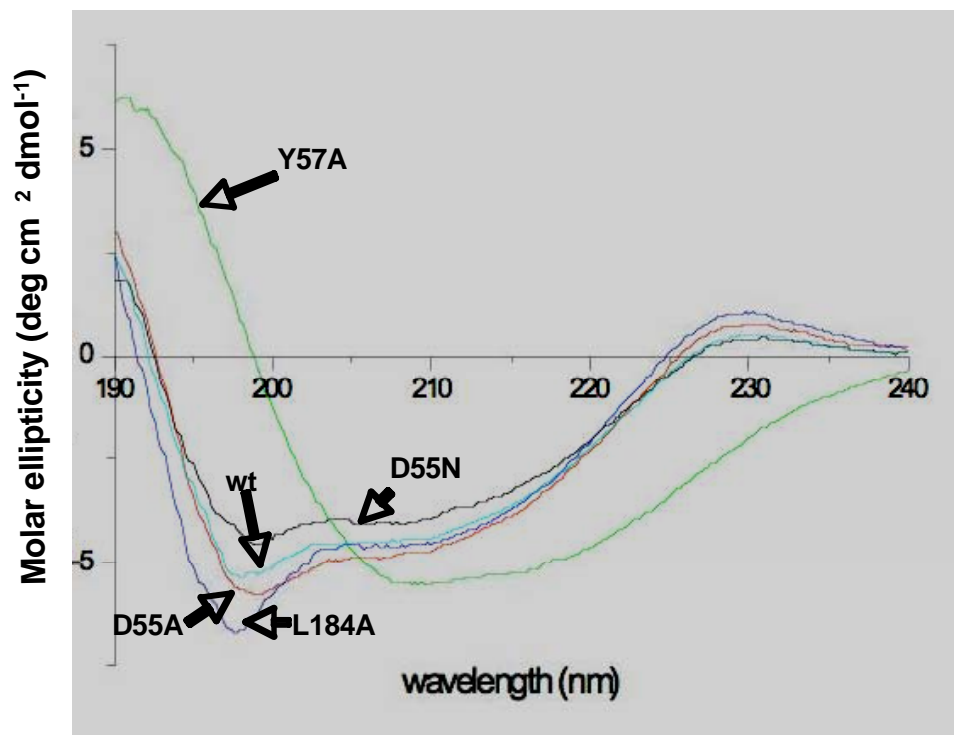


Figure 4-7. Circular dichroism spectrum of wild type hIL-5R α and variants. The qualitative analysis shows that D55A, D55N and L184A proteins possess similar secondary structure elements as wt- hIL-5R α . The Y57A variant shows a different spectra indicating variation in the secondary structure.

Mass spectrometry was used to analyze the molecular weight of the purified proteins (3.14.3). The purified wt-hIL-5R α and hIL-5R α variants, which contain Cys66, were found to exceed the predicted molecular weight by approximately 76.0 Da (Table 4-3).

Different observations suggested the possibility that the Cys66 could be the residue responsible for the increased molecular weight of these proteins. The first observation leading to this hypothesis was that the Del 1 hIL-5R α variant, which lacks Cys66, exhibits the expected molecular weight (Table 4-3).

The second observation in the SDS-PAGE analysis was that Del 2 and Del 3 hIL-5R α variants, which harbor Cys66, appeared highly pure after final gel filtration, but they formed aggregates after concentration by ultrafiltration. The aggregates disappeared only after mutating Cys66 to Ala. On the other hand, the molecular

weight of two variants with the C66A mutation showed the expected molecular weight.

Finally, in wt-hIL-5R α the cysteine at position 66 appears to undergo covalent modification with isothiazolone compounds (Devos et al., 1994) which modify the molecular weight of the receptor protein, thus indicating that the sulfhydryl group is highly reactive. Furthermore, recombinant proteins with highly reactive thiol groups can form disulfide adducts with reducing agents normally used in protein purification (Gillian E. Begg., 1999).

Table 4-3. Mass spectrometry of hIL-5R α proteins

Receptor α	Expected mass	Measured mass	Difference in Da
WT	35936.065	36011.893	75.8
D55E	35950.081	36025.814	75.7
Y57F	35920.070	35995.806	75.7
C66A	35903.091	35903.151	0.06
F182A	35859.030	35935.614	76.5
I183A	35894.018	35970.342	76.3
R188K	35908.059	35984.013	75.9
Del 3 C66A	25018.636	25017.968	0.00

Based on the results employing isothiazolone compounds and disulfide adduct interaction with highly reactive free cysteines, it seems highly probable that Cys66 residue of wt-hIL-5R α reacts with β -mercaptoethanol (β -ME), which is used in the buffer for the wt-hIL-5R α preparation (3.12.1). The molecular weight difference of 76.0 Da found in purified hIL-5R α proteins with Cys66, corresponded exactly to the molecular weight of β -ME (78.1 g/mol), thus suggesting that the chemical modification occurs by disulfide bond formation (Cys66 + β -ME \Rightarrow Cys66-S-S- β -ME + 2H + 2e⁻).

With Cys66 mutated to Ala (C66A), we found that the measured weight matched the expected weight within the error limit of the method (Table 4-3). For Se-labeled proteins 100% incorporation of Se-Met instead of S-Met could be confirmed by mass spectrometry.

4.1.3 Expression, refolding and purification of the human IL-5

The human IL-5 cDNA was cloned into the pET-3d expression vector using Nco I and BamH I restriction sites. *E. coli* Rosetta cells were transformed with the expression vector pET-3d/hIL-5. The transformed bacteria were grown in LB medium under the same conditions as described for the hIL-5R α expression. A whole cells lysate (0.01 ml) was loaded onto a SDS-PAGE for the analysis of protein induction (Figure 4-8 B, lane 2). A main protein band of 13 kDa corresponding to the hIL-5 monomer appeared after IPTG-induction and this protein was accumulated in inclusion bodies.

The inclusion bodies were 20-30 % of the wet weight of the total bacteria. Protein was purified under denaturing conditions by gel filtration chromatography (Sephacryl 200) and 6 M guanidinium hydrochloride. Yield was approximately 60-70 mg per L culture medium (3.13.1).

Human IL-5 was refolded in a single step refolding procedure overnight in the presence of urea and oxidized and reduced glutathione (3.13.3). This redox system facilitates the formation of the disulphide bridges. The refolding buffer was removed by dialysis. After dialysis, recombinant hIL-5 was concentrated up to 10 mg/ml and loaded onto a Superdex 200 column (16/60). A clear separation of the high molecular weight aggregates (20-40 ml or 13-26 min), hIL-5 dimer (40-60 ml or 26-40 min) and hIL-5 monomer (after 90 ml or after 60 min) was obtained (Figure 4-8 A). The purified hIL-5 dimer was analyzed by SDS-PAGE. It migrates as a protein band of approximately 26 kDa (Figure 4-8 B). Yield of the pure dimeric hIL-5 was approximately 6 mg per L of cell culture.

The molecular weight of hIL-5 (26473 Da), as determined by mass spectrometry, corresponded to the predicted molecular weight based on protein sequence.

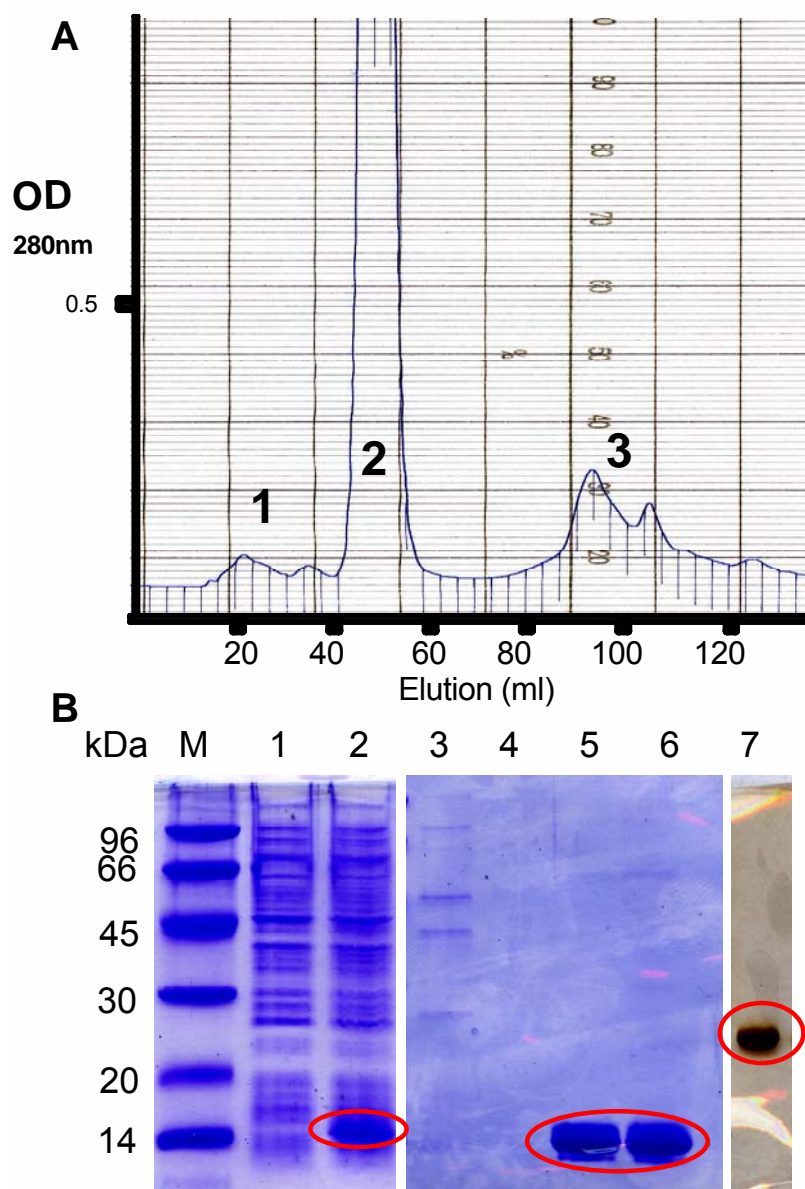


Figure 4-8. Expression and purification of hIL-5. (A) Gelfiltration chromatography indicates high molecular weight aggregates (number 1), hIL-5 dimeric protein (number 2) and the hIL-5 monomer (number 3). (B) SDS-PAGE was used to verify the protein expression and purification (red ovals). Lanes represent: M, MW; 1, non-induced cells; 2, IPTG induction for 3 hours; 3 and 4 supernatant after washing of inclusion bodies; 5 and 6, protein in IB; and 7 and 8 purified protein. Proteins were separated by reducing (lanes 1-6) and non-reducing (lane 7) SDS-PAGE and stained with Coomassie Blue (lanes 1-7) or silver staining (lane 8).

4.1.4 Biomolecular interaction analysis (BIAcore)

Protein-protein interaction between hIL-5R α and hIL-5 was analyzed using surface plasmon resonance (3.14.5). For measurements, chemically biotinylated hIL-5 was immobilized on a streptavidin-coated BIAcore sensor CM5 chip and the different

hIL-5R α proteins were perfused to distinct concentrations (3.14.5). For the BIAcore experiments the immobilized hIL-5 on the sensor chip was found to be a more efficient system than the immobilized receptor, due to the fact that when the receptor was immobilized on the sensor chip, the receptor lost significant binding capabilities after regeneration (3.14.5). This phenomenon was also reported by Brown and colleagues in 1995 using the hIL-5R α (Brown et al., 1995).

Table 4-4. Biomolecular interaction analysis of hIL-5R α and hIL-5

Receptor	$k_{on} \times 10^{-5} [s^{-1} M^{-1}]$	$k_{off} \times 10^3 [s^{-1}]$	K_D (nM)
Wild type	3.0 ± 1.0	2.4 ± 0.6	8.5 ± 4.0
hIL-5R α D55E	3.9 ± 0.11	13.0 ± 1.5	34.8 ± 10.0
hIL-5R α Y57F	4.4 ± 2.0	5.2 ± 0.05	14.9 ± 9.7
hIL-5R α C66A	5.2 ± 1.8	1.4 ± 0.4	3.0 ± 0.04
hIL-5R α F182A	5.0 ± 1.3	4.2 ± 0.1	8.8 ± 2.5
hIL-5R α I183A	8.4 ± 2.3	12.0 ± 1.1	16.0 ± 7.6
hIL-5R α R188K	4.6 ± 1.6	18.0 ± 2.2	35.6 ± 17.0
$\Delta 10R\alpha$	8.8 ± 1.0	2.1 ± 1.2	2.4 ± 1.0
Del 1	nb	-	-
Del 2	nb	-	-
Del 3	na	na	na

nb: no binding

na: no analyzed (protein precipitated at room temperature)

The K_D is defined as $K_D = k_{off}/k_{on}$

Analysis of the data from the last 10% of the association phase before reaching steady state and the first 10% of the dissociation phase yielded k_{on} and k_{off} values. The equilibrium binding constant K_D was calculated from the equation $K_D = k_{off}/k_{on}$. The hIL-5R α variants F182A and I183A had binding properties almost identical to wt-hIL-5R α , indicating that Phe or Ile substitutions for Ala residues did not alter the overall structure and that these residues are not involved in critical interactions (Table 4-4). The hIL-5R α variants D55E (Figure 4-9) and R188K,

however, exhibit a lower binding affinity, indicating that Asp55 or Arg188 are involved in receptor binding (Table 4-4).

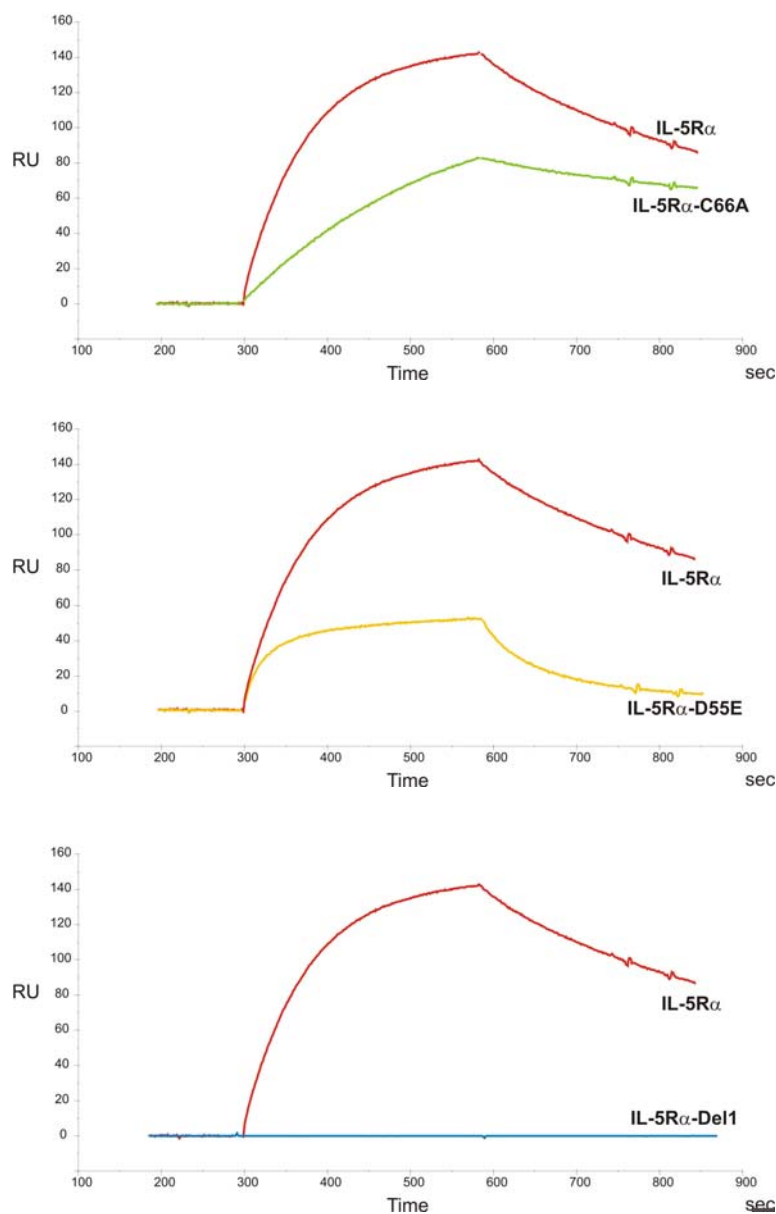


Figure 4-9. BIAcore analysis of human IL-5R α variants. Solutions of the indicated IL-5R α variants (concentration 140 nM) were perfused over a sensor chip with immobilized hIL-5.

BIAcore analysis also showed that the two hIL-5R α variants, hIL-5R α C66A (Figure 4-9) and Δ 10R α had a similar affinity for the ligand compared with wt-hIL-5R α . Remarkably, the mutations hIL-5R α C66A and Δ 10R α caused a decrease in the k_{off} value and a slight increase in k_{on} value (hIL-5R α C66A, see figure 4-9) or only increasing the k_{on} value (Δ 10R α). These receptor variants bind stronger, due to low off-rate and higher on-rates (Table 4-4). The BIAcore results reflect the interaction

of β -ME with the Cys66 leading to a decrease in the affinity binding of the wt-hIL-5R α .

Our data also show that the deletion of the first N-terminal Fn-III-like domain totally disrupts the receptor affinity (Del 1). Deletion of the third Fn-III-like (C-terminal) showed also significant reduction in affinity, but the data could not be analyzed, possibly due to protein precipitation at room temperature.

4.1.5 Limited proteolysis approaches

Flexible protein loops can disturb crystal growth as well as crystal diffraction. Removing such unstructured regions may considerably improve the crystal quality. Limited proteolysis was used to detect possible flexible loop(s) or termini in the components of the binary complex (hIL-5R α /hIL-5) which can disturb crystal growth.

In order to identify parts of the IL-5 complex sensitive to protease digestion, receptor plus ligand was mixed in a 1:1.1 ratio. The complex was purified by gelfiltration and afterwards digested with trypsin (3.15).

The protease trypsin cuts at the C-terminal end of the Lys and Arg residues. Mass spectrometry analysis was used to analyze the peptides resulting from the trypsin proteolysis of the wt-hIL-5R α /hIL-5 complex (Table 4-5). The largest peptides were identified as a flexible stretch spanning the first 40 N-terminal residues of the wt-hIL-5R α . Other peptides were also identified as the first 8, 20, 31 or 40 N-terminal residues of the wt-hIL-5R α (Table 4-5). No other peptides from hIL-5 were found after trypsin digestion. In addition, the SDS-PAGE confirmed the absence of corresponding peptides in the digested complex (Figure 4-10).

In line with these results, several deletion variants of hIL-5R α with a truncated N-terminus were generated. The new hIL-5R α variants were designated Δ 10R and Δ 20R, but generated with the hIL-5R α C66A cDNA.

Table 4-5. Analysis of peptides by mass spectrometry

m/z (mass/charge)	Peak Intensity	Residues	Peptide Sequence
2320.2	19.0	21-40 aa	VTGLAQVLLQWKPNPDQEQ
			ADLLPDEKISLLPPVNFTIKVTGLAQVLLQWKPNPDQEQ
4524.6	14.5	1-40 aa	
1341.8	9.3	9-20 aa	ISLLPPVNFTIK
3643.0	1.1	9-40 aa	ISLLPPVNFTIKVTGLAQVLLQWKPNPDQEQ

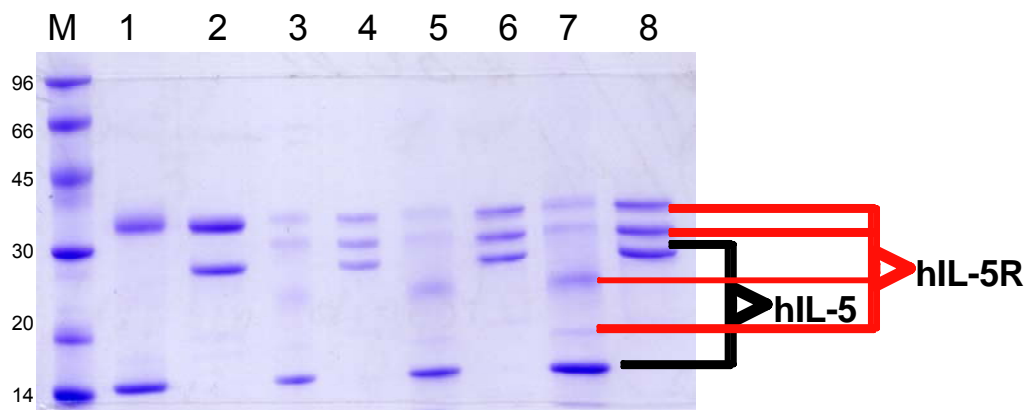


Figure 4-10. Complex proteolysis. Purified complex was digested with trypsin protease at 37°C for 40 min at ratio 200:1 (complex:trypsin). Untreated complex (5.0 μ l) was used as a control and only two bands were observed (lanes 1 and 2). Different volumes of digested complex were loaded onto the gel: lanes 3 and 4 (2.5 μ l); lanes 5 and 6 (5.0 μ l), and lanes 7 and 8 (7.5 μ l). Reducing conditions lanes 1, 3, 5, and 7; non reducing conditions lanes 2, 4, 6, and 8.

4.1.6 Crystallization

To crystallize the hIL-5R α /hIL-5 complex it was necessary to 1. produce sufficient amounts of highly pure proteins (above), 2. to evaluate the stoichiometric interaction and 3. to find the specific crystallization conditions. Although previous reports suggested that hIL-5 and wt-hIL-5R α interact in a 1:1 ratio (Devos et al., 1993; Johanson et al., 1995), we experimentally tested the stoichiometry via different molar ratios of receptor and ligand (Figure 4-11).

Gelfiltration chromatography of the complexes formed in the presence of a molar excess of receptor showed a different elution profile compared to that of complexes formed at a near equimolar ratio (Fig 4-11). SDS-PAGE analysis of single fractions indicated that a high excess of the wt-hIL-5R α formed aggregates that eluted ahead of the complex (Fig 4-11 A, first and second peak, respectively).

The unbound wt-hIL-5R α and hIL-5 eluted as a little shoulder of the highest peak (Fig 4-11 A). However, fractions belonging to the complex formed with a small excess of ligand (1:1.1 ratio) suggest that all fractions present a complex of 1:1 ratio (Fig 4-11 B). An unbound ligand was not detected by SDS-PAGE. In conclusion, both ratios 2:1 or 1:1.1 (receptor:ligand) showed the same elution times (40-60 min, Superdex 200 16/60) for the fractions that contain 1:1 stoichiometry. The 1:1 complex is maintained during the chromatography procedure.

These results confirm, indeed, the previously reported stoichiometry for the IL-5 and IL-5R α ecto-domain interaction as 1:1, despite the dimeric structure of the ligand suggesting two receptor binding sites. Mixing 1 equivalent of hIL-5R α with 1.1 equivalent of the hIL-5 the binary complex of hIL-5R α with hIL-5 was subsequently formed.

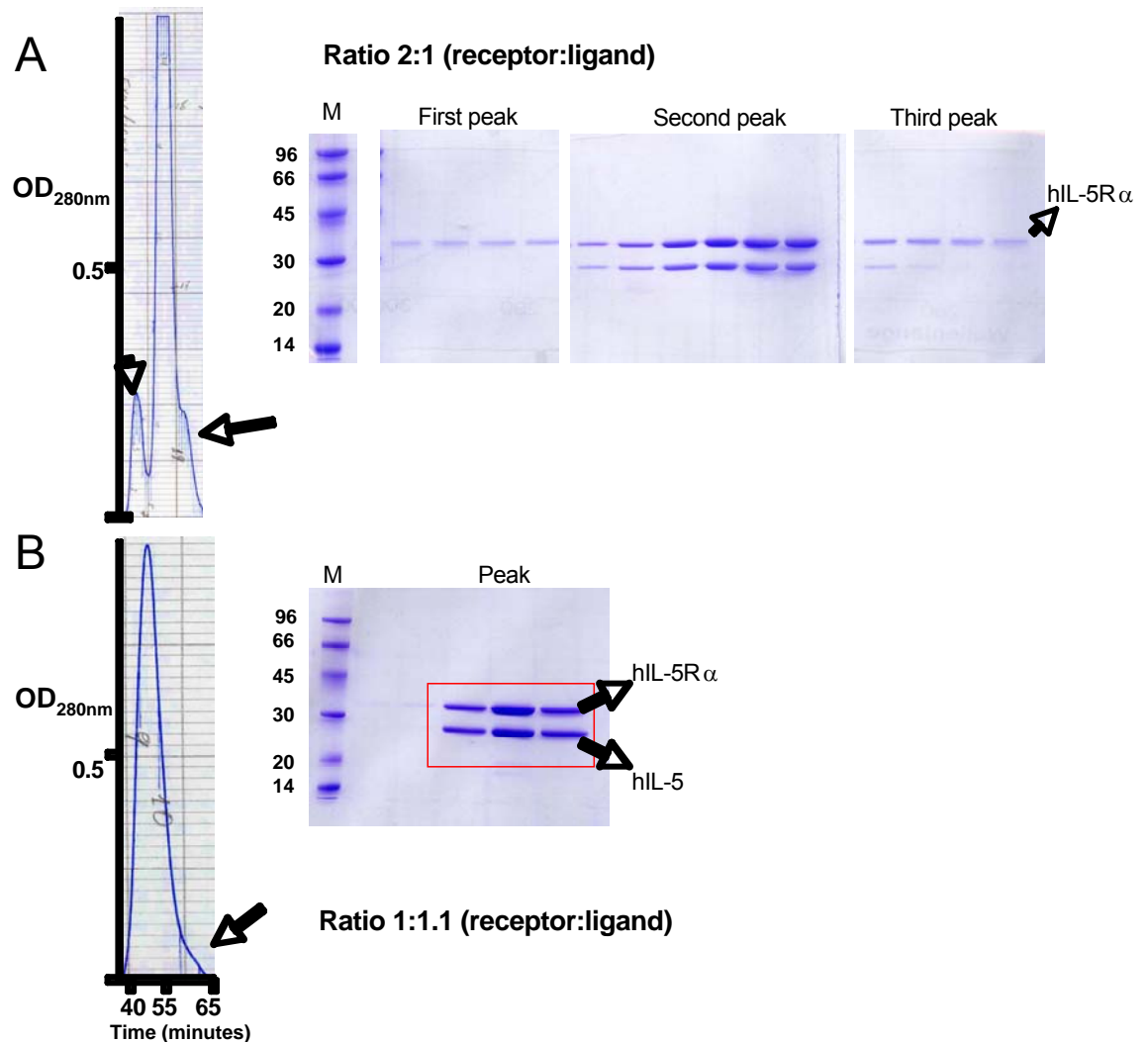


Figure 4-11. Gelfiltration chromatography and SDS-PAGE analysis of the wt-hIL-5R α /hIL-5 complex. (A) Complex was formed with a two fold molar excess of wt-hIL-5R α . The chromatogram shows small additional peaks (arrows). (B) Complex was formed with a small excess of ligand (10%). Only one peak was formed and the analyzed fractions showed equal amounts of receptor and ligand. The highest peak in both chromatograms display similar amounts of receptor and ligand.

The complex containing fractions were pooled and concentrated to 10 mg ml⁻¹. An aliquot from this concentrated complex was analyzed again by gelfiltration using a FPLC system with a Superdex 200 chromatography column (analytical column) to verify the quality of the complex (Fig 4-12). The chromatogram of the complex shows a high sharp peak followed by small peak (Fig 4-12).

The highest peak contained the wt-hIL-5R α /hIL-5 complex, which has a predicted molecular weight of 62 kDa. The elution time of the highest peak of 28-30

min corresponds to a molecule with a molecular weight of 61-63 kDa. The small peak that contains hIL-5 has an elution time of 31 min. This corresponds to a protein with a molecular weight of approximately 26 kDa. The small peak could be detected in this chromatography only after complex concentration. Both proteins also display high purity and there were not aggregates formed after complex concentration (Fig 4-12).

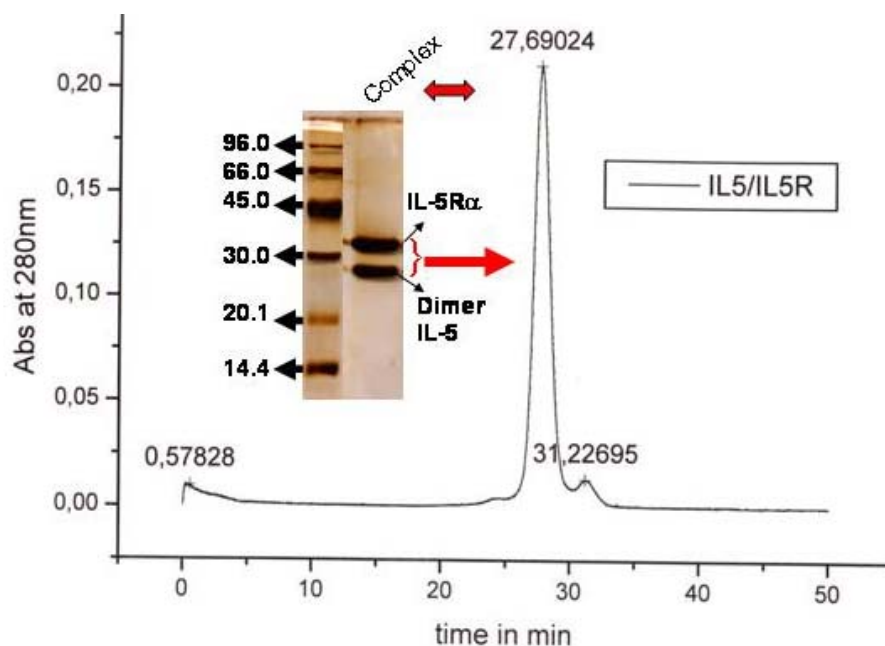


Figure 4-12. Concentrated complex analyzed by Fast Protein Liquid Chromatography (FPLC). Elution profile shows one peak at 28 min and one peak at 31 min. The major peak (28 min) corresponds to the 1:1 complex. In addition, the human IL-5 dimer can be seen (the small peak at 31 min). SDS-PAGE analysis under non-reducing conditions of the peak eluted at 28 min shows two bands corresponding to hIL-5R α and hIL-5 that migrated to 36 kDa and 26 kDa, respectively.

Initial crystallization trials (3.16.1) were performed with a complex concentration of 10 mg per ml. Using commercial crystallization kits following the sparse matrix screening, crystals with different morphologies were obtained (needles, dendrites, spherulites, and plates), but after the initial screening none of these crystals proved suitable as three-dimensional single crystal for further analysis (Table 4-6). Varying individual parameter such as the buffer composition, pH value, complex concentration, the precipitant/protein, temperature and the additives, the initial conditions were subsequently optimized.

Table 4-6. Crystallization buffers

Screen	Number	Buffer	Result
Crystal Screen1	36	8% PEG 8.000, 0.1M Tris-HCl pH 8.5	Needles
Crystal Screen2	22	12% PEG 20.000, 0.1M MES pH 6.5	Needles and Plates
Crystal Screen2	37	10% PEG 8.000, 0.1M HEPES pH 7.5, 8% Ethylene Glycol	Needles
Crystal Screen2	38	20% PEG 10.000, 0.1M HEPES pH 7.5	Needles
Crystal Screen2	42	12% Glycerol, 0.1M Tris pH 8.5, 1.5M Ammonium Sulphate	Needles
PEG/Ion	2	0.2M Potassium Fluoride, 20% PEG 3.350	Small needles
PEG/Ion	40	0.2M di-Sodium hydrogen Phosphate, 20% PEG 3.350	Small needles and spherulites
PEG/Ion	42	0.2M di-Potassium hydrogen Phosphate, 20% PEG 3.350	Long needles
PEG/Ion	44	0.2M di-Ammonium hydrogen Phosphate, 20% PEG 3.350	Needles
JBS5	A2	12% PEG 8.000, 10% Glycerol, 0.5M K Chloride	Needles
JBS5	B3	18% PEG 8.000, 0.1M Tris-HCl pH 8.5, 0.2M Li Sulphate	Spherulites
JBS5	D4	10% PEG 20.000, 0.1M Na MES pH 6.5	Needles

Optimization with buffer 36 from crystal screen 1 (8% PEG 8.000, 0.1M Tris-HCl pH 8.5), buffer 2 (0.2M Potassium Fluoride, 20% PEG 3.350), 40 (0.2M di-Sodium hydrogen Phosphate, 20% PEG 3.350), 42 (0.2M di-Potassium hydrogen Phosphate, 20% PEG 3.350) and 44 (0.2M di-Ammonium hydrogen Phosphate, 20% PEG 3.350) from PEG/Ion, and buffer A2 (12% PEG 8.000, 10% Glycerol, 0.5M K Chloride) from JBS5 showed the same spherulites and needle crystals. These crystal

forms, however, did not improve, although various parameters were modified in the fine screening procedure.

Improvement was observed using buffer B3 (18% PEG 8.000, 0.1M Tris-HCl pH 8.5, 0.2M Li Sulphate) from JBS5 leading to the growth of long needles. However, all attempts to increase the crystal size were finally unsuccessful. Optimization of the initial crystallization results with buffer 37 (10% PEG 8.000, 0.1M HEPES pH 7.5, 8% Ethylene Glycol), 38 (20% PEG 10.000, 0.1M HEPES pH 7.5) and 42 (12% Glycerol, 0.1M Tris pH 8.5, 1.5M Ammonium Sulphate) from crystal screen2 and buffer D4 (10% PEG 20.000, 0.1M Na MES pH 6.5) from JBS5 only led to protein precipitation.

The best results were obtained with buffer 22 (12% PEG 20.000, 0.1M MES pH 6.5) from crystal screen 2 in which the crystal improved the size and morphology (Table 4-6). Under these conditions, the complex could be reproducibly crystallized in two different forms such as long needles and thin but three-dimensional plates (Fig 4-13 A). Nevertheless, first X-ray diffraction experiments revealed that these crystals did not diffract. A breakthrough was the use of the hIL-5R α C66A variant that yielded single morphology crystals of the complex (Fig 4-13 B). Although the X-ray diffraction also failed with this receptor, the crystal morphology was significantly improved (Figure 4-13 B). The hIL-5R α C66A variant was subsequently used for all further crystallization experiments.

In order to further improve the crystallization properties of the complex, the detergent 3-[(3-cholamidopropyl) dimethylammonio]-1-propanesulfonate (CHAPS) was used to minimize protein aggregation and to increase protein complex stability. CHAPS was added after complex purification by gel filtration. The pool fraction of the complex was divided in three aliquots and each aliquot was supplemented with distinct concentrations of CHAPS (0.1%, 0.2% and 0.3%). Crystals were grown from 0.1 M MES pH 6.5, 12 % PEG 20000 buffer (crystal screen 2, buffer 22). Only one condition showed improved crystal growth, after addition of CHAPS. With 0.3% CHAPS concentration, the resulting crystals grew in about five days. The CHAPS screen indicated that three-dimensional growth of the crystals could be induced in a reproducible way by the addition of 0.3% CHAPS and not by 0.1% or 0.2% CHAPS. At 0.1% and 0.2% of CHAPS concentration crystals displayed a more cluster-like morphology.

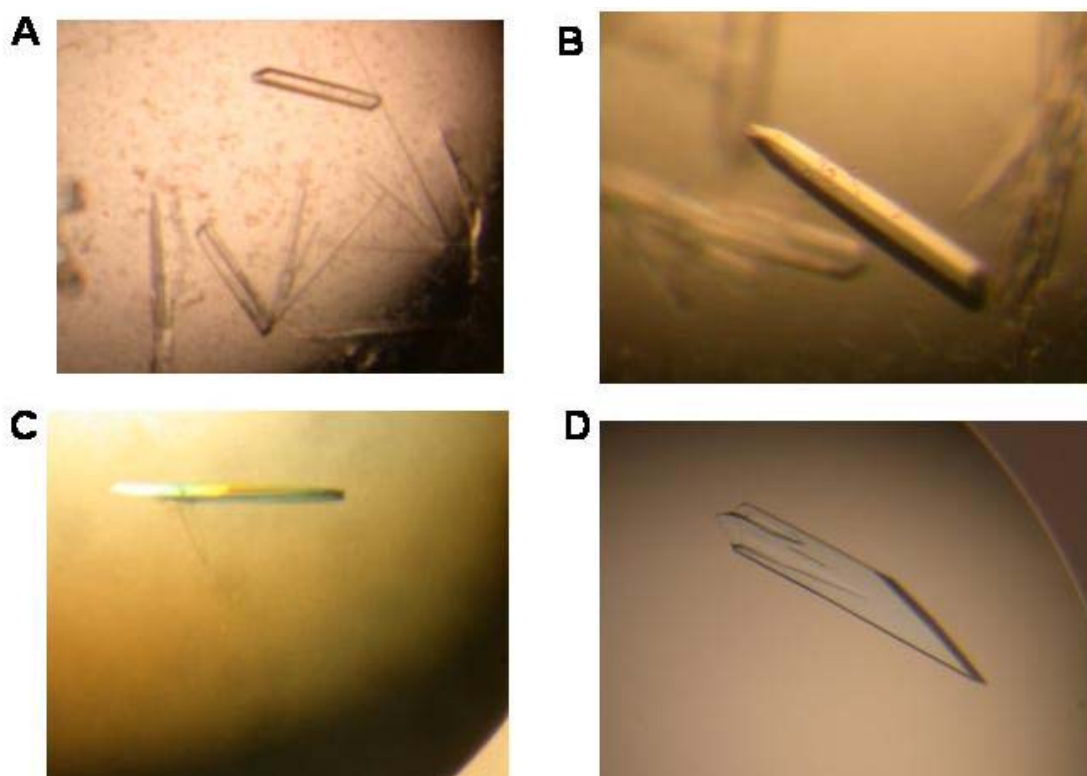


Figure 4-13. Optimization of crystallization conditions for the complex hIL-5R α /hIL-5. Crystals of the hIL-5R α /hIL-5 complex were grown under different crystallization conditions. (A) Complex comprising wild type hIL-5R α /hIL-5 grown from 0.1 M Imidazol pH 6.5, 10% PEG 20.000. (B) Complex comprising hIL-5R α C66A/hIL-5 grown from 0.1 M Imidazol pH 6.5, 10% PEG 20.000. (C) Complex consisting of hIL-5R α C66A/hIL-5, the complex prepared with buffer containing 0.3% CHAPS, the crystals grown from 0.1M KH₂PO₄ pH 6.5, 10% PEG 20.000, 20% glucose and 2.5% MPD. (D) Complex comprising hIL-5R α C66A/hIL-5 prepared with buffer containing 0.3% CHAPS and crystals grown from 0.1M MOPS, pH 6.5, 10% PEG 20.000, 20% glucose and 2.5% MPD.

In addition, the complex was also prepared by adding 0.3% CHAPS to the individual complex components (hIL-5R α C66A and hIL-5). Subsequently, the complex was formed. The complex was purified by gelfiltration and crystallized under the same conditions mentioned above. Despite of maintaining these conditions, the crystal morphology was different resulting in only small needles.

In order to test whether the chemical composition of the buffer could influence crystallization and diffraction properties of the crystals, different buffers were used in the optimization screening (Fig 4-13). Buffer screen could be shown that crystals diffracted only from very few buffers such as Bis-Tris (8.0Å), KH₂PO₄ (4.0-5.0Å) and MOPS (3.5-4.0Å). Crystals grown from Imidazol, Tris-HCl, CHES

and MES buffer did not diffract at all. Since crystals grown from MOPS buffer showed the best diffraction properties, MOPS buffer was used for further crystallization optimization (Fig 4-13 D).

Small concentrations of additives such as ethanol, NiCl₂, MPEG 400, MEG 550, and 2-methyl-2,4-pentanediol (MPD) were included in order to determine whether they could improve crystal size and quality (Wilmanns, 1999). Long thin cluster crystals grew from crystallization buffer supplemented with ethanol or PEG 400 (compare Fig 4-14 B and C). Using 2.5% MPD (v/v) resulted in more single crystals in comparison to those from buffer without MPD (compared Fig 4-14 A and D).

Finally, glucose was evaluated as a cryoprotectant reagent, and various glucose concentrations were examined. With 20% glucose, the resulting crystals had clearly the same morphology and size as those crystals grown without glucose.

These conditions were also examined with various complex concentrations (3, 5, 7.8, 10 and 11.0 mg ml⁻¹) and different ratios of protein solution buffer (1:1, 1:1.5, 1:2 and 1:3). A complex concentration greater than 3 mg per ml in the drop leads to precipitation of the complex. However, at a complex concentration below 2.4 mg per ml only crystals with morphologies like thin plates and needles could be obtained. The best complex concentration was found to be 2.6 mg per ml, but concentrations in the range of 2.4-2.8 mg ml yielded single crystals in a reproducible way.

Additionally, different crystallization temperatures as 4°C, 12°C and 37°C along with paraffin- and silicon oil to vary the rate of vapor diffusion were tested. At low temperatures e.g, 4°C no crystallization was observed. At 12°C the complex crystallized in small needles after 15 days. Only small needles were also obtained at 37°C but they appeared already within 24 hours. Using oils to control the rate of vapor diffusion did not improve crystallization and was, therefore, abandoned. In summary, the addition of 0.3% (v/v) CHAPS after complex preparation, and crystallization in 0.1M MOPS pH 6.5, 10% PEG 20.000, 20% glucose and 2.5% MPD buffer with 1:2 ratio protein:buffer (7.2-7.8 mg ml⁻¹) promotes in a reproducible way the growth of single crystals with an approximate size of 400 µm x 200 µm x 50 µm, at room temperature in approximately 3-5 days (Figure 4-14 D). Under these conditions, the growth of cluster was significantly reduced. Crystals of

selenomethionyl complex (Se- hIL-5R α C66A and Se-hIL-5) were obtained with the same crystallization conditions.

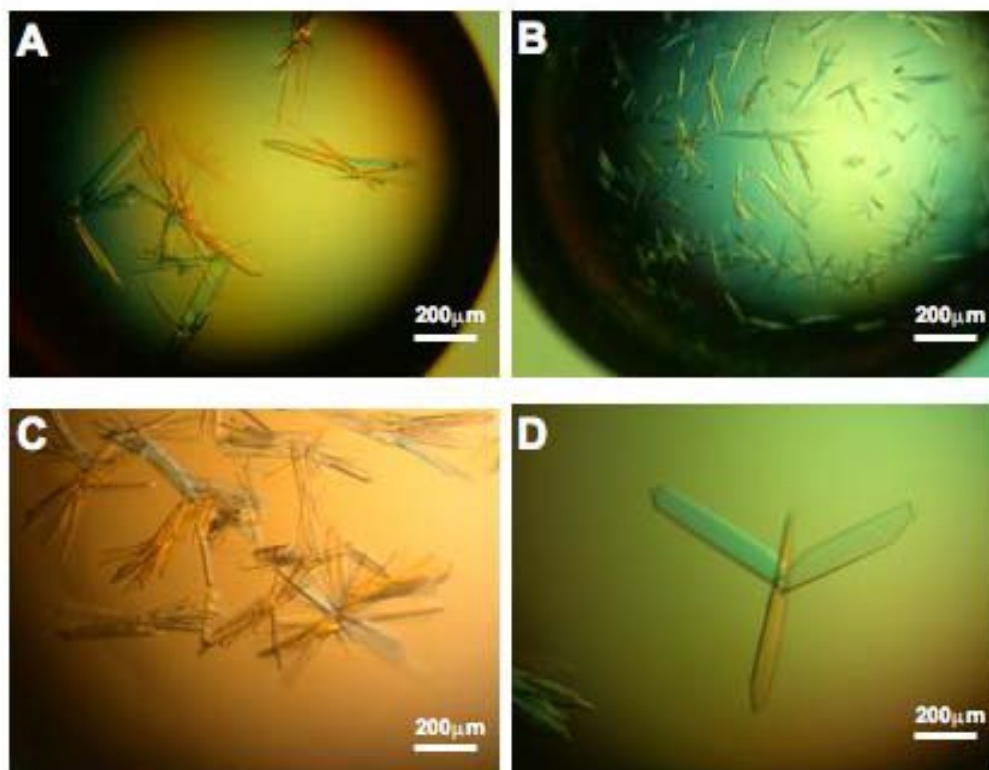


Figure 4-14. Optimization of the crystallization of the hIL-5R α C66A/hIL-5 by detergent use. Complex was prepared with 0.3% (v/v) CHAPS and crystals grown in 0.1M MOPS, pH 6.5, 10% PEG 20.000, 20% glucose. Crystals of hIL-5R α C66A/hIL-5 complex were grown in the presence or absence of additives (A) without additives; (B) 2.5% (v/v) ethanol (C) 2.5% (v/v) PEG 400, and (D) 2.5% (v/v) MPD.

Additionally, the Δ 10R α variant was used to crystallize in complex with hIL-5. Complex preparation was performed as described above for the hIL-5R α C66A/hIL-5 complex. The complex was concentrated to 10 mg per ml or 7.8 mg per ml in the presence of CHAPS. The highest complex concentration was used to set up initial screens at a 1:1 ratio (crystallization screen 1 and 2). In these screens, the Δ 10R α /hIL-5 complex precipitated under the following conditions: crystallization screen 1; buffer #3 (0.4 M Ammonium Phosphate) and buffer #12 (30% Isopropanol, 0.1 M Na HEPES pH 7.5, 0.2 M Magnesium Chloride). However, the majority of the crystallization conditions only led to clear drops. Long needle clusters grew from two conditions: buffer #22 (12% PEG 20000, 0.1M MES pH 6.5) and buffer # 42

(12% Glycerol, 0.1M Tris pH 8.5, 1.5M Ammonium sulphate). The optimization of these two conditions did not improve the crystallization.

Alternatively, the $\Delta 10R\alpha$ /hIL-5 complex was crystallized applying the same conditions found for hIL-5R α C66A/hIL-5 (0.1M MOPS pH 6.5, 10% PEG 20.000, 20% glucose and 2.5% MPD) using 7.8 mg ml⁻¹ complex concentration. But, although crystallization followed the same procedure, crystals obtained exhibited a different morphology (small needles). Fine-tuning using different concentrations of PEG 20000 or MPD was performed, but only very small needles or medium size needles could be obtained depending on the PEG concentration. These results suggest that, although the $\Delta 10R\alpha$ has a similar affinity as hIL-5R α C66A, as well as the purification characteristics of the $\Delta 10R\alpha$ /hIL-5 complex are similar to those of hIL-5R α C66A/hIL-5 complex, this $\Delta 10R\alpha$ /hIL-5 complex requires other crystallization conditions.

4.1.7 X-ray analysis and complex structure

A preliminary dataset was collected from a single crystal (hIL-5R α C66A/hIL-5 complex) using a Rigaku X-ray machine (Rigaku, MSC, USA). Crystals were mounted in a nylon loop and immediately flash-frozen in liquid nitrogen. Crystal-to-detector distance was set to 130 mm, wavelength was 1.54 Å, and data collection was performed at 100 K. The crystal diffracted at a resolution of 3.2 Å. Data analysis indicated a monoclinic space group P2₁ with unit cell parameters $a = 85.13$ Å, $b = 60.03$ Å $c = 139.64$ Å; and $\alpha = \gamma = 90^\circ$, and $\beta = 97.98^\circ$.

After data acquisition, the crystal was removed, washed three times in fresh reservoir buffer and dissolved in non-reducing SDS sample buffer. SDS-PAGE analysis showed that the crystal was composed of hIL-5R α and hIL-5 in a 1:1 ratio (Figure 4-15), indicating that the dataset obtained was derived from a 1:1 complex of hIL-5 : hIL-5R α C66A extracellular domain.

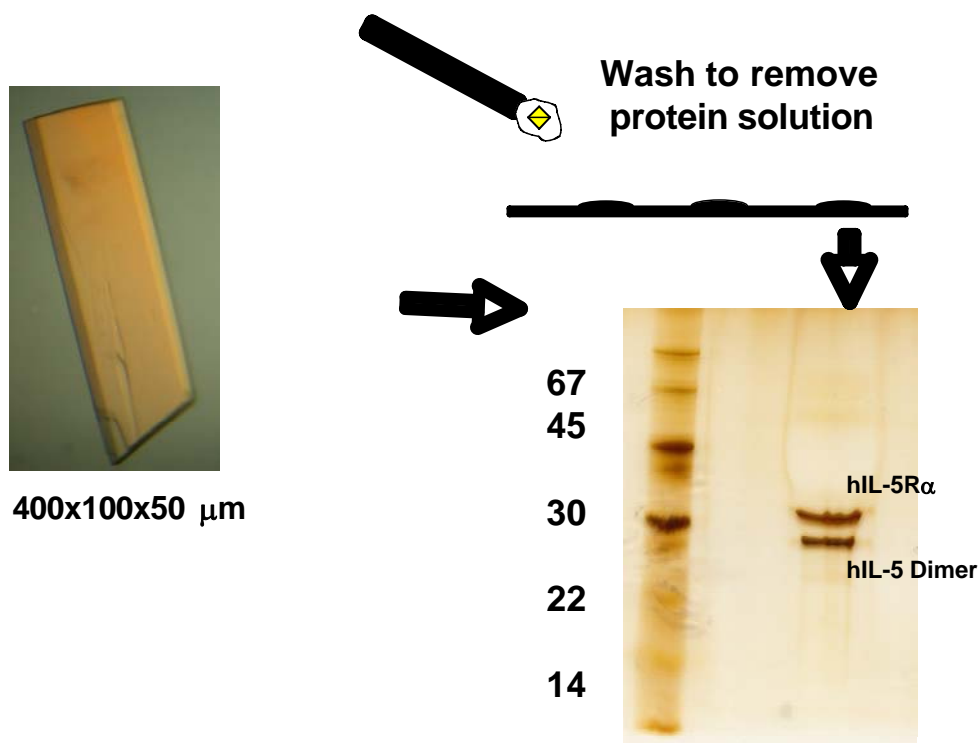


Figure 4-15. hIL-5R α /hIL-5 crystal content analysis. A SDS-PAGE silver stained gel revealed that the crystal consisted of hIL-5R α C66A/hIL-5. The crystal was washed three times in 0.1M MOPS pH 6.5, 10% PEG 20.000, 20% glucose and 2.5% MPD buffer, solubilized in SDS-sample buffer and analyzed onto a 12 % polyacrylamide gel.

The final data were collected from a single crystal (Se-hIL-5R α C66A/Se-hIL-5 complex) using a Cyclotron beam line (SLS, Switzerland). The data analysis of the selenomethionyl complex (Se-complex) showed the same space group and the same unit cell parameters as determined before. The preliminary data processing and refinement statistics for Se-complex are summarized in table 4-7.

Table 4-7. Data collection of hIL-5R α _{C66A}/hIL-5 complex

Crystal	hIL-5R α _{ECD} (C66A):hIL-5		
Space group	P2 ₁		
Cell constants	a = 85.13 Å, b = 61.03 Å, c = 139.64 Å $\alpha = 90.0^\circ$, $\beta = 97.98^\circ$, $\gamma = 90.0^\circ$		
Solvent content (% v/v)	57.23		
	Se-Met (λ 1)	Se-Met (λ 2)	Se-Met (λ 3)
Wavelength	0.97972	0.97955	0.90794
Resolution (Å) ^a	46.10-2.58 (2.67-2.58 Å)	38.71-2.64 Å (2.73-2.64 Å)	38.80-2.60 Å (2.69-2.6 Å)
	λ 1 (inflection)	λ 2 (peak)	λ 3 (remote)
Number of measurement reflections ^b	159539	165069	131037
Number of unique reflections ^b	86507	79327	79783
Completeness	98.8 (98.6)	96.7 (96.6)	90.2 (91.7)
R _{sym} for all reflections ^c	0.062 (0.464)	0.062 (0.440)	0.055 (0.399)
\langle intensity/ σ \rangle	6.8 (1.5)	7.2 (1.8)	7.7 (1.6)
a)	Numbers in parentheses indicate highest resolution shell		
b)	Cut-off for reflections $F > 0\sigma$		
c)	$R_{\text{sym}} = \sum_{hkl} I_{hkl} - \langle I_{hkl} \rangle / \sum_{hkl} \langle I_{hkl} \rangle$ where $\langle I_{hkl} \rangle$ is the mean intensity of symmetry related observations of a unique reflection		

The density map shows coherent density areas resulting from proteins, and empty areas occupied by water (Fig 4-16). Thus, at first glance, the electron density map revealed a crystal suitable for structure analysis. The structure of the hIL-5 could be easily placed into the electron density map confirming the presence of two molecules in the electron density (PDB file: 1HUL). The main feature of the hIL-5 is the four α -helices bundle patterns, which form a symmetric homodimer. The ribbon representation (green) of IL-5 in the electron density map shows its position in the unit cell (Fig 4-16). The structure of hIL-5R α C66A was partially traced by automated building/tracing routine using RESOLVE program.

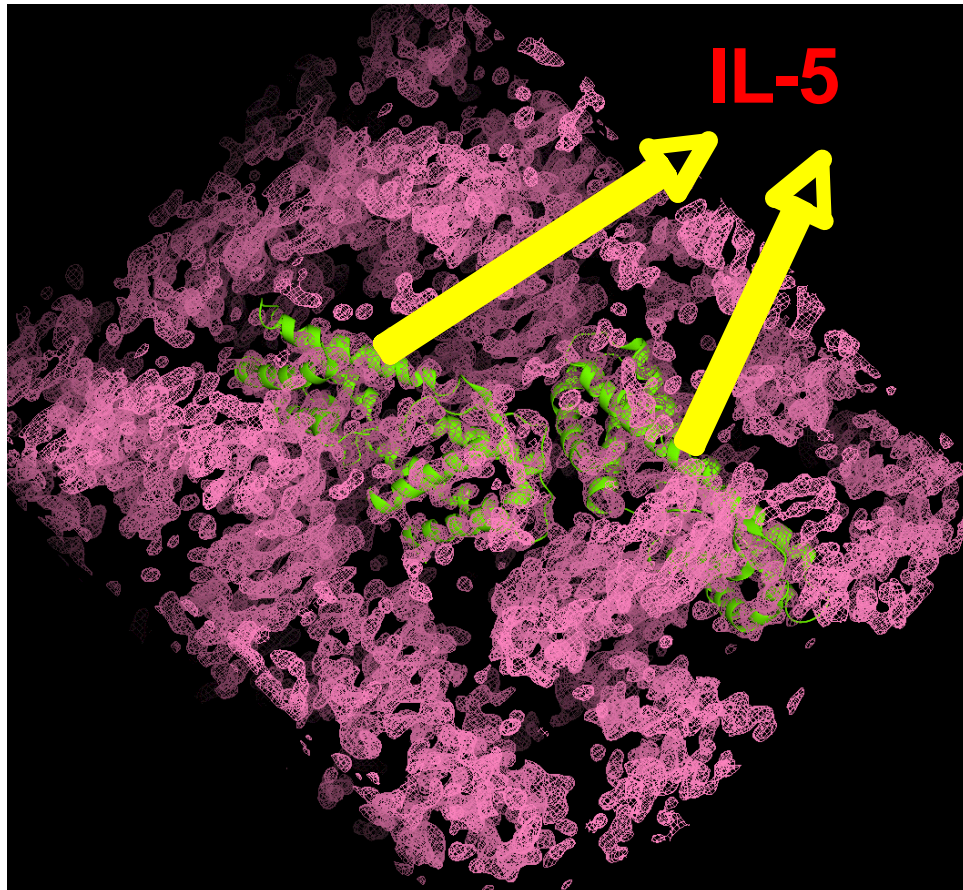


Figure 4-16. Electron density map of the hIL-5R α /hIL-5 complex. The electron density map displays density areas occupied by proteins (magenta) in which the IL-5 molecules (green ribbon) are placed, and empty areas corresponding to crystal solvent molecules that are not ordered.

The extracellular domain of the hIL-5R α C66A consists of three modules/domains, each comprising approximately 100 residues which are linked by loops. Each domain was described to contain a Fn-III like domain/motif (Bazan, 1990). The preliminary structure obtained from initial data analysis of the hIL-5R α C66A and hIL-5 complex demonstrated that hIL-5 binding requires the participation of all Fn-III like domains (Fig 4-17).

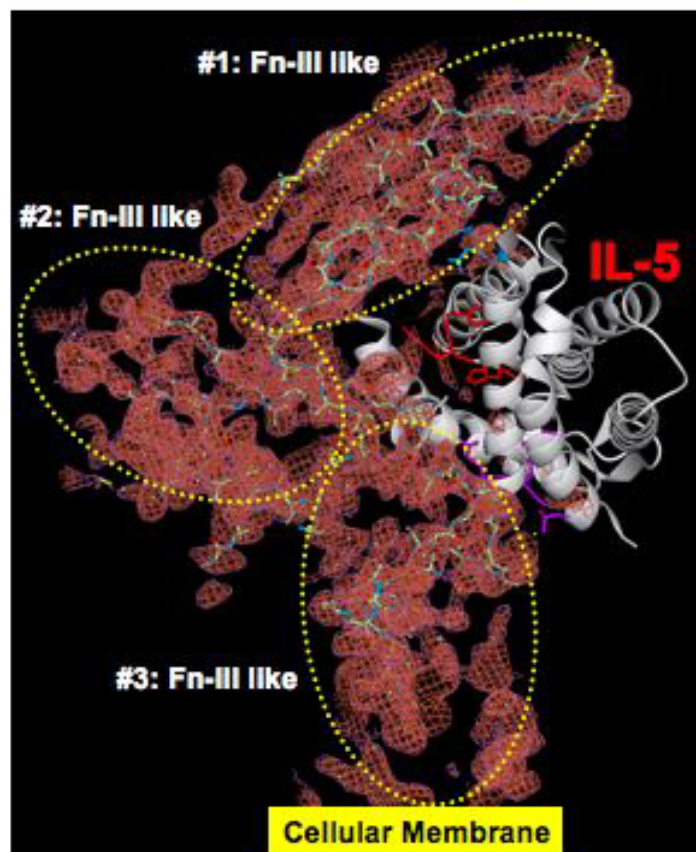


Figure 4-17. Schematic representation of the hIL-5R α C66A/hIL-5 complex. The initial trace of the complex in the electron density map shows the three Fn-III domains (labeled with numbers 1, 2 and 3) of the receptor appearing in contact with IL-5. The C-terminus of the receptor is in proximity to the cellular membrane. The N-terminus is at the top of the figure.

This finding is in agreement with previously reported results which provided evidence by use of site directed mutagenesis and interaction analysis that two clusters contain the crucial residues required for the interaction with hIL-5 (Ishino et al., 2005). In particular, the mutagenesis studies showed that the first cluster consists of residues Asp55 and Tyr57 of the first Fn-III like domain, whereas the second cluster is formed by residues Ile183 and Arg188 of the second Fn-III like domain and Arg297 of the third Fn-III like domain, respectively (Ishino et al., 2005).

Our preliminary results of the hIL-5R α C66A/hIL-5 complex structure demonstrate a unique binding topology in which the participation of all three Fn-III like domains of the IL-5R α is required for binding of IL-5. Hence, the three Fn-III like domains of the receptor appear to form a cytokine binding cleft to accommodate

the IL-5. Further refinement of the structure is currently ongoing, in order to reveal more details of the molecular hIL-5-hIL-5R α interaction.

On the ligand side, three regions are supposed to be in contact with the receptor (Fig 4-17), thus confirming the results of the mutagenesis studies of IL-5 (Graber et al., 1995; Tavernier et al., 1995b). These three interaction regions of IL-5 are located in the β -sheet 2 (Glu89 to Arg91), in the loop between β -sheet 1 and α -helix B (His38, Lys39 and His41), and at the C-terminal end of α -helix D (Thr109, Glu110, and Trp112). The mutant variants in which Ala replaced these residues confirmed their crucial function in binding. These mutants reduced the binding behaviour and activity as determined by interaction analysis and cell-based assays (Graber et al., 1995; Tavernier et al., 1995b)

Taken together, this result suggests that the binding interface between hIL-5R α /hIL-5 in the dimeric complex is composed of: (i) the interaction between the first Fn-III domain residues Asp55, Asp56 and Glu58 of the hIL-5R α with the residues Glu89 and Arg91 of IL-5; (ii), the second Fn-III domain residue Arg188 of the receptor with His38, Lys39 and His41 of IL-5, and (iii), the third Fn-III domain residue Arg 297 of the receptor with Thr109, Glu110 and Trp112 of IL-5 (Figure 4-17). The data of the crystal structure are absolutely in line with all the previously published mutations on the hIL-5R α or hIL-5.

The knowledge of the hIL-5R α C66A/hIL-5 complex structure also gives an explanation for the unexpected 1:1 stoichiometry of the hIL-5R α /hIL-5 complex. The hIL-5R α interaction site is spread over the dimer interface and, as a consequence, only one hIL-5R α can bind to each hIL-5 dimer (Devos et al., 1993; Johanson et al., 1995). A possible second binding site on IL-5 appears to be blocked by the first receptor. Additionally, the residues of IL-5 in contact with the residues N-terminal to C-terminal of the hIL-5R α are on the opposite side of each IL-5 monomer (see Fig 4-18 yellow arrow for the second receptor). This suggests that, if a second hIL-5R α molecule binds, this molecule is derived from a second cell, leading to a sandwich structure, in which IL-5 being is shared (sandwiched) between the two cells (Figure 4-18, see red arrow for the second receptor). So far, this possible cell organization has only been observed during the interaction of antigen presenting cells and T-cells.

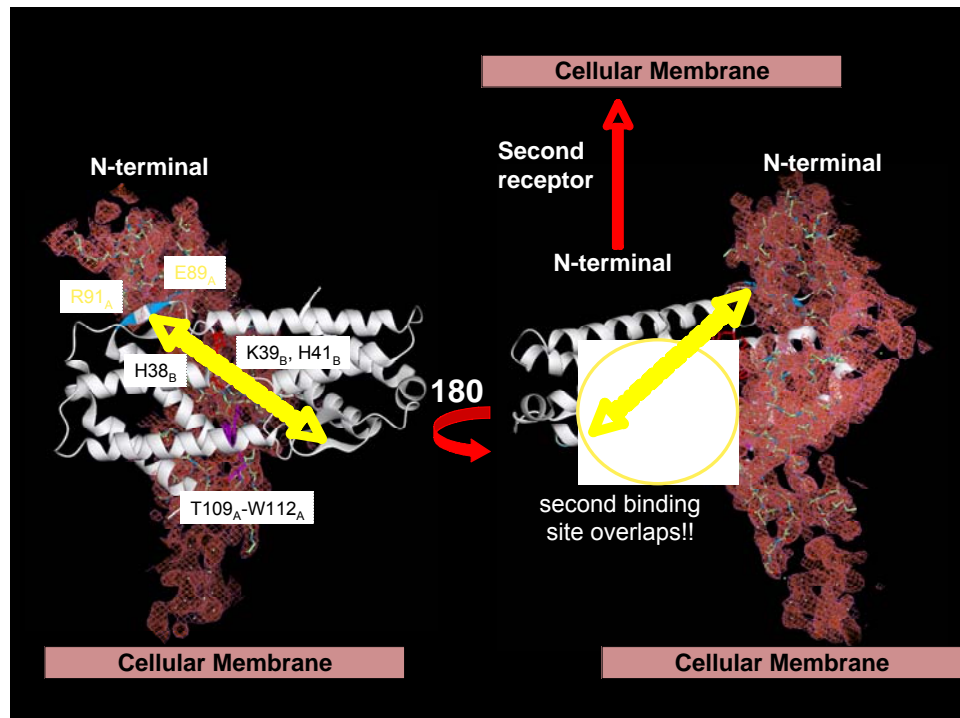


Figure 4-18. Stoichiometry of the hIL-5R α /hIL-5 complex. The location of the hIL-5 residues in contact with hIL-5R α C66A (yellow arrows). The hIL-5R α C66A binds the ligand in the center of its homodimeric structure (left) and in this way leads to a blockade of the second binding site by the first bound receptor molecule (right). The red arrow indicates the hypothetical direction of the second receptor.

In conclusion, this is the first experimental approach so far which presents the crystal structure of the binary complex of the hIL-5R α _{ECD} with hIL-5 at a resolution of 2.5 Å. This structural data may lay the ground to study the molecular architecture of both proteins and depict the molecular assembly of the complex required for signal transduction.

4.2 Structural studies of the mouse interleukin-5

4.2.1 Expression, refolding and purification of mouse IL-5 (mIL-5)

So far, there are no reports available on the structure of the mIL-5 protein expressed in *E. coli*. The first approach was to amplify the cDNA by PCR using the wt-mIL-5.wt-BiP (pMT/V5-HisA) as template and specific oligonucleotide primers (3.7). The PCR products were digested (3.8.1) with restriction enzymes (Nco I and BamH I) and cloned into different expression vectors such as pET-3d, pET-28b (Novagen)

and QKA (Qiagen). Transformed Rosetta cells with each vector failed to express wild type mIL-5. The first 10 or 20 residues on mIL-5 were subsequently replaced by their respective human counterpart residues. However, these chimeric mIL-5 molecules also failed to be expressed in the bacterial expression system.

The cDNA that encodes the wt-mIL-5 was cloned into pET-32a and pET-44a vectors to express mIL-5 as a fusion protein with thioredoxin or NUS A, respectively. AD 494 or Rosetta cells were transformed with pET-32a/wt-mIL-5 and pET-44a/wt-mIL5, respectively, and the cells were grown in TB medium. Wild type mIL-5 was expressed in fusion with thioredoxin- or NUS A protein after IPTG induction and the fusion protein accumulated in inclusion bodies (IB). The inclusion bodies were solubilized with high concentrations of guanidinium hydrochloride and the fusion protein was recovered under denaturing conditions with 6 M guanidinium hydrochloride (GuHCl). The digestion of the fusion protein with thrombin or enterokinase proteases was unsuccessful, because GuHCl denatures the protease. As consequence, chemical cleavage was chosen, in order to digest the fusion protein, and this cleavage could be performed under denaturing conditions. One of the most frequently used reagents for chemical cleavage is cyanogen bromide (CNBr). CNBr cleaves specifically C-terminal of Met residues using acidic conditions such as 70-80% formic acid.

The mIL-5 contains 6 methionine residues (Met 1, Met 5, Met 29, Met 65, Met 105, and Met 111, according to mIL-5 numbering). Multiple sequence alignments of IL-5 were performed with 6 different species (Fig 4-19). Several interesting substitutions were observed on the IL-5 sequence level between the different species. The sequence alignments showed that these methionine residues are not conserved in the different species (Fig 4-19). Thus, these observations were taken as a useful starting point to decide which residues could be used for the replacement of the methionine residues on mIL-5. Any Met residue of IL-5 was shown to participate in receptor binding.

Sequence alignment also showed the amino acid counterpart of the six mIL-5 methionines in hIL-5. To generate a methionine deficient mIL-5 protein, We replaced five mIL-5 methionines by the respective amino acid of hIL-5. The mutations generated were M5T, M29L, M65R and M111I. The only conserved methionine (M105L) was mutated to leucine. Mutations were performed in pET-32a/mIL-5, which was used as template DNA for PCR (3.7.2). The clones obtained

were verified by DNA-sequencing using DTCS Quick Start kit. The resulting variant is referred to as mIL-5^{nullMet}.

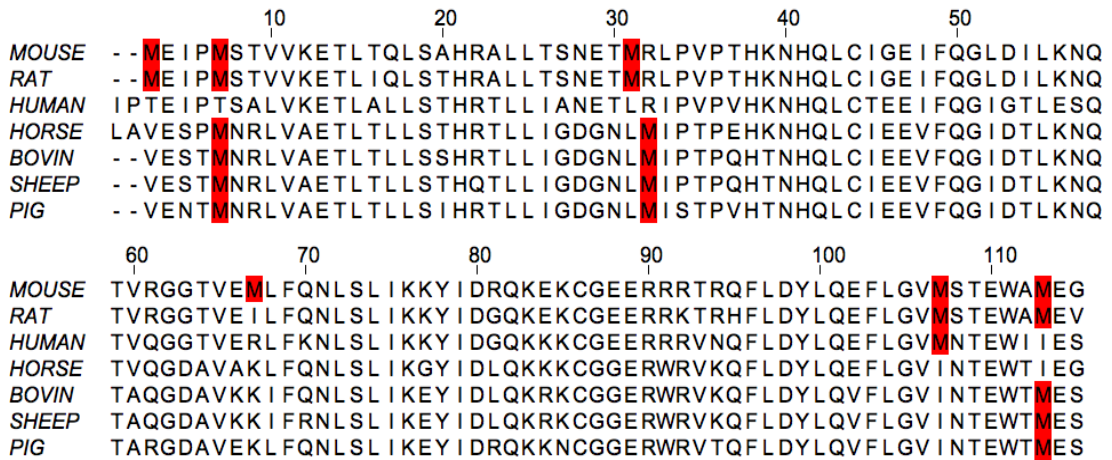


Figure 4-19. Sequence alignment of IL-5 from six different species. Methionine positions are shown in red. The sequence alignment was performed using the program JalView (Clamp et al., 2004).

Expression and purification of the protein was carried out as described for hIL-5 using the pET-32a/mIL-5^{nullMet} and AD 494 (DE3) *E. coli* strain. The expression of Trx-mIL-5^{nullMet} fusion protein was confirmed by SDS-PAGE showing a major band of approximately 26 kDa corresponding to the molecular weight expected for Trx/mIL-5^{nullMet}. Subsequently, CNBr cleavage of denatured Trx-mIL-5^{nullMet} was performed under acidic conditions (80 % formic acid). Cleaved protein was dialyzed in GuHCL buffer for 48 hours. Later on, the protein was loaded onto Sephacryl 200 column to purify the mIL-5 monomer from any remaining bacteria components and peptides derived from bacterial proteins and thioredoxin (3.13). Protein refolding was performed using the same parameters and conditions as for hIL-5. After protein renaturation, the mIL-5 was loaded onto S200 column using Tris-HCl buffer (3.13.4), but surprisingly the elution profile of refolded mIL-5^{nullMet} was totally different to that of hIL-5. The SDS-PAGE analysis showed that the mIL-5 dimer did not elute as a pure fraction. Different peptides possibly derived from thioredoxin were found after CNBr cleavage. Further chromatography purification steps implemented to remove these peptides were unsuccessful.

We took advantage of the pET-31b vector as it harbours a unique *A*lwn I cloning site allowing the unidirectional insertion of several tandem-coding regions.

The fusion protein (ketosteroid isomerase) does not have internal methionine and, thus, does not produce additional peptides after CNBr cleavage (Fig 4-20). The mIL-5^{nullMet} was cloned into the pET-31b vector and expressed as a fusion protein with bacterial ketosteroid isomerase (KSI) under the same conditions used before (3.11).

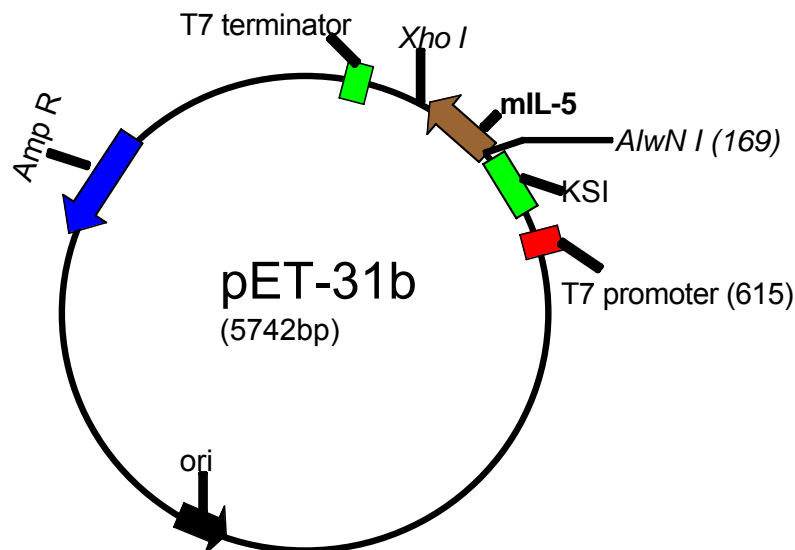


Figure 4-20. Schematic representation of the pET-31b/mIL-5^{nullMet} vector. The cDNA of mIL-5^{nullMet} (brown) was cloned between AlwNI and XhoI restriction sites. T7 promoter is used for KSI/mIL-5 transcription. pET-31b carries Ampicillin resistance gene. The KSI is shown in green.

After IPTG-induced protein expression, a band of approximately 26 kDa molecular weight appeared corresponding to the KSI/mIL-5^{nullMet} fusion protein (Fig 4-21, lane 2). The fusion protein was exclusively targeted into inclusion bodies (Fig 4-21, lane 4). Cells were sonicated and inclusion bodies were prepared following the protocol of Hoppe and collaborators (3.12.2) (Hoppe et al., 1989; Hoppe et al., 1990). The fusion protein isolated from inclusion bodies was precipitated with acetone and subsequently dissolved in 80% formic acid. The fusion protein was chemically cleaved with CNBr at the single Met residue between KSI and mIL-5 (Fig 4-21). After protection of the thiol groups by S-sulfonation with Na₂SO₃ and Na₂S₄O₆ (Hoppe et al., 1989; Hoppe et al., 1990), mIL-5^{nullMet} monomers were purified by S200 column under denaturing conditions (Fig 4-21, lanes 5-7). Refolding (3.13.3) and purification (3.13.4) of the mIL-5^{nullMet} dimer was performed under identical conditions as for hIL-5. No additional peptides could be observed

after CNBr cleavages. The mIL-5^{nullMet} represented a final yield of about 2-3% of refolded protein (2-4 mg/L).

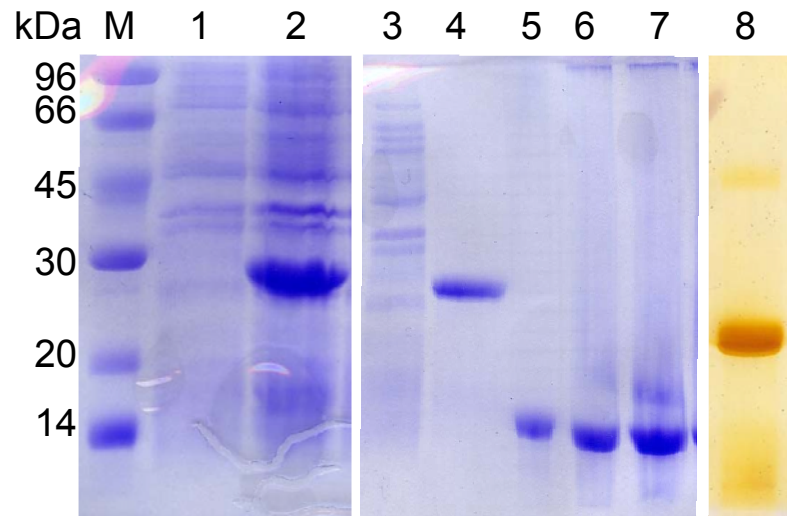


Figure 4-21. Expression of mouse IL-5^{nullMet} in *E.coli* Rosetta cells (red oval). Protein expression was induced with 1 mM IPTG for three hours. Protein was analyzed on 12% SDS-PAGE. The gel shows: lane M; the protein marker, lane 1; non-induced cells, lane 2; IPTG induction of fusion protein (3 hours), lane 3; supernatant after washing of inclusion bodies (IB), lane 4; protein main-extraction of IB, lanes 5-7; fractions from gelfiltration after CNBr cleavage, and lane 8; mIL-5^{nullMet} dimer. Proteins were separated by reducing (lanes 1-7) and non-reducing (lane 8) SDS-PAGE and stained with Coomassie Blue (lanes 1-7) or silver staining (lane 8).

The hIL-5 E13Q is an antagonistic mutant that causes a reduced activation of the hIL-5 receptor. The Glu13 of IL-5 is highly conserved in different species (Figure 4-19). Based on the hIL-5 data, we engineered an antagonist molecule targeted against mIL-5 by replacing Glu13. The mIL-5^{nullMet} E13Q variant was generated by PCR mutagenesis using the cDNA of mIL-5^{nullMet} as template (3.7.1). mIL-5^{nullMet}E13Q cDNA was used to transform Rosetta *E.coli* cells as described for mIL-5^{nullMet} variant protein. This protein was expressed, and refolded under the exactly same conditions utilized for mIL-5^{nullMet}. Surprisingly mIL-5^{nullMet}E13Q precipitated during the concentration step almost completely.

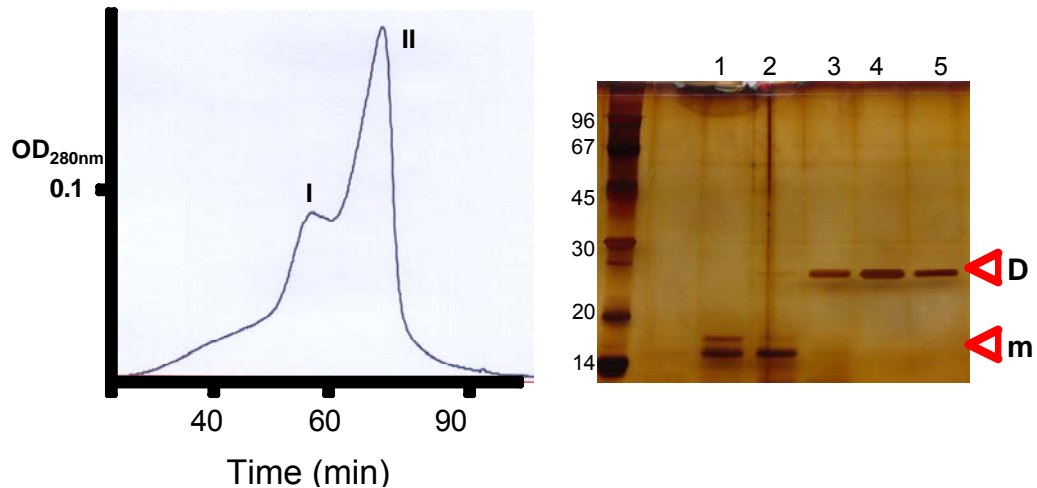


Figure 4-22. Purification of mIL-5^{nullMet} E13Q. Chromatogram of gel filtration chromatography using Superdex 75 (left). The flow rate was controlled a 0.25 ml/min. SDS-PAGE analysis shows: momomers (lanes 1 and 2) and dimer (lanes 3-5) from the peak I and peak II, respectively. Proteins were separated by non-reducing SDS-PAGE and stained with silver staining. The protein dimer is indicated by D and the protein monomer by m.

The remaining soluble mIL-5^{nullMet} E13Q protein was applied to Superdex 200 column (preparative grade, 16/60), in order to eliminate monomeric protein and high molecular weight aggregates. Usually after this chromatography, the IL-5 dimer was eluted as a pure fraction as observed in the case of wt-hIL-5 and mIL-5^{nullMet}. However, in this case, the mIL-5^{nullMet} E13Q dimer did not appear highly pure. It was concluded that the impurities could not be eliminated by anion exchange or RP-HPLC. The mIL-5^{nullMet} E13Q dimer was then purified using analytical superdex 75 column. 200 μ l of concentrated mIL-5^{nullMet} E13Q were applied to FPLC analytical superdex 75 column (3.13.4.2). The chromatogram profile showed that the monomeric protein was eluted in the first peak (see chromatographic peak I on Figure 4-22) and the mIL-5^{nullMet} E13Q dimer was eluted in the second peak (see chromatographic peak II on Figure 4-22). SDS-PAGE analysis confirmed that the mIL-5^{nullMet} E13Q dimer was obtained as a pure fraction. This unexpected elution profile using the analytical Superdex 75 is possibly due to an total unfolding state of mIL-5 monomers. The concentration of the protein was estimated by coomassie blue staining of the gel against known/defined concentrations of hIL-5, since the UV-spectrum did not show a regular UV-spectrum of a protein. The mIL-5^{nullMet} E13Q yield was 50 μ g for each 100 mg of refolded protein (50 μ g/L of cell culture).

In order to compare if mIL-5 E13Q mimics the known antagonistic effect of hIL-5 E13Q (Graber et al., 1995; McKinnon et al., 1997; Tavernier et al., 1995b), The hIL5 E13Q antagonist variant was generated by cycle PCR using the cDNA of wt-hIL-5 as a template. Human IL-5 E13Q cDNA was cloned into the pET-3d vector using Nco I and BamH I restriction sites (see Fig 4-1) and the resulting vector was used to transform *E.coli* cells. Expression, renaturation and purification were carried out under the same conditions used for hIL-5 (3.13.2 and 3.13.3). The yield of the IL-5 E13Q mutant was 2-4 mg/L of cell culture.

4.2.2 Biological activity assay

The biological activity of recombinant mIL-5^{nullMet}, mIL-5^{nullMet} E13Q, wild type hIL-5 and hIL-5 E13Q was examined using cell proliferation assays (3.14.6). The human erythroleukemia cell line (TF-1) was established from the bone marrow of a patient with erythroleukemia. This disease is characterized by erythroblastic and leukoblastic tissue proliferation (Kitamura et al., 1989). TF-1 cells grow in the presence of different cytokines including IL-5 (Kitamura et al., 1989).

The TF-1 cells were shown to proliferate when incubated in the presence of hIL-5 or mIL-5^{nullMet} (Fig 4-23). The TF-1 cell proliferation was monitored by measuring DNA synthesis by [³H] thymidine incorporation (Fig 4-23). Our results confirm previous findings which have shown that mIL-5 is active in human cells (Cornelis et al., 1995; Kitamura et al., 1989; Kodama et al., 1991; McKenzie et al., 1991a). The concentration of hIL-5 or mIL-5^{nullMet} required for the half-maximal proliferative response (EC₅₀) was <17 and <200 pM, respectively. The EC₅₀ of both cytokines were close to those values reported in the literature. Additionally, the EC₅₀ value shown for mIL-5^{nullMet} was similar to the EC₅₀ value (<180 pM) of commercially available mIL-5 expressed in insect cells (R&D systems). The proliferation of TF-1 cells with mIL-5^{nullMet} also demonstrates for the first time that the glycosylation moiety of mIL-5 is not required for biological activity as it was similarly shown for hIL-5.

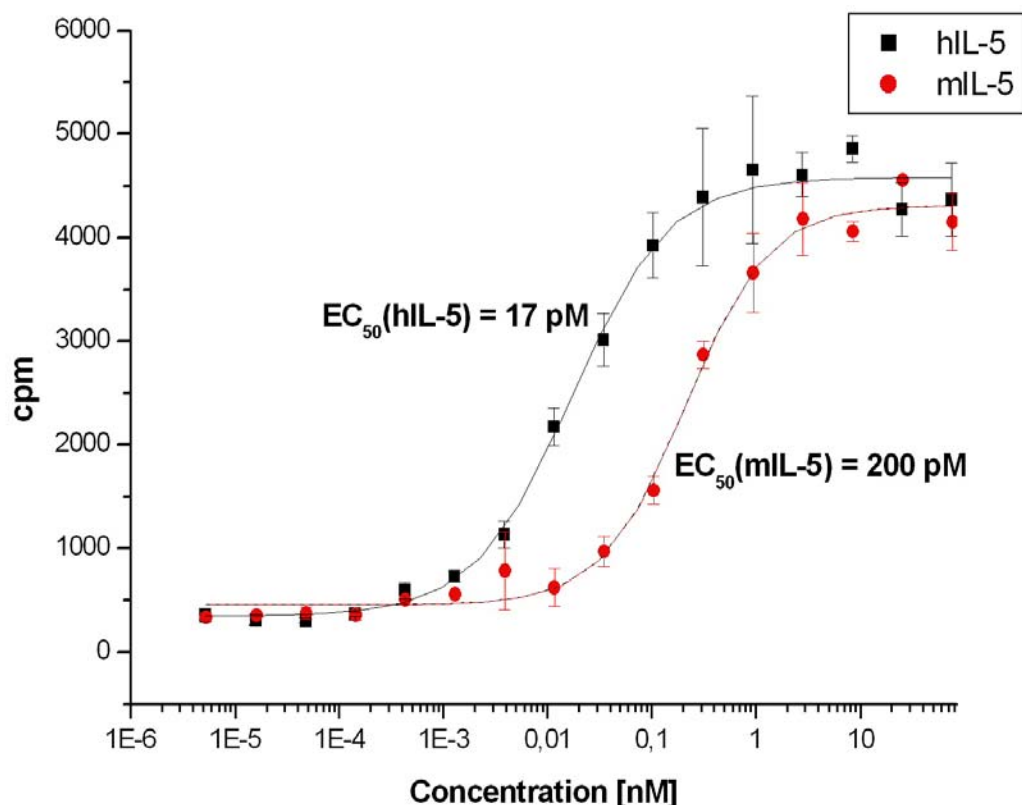


Figure 4-23. Proliferation of the TF-1 cells by IL-5. The ability of hIL-5 or mL-5nullMet causes proliferation of TF-1 cells in a dose-dependent manner. EC₅₀ values were calculated by Origin program. Data are shown from three independent experiments.

The TF-1 cells were also used to evaluate the antagonistic ability of hIL-5 E13Q from *E. coli* in proliferation assays. The TF-1 cells did not proliferate in the presence of this protein, although high protein concentrations were used. When the TF-1 cells were cultured in the presence of a fixed concentration of wt-hIL-5 (2 nM) and serial dilutions of hIL-5 E13Q, hIL-5, the molecule E13Q was capable to confer a complete antagonist effect with a half maximal inhibition concentration IC₅₀ of 0.7 nM (Figure 4-24). Our IC₅₀ (0.7 nM) was relatively similar to the IC₅₀ previously reported by Tavernier and colleagues (0.3 nM) (Tavernier et al., 1995b). The inhibition properties of the hIL-5 E13Q are based on its incapacity of activate the TF-1 cells through the IL-5 receptor, although hIL-5 E13Q presented the same interaction and the same affinity constant with hIL-5R α as those of wt-hIL-5 (Tavernier et al., 1995b).

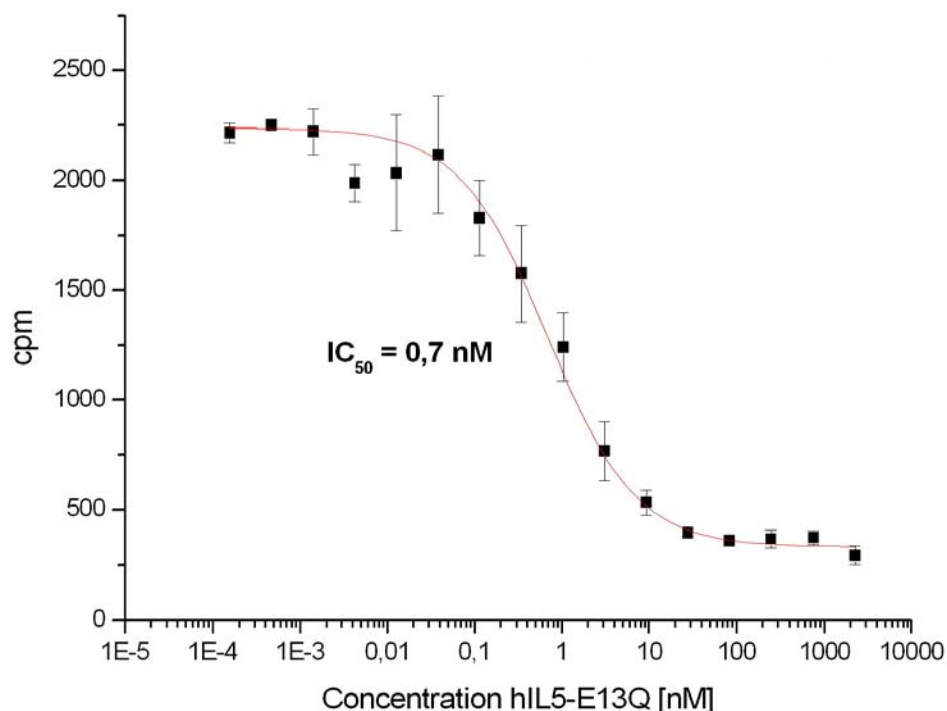


Figure 4-24. Analysis of human IL-5 E13Q on TF-1 cells. The graphic shows the half maximal inhibition concentration (IC_{50}). TF-1 proliferation was measured by [3H] thymidine incorporation for serial dilutions of mutant E13Q. Data are shown from three independent experiments.

The fusion protein of KSI/mIL-5^{nullMet} E13Q was well expressed in the bacterial system and the mIL-5^{nullMet} E13Q antagonist could be purified after CNBr cleavage. But the mIL-5^{nullMet} E13Q dimer was very difficult to purify after renaturation and the yield obtained was very low. The low amounts did not allow a further analysis of the possible antagonistic properties in TF-1. Therefore, in this case, the corresponding biological assay could not be performed.

4.2.3 Crystallization of mIL-5^{nullMet} variant

Crystallization trials were performed using a fine screen of the crystallization conditions published for hIL-5 (Graber et al., 1993; Hassell et al., 1993; Milburn et al., 1993). In addition, conditions of commercial crystal screen 1 and 2 (Hampton) were used. The mIL-5^{nullMet} protein was found to precipitate in most of the individual setups of either two screening kits (Crystal screen 1 and 2).

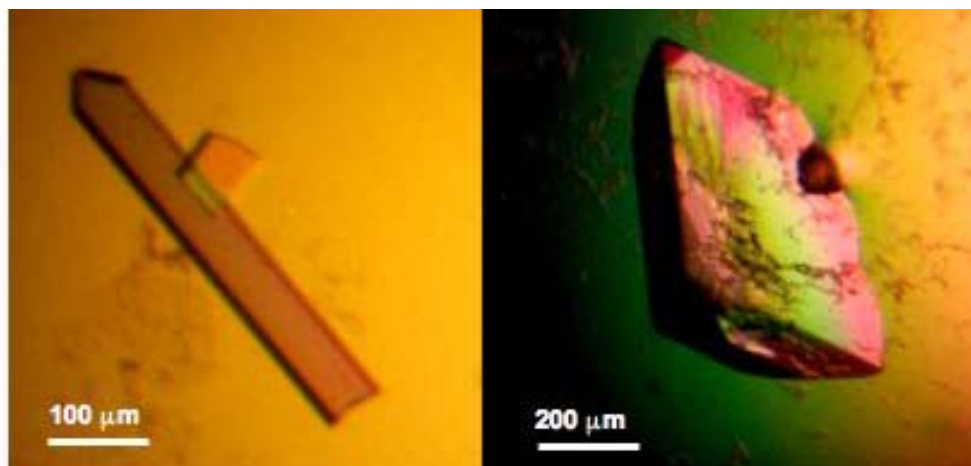


Figure 4-25. Crystals from mL-5^{nullMet} (left) or hIL-5 (right). Both proteins crystallized in the same setup (100 mM Tris-HCl pH 8.5, 210 mM sodium acetate, 24% PEG 4000). Crystals exhibit different morphology. The diffraction limits were 2.5 Å and 2.7 Å for mL-5^{nullMet} (left) and hIL-5 (right), respectively.

Hence, mL-5^{nullMet} was crystallized under the same crystallization conditions reported for the crystallization of hIL-5 (Graber et al., 1993; Hassell et al., 1993; Milburn et al., 1993). The setup for mL-5^{nullMet} was 100 mM Tris-HCl, pH 8.5, different concentrations of PEG 4000 (22-26 %), and sodium acetate (0.2-0.23 mM) at room temperature. The crystallization set up was performed by the hanging drop vapor diffusion method. Each hanging drop contained 1 μl of protein (5-8 mg ml⁻¹) and 1 μl of reservoir solution. Crystals grew from almost all setups after 5 days, but an elevated PEG 4000 concentration resulted in larger and more three dimensional crystals. For the X-ray analysis, crystals were grown from 100 mM Tris-HCl, pH 8.5, 26 % PEG 4000, and 0.21 mM sodium acetate with protein concentration of 6.0 mg ml⁻¹. The morphology shown for the mL-5^{nullMet} crystal was different to that of hIL-5 crystallized in the same buffer (Fig 4-25).

4.2.4 Structure of mL-5^{nullMet} variant

A flash-frozen crystal was mounted onto a nylon loop and a full dataset was acquired on Rigaku Micro Max 007 equipped with VariMax HighRes optics. A native dataset of 360° images was collected at 100 K from a single crystal grown from 0.1 M Tris pH 8.5, 26% (v/v) PEG 4000, 0.21 M sodium acetate. The crystal to detector distance was set to 130 mm and each frame had exposure times of 180 sec for 1°

oscillation. The dataset was processed using the software package Crystal Clear. The crystals belong to the monoclinic space group $P2_1$ with unit cell parameters $a = 39.19 \text{ \AA}$, $b = 47.08 \text{ \AA}$, $c = 55.05 \text{ \AA}$, $\alpha = 90^\circ$, $\gamma = 90^\circ$, and $\beta = 96.41^\circ$. Calculation of the Matthews coefficient suggested either the presence of an IL-5 monomer in the asymmetric unit requiring the two-fold screw axis to overlap with the two-fold symmetric of the IL-5 dimer, or the presence of the complete IL-5 dimer in the asymmetric unit.

The latter would result in rather tight packing with a relatively low solvent content in the crystal. Self-rotation function using the software GLRF suggested the presence of a two-fold non-crystallographic symmetry indicative for the IL-5 dimer present in the asymmetric unit. Molecular replacement using the software Phaser and the PDB file of hIL-5 (PDB 1HUL) as an input model were employed to solve the structure of mIL-5^{nullMet}. The initial analysis confirms the mIL-5^{nullMet} structure as a symmetrical homodimer. A full dimer was found in the asymmetric unit resulting in a low solvent content of 37% in the crystal. This low solvent content reveals that the molecules of mIL-5^{nullMet} are densely packed. The data processing and refinement statistics for mIL-5^{nullMet} are summarized in table 4-8.

The overall dimension of the mIL-5^{nullMet} structure is about $57\text{\AA} \times 21\text{\AA} \times 19 \text{ \AA}$ (Fig 4-26). The monomer subunit is composed of four α -helices and two β -sheets (β). Analysis of the crystal structure shows that mIL-5 forms the expected left-handed four helical bundle. As it holds true for hIL-5, the mIL-5 exists as an intertwined dimer with three helices A, B, and C provided by one chain and helix D coming from the second chain (Figure 4-26). The N- and C-terminal are disordered in the structure and are probably flexible. The arrangement and location of the secondary structure elements of mIL-5 are similar to hIL-5, all α -helices exhibit similar length (helix A: Val8-Ser25; helix B: His39-Glu56; helix C: Thr62-Gly85; helix D: Thr91-Leu107).

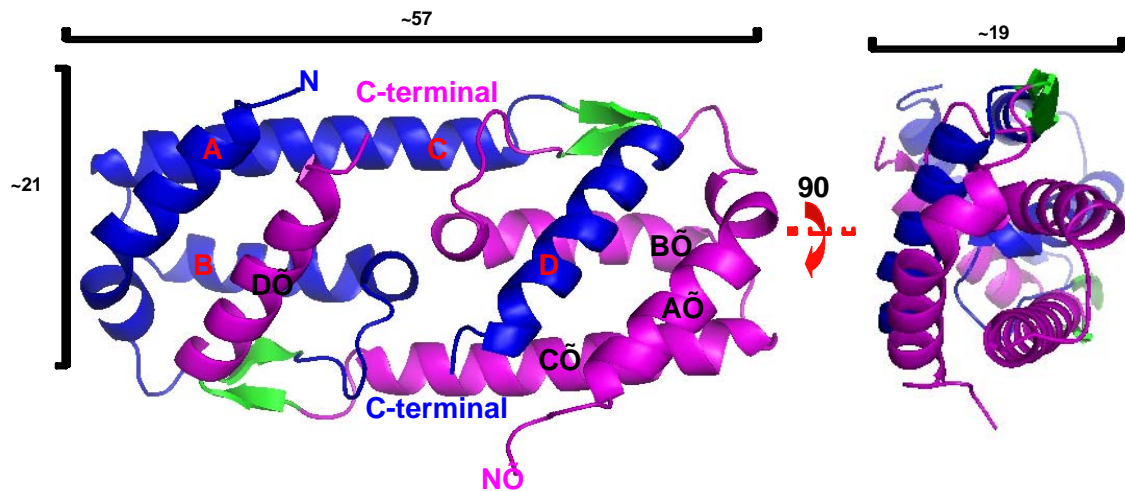


Figure 4-26. Structure of the mIL-5^{nullMet}. The monomers are shown in blue and magenta. Each monomer consists of four helices A-D and A'-D'. The β_1 -strand connects the helices A and B or A' and B', and β_2 -strand connects the helices C and D or C' and D' (green). The N-terminus (N) is found in the start of helix A or A', and C-terminus (CO) is in the end of helix D or D'.

The two β -sheets are formed by residues Arg32 to Pro34 (β_1) and Glu89 to Arg91 (β_2). The β -sheet 1 is tightly packed against the hydrophobic core of the four helices bundle, with the C-terminal of the Arg32 residue involved in hydrophobic interaction with residues of helix B, i.e., Gly51, Ile54 and Leu55. The β -sheet 2 is located at the solvent-accessible surface. The exposed residues Glu89 to Arg92 were found to be important for binding to IL-5R α . Interestingly, the residues in the β -sheet 2 are highly conserved in mIL-5 and hIL-5. This is in contrast, to the residues in β -sheet 1 which are not conserved.

Since the full mIL-5 dimer is located in the asymmetric unit, dimer symmetric or its absence can yield valuable insights into the flexibility of the mIL-5 molecule. By superimposing the two-monomer subunits it can be seen that the backbone of the two monomeric subunits is basically identical (r.m.s. deviation is 0.5Å for 208 C α atoms), only the C-termini (helix D) and the N-termini (helix A) deviate significantly.

Of the 74 water molecules observed in the mIL-5 structure only three molecules occupy identical positions in both monomers. These water molecules are located in a hydrophobic environment between helices B and C and form a

hydrogen-bond network connecting the carbonyl oxygen of Phe49 and Phe69. They are shielded from the access of bulk solvent by the residues Lys56 and Lys76.

Table 4-8. Data processing and refinement statistics for mIL-5^{nullMet}

A. Data processing		
Space group	P2 ₁	
Cell constant	a = 39.19 Å, b = 47.08 Å, c = 55.05 Å $\alpha = 90.0^\circ$, $\beta = 96.41^\circ$, $\gamma = 90.0^\circ$	
	Low	High
Resolution (Å)	50.0-2.55	2.62-2.55
No unique reflections	5940	435
Completeness (%)	94.63	91.77
B. Refinement statistics		
R _{free} (%)	25.7	22.4
R _{crys} (%)	21.0	22.1
Solvent content (% v/v)	37.0	
PROCHECK analysis		
Residues in most-favored regions (%)	88.9	
Residues in additional allowed region (%)	21.0	
Residues in generously allowed region (%)	0.0	
Residues in disallowed region (%)	0.0	

In summary, the structure of mIL-5^{nullMet} is well defined, with exceptions of the N-terminal residues Glu2 to Ser6, and the C-terminal residues Trp108 to Glu113 indicating that the N and C-termini are not ordered and likely flexible. The final model of mIL-5^{nullMet} has a good overall stereochemistry with 169 residues (88.9 %) in most the favorable region of the Ramachandran plot (PROCHEK) and no residues in the disallowed regions (Table 4-8).

5 DISCUSSION

5.1 Production of recombinant mouse IL-5 in *E. coli*

Airway hyperresponsiveness is a hallmark of asthma pathogenesis, which occurs as a consequence of tissue damage due to the accumulation of large numbers of eosinophils within the airways (Enokihara et al., 1990; Magnan and Vervloet, 1998). Different cytokines and chemokines are crucially involved in this process. IL-5 influences the development of eosinophils at the bone marrow level and increases the number of eosinophils within the inflammation area (Kay, 2005; Wills-Karp and Karp, 2004). Different strategies to ablate eosinophil populations have shown that these cells constitute an integral part of experimental allergic asthma development (Humbles et al., 2004; Lee et al., 2004). Animal models that mimic allergen-airway remodeling has proven to be a valuable tool to study this disease condition.

The murine model exhibits the same pulmonary pathogenesis as observed in human asthma. Mice display allergen induced eosinophilia (Hogan et al., 2003) and eosinophil accumulation leads to airway and bronchial hyperresponsiveness (Cho et al., 2004). Although other animal models are also available for the study of the pathophysiology of asthma, the extensive use of mice in immunological research provides a clear advantage for the analysis of the molecular mechanisms underlying this disease. In addition, the availability of a wide range of different transgenic and knockout mice, together with the availability of athymic nude mice, provides excellent *in vivo* systems to study the molecular mechanisms of tissue inflammation. However, there is no report on the expression of murine IL-5 in *E. coli*. Prokaryotic expression system looks more promising for the analysis of factors involved in asthma than eukaryotic expression system, due to its considerably cheaper production costs.

Our objective was to find a suitable protocol for the cloning, expression, fermentation and purification of mouse IL-5 which could serve as basis for large-scale production processes. At the same time, this protocol could also be used for the production of antagonistic molecules. The obtained mouse IL-5 could then be used in mouse trials and structural studies.

The initial approach consisted in the cloning of the mouse IL-5 cDNA into the commercial expression vectors pET-3d and pET-28b. Although the mouse IL-5 was cloned with NH₂-terminal tags of different length or without tags, respectively,

expression of a recombinant protein failed. In addition, different chimeric murine/human IL-5 constructs were tested. The cDNA encoding for the first 10 and 20 residues of mouse IL-5 was replaced by those of human IL-5, but the expression of these IL-5 chimeras in bacteria did also fail. Different factors that influence protein expression in *E.coli*, such as codon usage, secondary structure of the mRNA and stability of the mRNA are well known and may represent a limiting factor in recombinant protein expression (Jana and Deb, 2005; Kane, 1995; Schlax and Worhunsky, 2003).

The fusion of cytokines with *E. coli* proteins, such as thioredoxin, has become a suitable tool for protein expression. In our approach, thioredoxin was used as a fusion partner, because it can be overexpressed in bacteria without the formation of inclusion bodies (LaVallie et al., 1993). The mouse IL-5 was highly expressed in fusion with thioredoxin using the pET-32a vector. But the fusion protein accumulated in inclusion bodies, probably due to the dimeric nature of mouse IL-5. These inclusion bodies were solubilized using GuHCL (guanidinium hydrochloride), β -ME and EDTA, thereby preventing a proteolytic cleavage. Thus, a different strategy was required for the expression of the fusion protein of mouse IL-5 together with a chemical cleavage that could be performed under denaturing conditions.

Different reagents as 3-bromo-3-methyl-2 (2-nitrophenylmercapto)-3H-indole (BNPS-Skatole), 2-Nitro-5 thiocyanobenzoic acid (NTCB) and cyanogen bromide (CNBr) have been used for chemical cleavage of proteins under denaturing conditions. The reaction is carried out in acetic acid (70-80%), alkaline conditions (Tris, pH 8.5-9.0) or formic acid (70-80%), respectively. They are often accompanied by side reactions such as oxydation of tyrosine and histidine residues (BNPS-Skatole), cyanylation of the thiols groups (NTCB) and modification of methionine in homoserine (CNBr). The reagent most frequently used is CNBr, which cleaves specifically after Met residue. In contrast, BNPS-Skatole and NTCB cut at the C-terminal of Trp and Cys with much less specificity.

Although the mouse IL-5 contains six Met residues, these Met residues of the mouse IL-5 do not participate in receptor binding. In addition, they are not conserved in different species (see figure 4-19). It was further shown, that the biological activity of mouse IL-5 was dependent on its homodimer configuration, linked together by disulphide bridges (Tavernier et al., 1989). Interestingly, the Trp111 is highly conserved in distinct species (4.4 see figure 4-19) and the hIL-5 W111D (in

mouse Trp 109) mutation reduces the strength of the receptor binding by a factor of 500-fold (Graber et al., 1995). Therefore, the CNBr cleavage was the option to digest the fusion protein.

Of the six Met residues in mouse IL-5, only five Met residues of mouse IL-5 were substituted by the respective amino acids derived from the human counterpart (M5T, M29L, M65R, M105L and M111I, according to mIL-5 numbering). The first Met residue in mouse IL-5 was maintained for CNBr digestion. The resulting mouse IL-5 Met deficient mutant (plasmid pET-32a-Thioredoxin/mouse IL-5^{nullMet}) was highly expressed in *E.coli*. However, after CNBr cleavage different peptides from *E. coli* thioredoxin were generated. After allowing protein refolding, the mouse IL-5^{nullMet} dimer was formed as shown by SDS-PAGE, but the peptides generated after CNBr digestion prevented further purification. Thus, the mouse IL-5 dimer purity was very low.

In a following step, We took advantage of the pET-31b vector which harbors an unique *AlwN* I cloning site, thus allowing the unidirectional insertion with bacterial ketosteroid isomerase (KSI). The KSI does not have internal methionine and, as consequence, does not produce additional peptides after CNBr cleavage. The expressed fusion protein was found within inclusion bodies. Chemical cleavage with cyanogens bromide (CNBr) was used to release the mouse IL-5 monomer (see materials and methods 3.13.2). The mouse IL-5 dimer was obtained using the same refolding and purification conditions as for the human IL-5. Using different analytical methods (SDS-PAGE under non-reducing conditions as well as analytical RH-HPLC) the purity of mIL-5 could be estimated to be $\geq 96\%$

The first step was to evaluate the biological activity of mouse IL-5 in cell proliferation assays. The mouse IL-5^{nullMet} was able to induce proliferation of TF-1 cells in vitro. A comparison of the half maximal response (EC_{50}) value of the mouse IL-5^{nullMet} (200 pM) and mouse IL-5 (180 pM) from sf9 cells (R&D systems) reveals that the mouse IL-5^{nullMet} was biologically active and glycosylation of this protein was not necessary for activity.

5.2 Structural studies of the mouse IL-5

So far, only the structure of the human IL-5 (hIL-5) has been determined by X-ray crystallography. Depicting the X-ray structure of the mouse IL-5 system may provide an important clue towards our understanding of the mechanisms governing

the species-specific interactions of IL-5. After mouse IL-5 purification, the protein was crystallized under the same conditions described for human IL-5. Crystal structure analysis shows that mouse IL-5^{nullMet} exhibits the same topology compared to the human IL-5 (Milburn et al., 1993).

Table 5-1. Alignment of α -helix sequences of human IL-5 and mouse IL-5^{nullMet}

Secondary structure	Sequence Alignment	Similarity (%)
α -helix A	<pre> TSALVKETLALLSTHRTLII - - -VVKETLTQLSAHRALLT </pre>	64
α -helix B	<pre> HQLCTEEIFQGI GTLE - - HQLCIGEIFQGLDILKNQ </pre>	62
α -helix C	<pre> QGGTVERL FKNLSL IKKYIDGQKKK RGGTVEML FQNL SL IKKYIDRQKEK </pre>	80
α -helix D	<pre> VNQFLDY LQEF LGVMNT TRQFLDY LQEF LGVL - - </pre>	80

Upper sequence (human IL-5)

Lower sequence (mouse IL-5^{nullMet})

Conserved amino acids are in blue boxes. Gaps are designated with hyphen (-)

A detailed comparison of the structures of mouse IL-5^{nullMet} with its human homologue IL-5 (PDB 1HUL) reveals some structural differences. The length of α -helices differ slightly, e.g., the α helices A, B, and D are formed by 17, 18, and 15 residues in mouse IL-5^{nullMet} in contrast to 20, 16, and 17 residues in human IL-5. Nevertheless, the protein sequence appears highly conserved (Table 5-1). Helix C is formed by 25 residues in both cytokines (Table 5-1).

Superimposition of both IL-5 structures allows determining the exact positional differences of the N- and C-termini. The N-terminus of the helix A of

mouse IL-5 was moved 3.79 Å with respect to human IL-5 only in one monomer (Pro6); for the second monomer the Pro6 was absent at the N-terminus (Figure 5-1). In the case of the C-terminus of mouse IL-5 (Glu110), it differs 5.48 and 5.86 Å in comparison to human IL-5 (Figure 5-1).

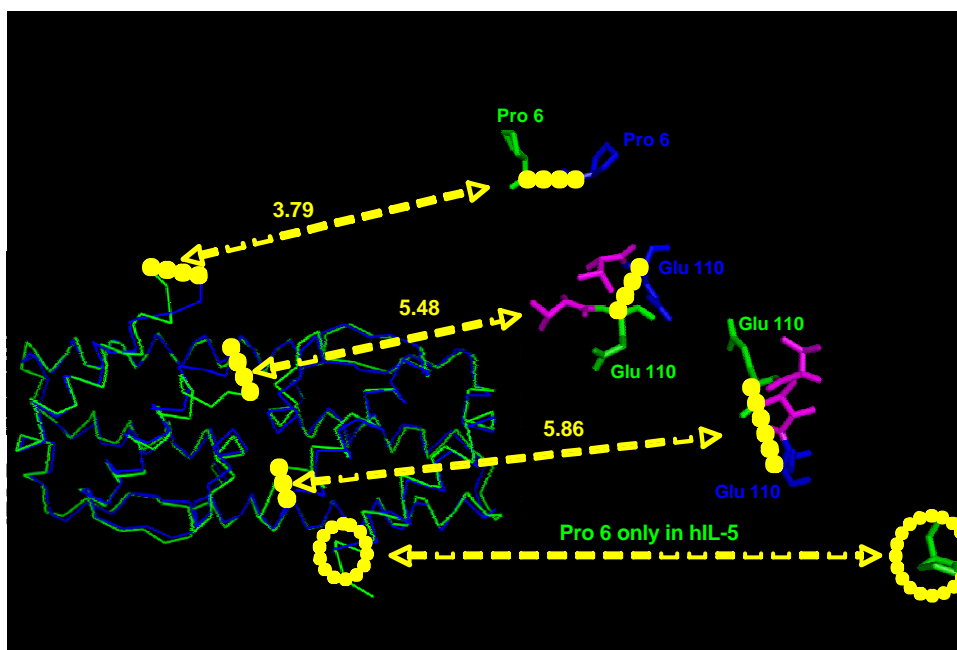


Figure 5-1. Alignment of mouse IL-5^{nullMet} structure with human IL-5 structure. Line representation illustrates the superimposition of both secondary structures from mouse IL-5^{nullMet} (blue) and hIL-5 (green) backbones. The N-terminal residue (Pro6 in green) was moved by 3.79 Å in mouse IL-5^{nullMet} in one monomer, but is not present in the second monomer. The C-terminal residue (Glu110 in green) appeared 5.48 or 5.86 Å away from its counterpart on hIL-5 (Glu110 in blue). The residue before of Glu110 (Thr109) is shown in magenta.

These and other small differences between the structures of mouse IL-5 and human IL-5 may explain the species-specificity observed for mouse IL-5 receptor activation. Superimposition of the mouse IL-5 and human IL-5 structures shows additionally, that the helix A of mouse IL-5 is shortened by one turn. Furthermore, the N-terminus of mouse IL-5 seems much less ordered despite the fact that traceable electron density can be observed from residue Thr7 in one monomer and from Pro5 in the other monomer.

These results suggest that the helix A of mouse IL-5 may be more flexible than the human IL-5 counterpart at the N-terminus due to the amino acid difference located further up in the helix A; Leu10 in human IL-5 is replaced by the smaller Val in mouse IL-5. The Leu10 residue in hIL-5 is, however, in close contact with Leu74 in helix C possibly forming a stable hydrophobic interaction. On the other hand, in mouse IL-5, the side chain of Val10 is supposed to be too short for this hydrophobic interaction; therefore, it can be hypothesized that a stabilization of the N-terminus cannot be achieved to this extent leading to a more flexible N-terminus in mouse IL-5.

Also the C-terminal helix D is shortened in mouse IL-5 by one turn if compared to hIL-5, and the C-terminal residues of the mouse IL-5 adopt a less regular secondary structure. The probable cause for the increased flexibility in the C-terminal end of mouse IL-5 could reside in the side chain conformation of residue Trp111. In one monomer the side chain of the Trp111 is more solvent exposed compared to hIL-5, due to the change in backbone conformation in the preceding residues Thr109 to Glu110. The C α -atom of Glu109 in mouse IL-5 occupies the same position as the C α -atom of Trp111 in hIL-5, leading to a significant shift of the C α -atom of the Trp111 of mouse IL-5. In the second monomer of the mouse IL-5 dimer, the electron density cannot be traced beyond the backbone atoms of Glu109, suggesting that the flexibility in the C-terminus is, indeed, higher in mouse IL-5. In line with this hypothesis, temperature factors of the residues in the C-terminal turns of both helices D of mouse IL-5 are higher as compared to the residues in the core helical part. Since the C-terminal residue Glu110 has been shown to be crucial for human IL-5R α binding and activation (Cornelis et al., 1995; Graber et al., 1995; Morton et al., 1995; Tavernier et al., 1995a), such differences in the backbone conformation might contribute to species specificity. Currently, there is no evidence that the residue Trp111 is involved in any direct interaction with the receptor IL-5R α , but it is believed to mediate anchoring of the C-terminal end of helix D in human IL-5.

The N-terminus of the helix B of mouse IL-5 appears extended by one turn with respect to human IL-5. The probable cause for this might be the fact that Thr45 in hIL-5 is replaced by Ile45 in mouse IL-5. The polar side chain of Thr45 is important for the access to the solvent via its hydroxyl end, thereby requiring a less

tight packing of the core. In contrast, the Ile45 in mouse IL-5 allows for tight packing, thereby stabilizing the N-terminal end of the helix B in mouse IL-5. Helices C and the short β -strands formed by overhand connections loops are identical in mouse IL-5 and hIL-5.

Our results show that the production of mIL-5^{nullMet} is feasible. Studies are underway, in order to produce antagonistic molecules of mIL-5 that could be evaluated in mice asthma model.

5.3 Human IL-5R α /IL-5 complex structure

After differentiation, precursor T cells develop into - at least - two effectors T cell subsets, called Th1 and Th2. Each one is characterized by their particular cytokine secretion pattern. The Th1 subset mainly produces the cytokine interferon- γ , which is a key messenger for killing of intracellular pathogens. The Th2 cells secrete IL-4, IL-5, IL-10 and IL-13, all of which are required to fight extracellular infections, such as helminth parasites. It is well known that these Th2 cytokines also play a very important role in the pathophysiology of asthma. In particular, a strong correlation between disease severity and IL-5 production was found (Enokihara et al., 1990; Magnan and Vervloet, 1998). It is unclear why certain antigens (allergens) cause asthma. Once Th2 cells release higher amounts of IL-5, which induce terminal differentiation, activation and survival of eosinophil cells (Woodcock et al., 1997), airway remodeling is induced as a consequence of tissue damage (Kay, 2005; Wills-Karp and Karp, 2004). The first step in eosinophil activation is the interaction of IL-5 and the corresponding IL-5 receptor. The cellular IL-5 receptor is a heterodimer consisting of an IL-5 specific alpha subunit (IL-5R α) mediating binding and a common beta subunit (β_c), which is also shared by the IL-3 and GM-CSF receptors (Wells and de Vos, 1996). The IL-5R α is the highly-specific binding subunit, whereas the association of the low-affinity β_c subunit mediates signaling into the effector cell (Wells and de Vos, 1996).

Because of the central role of eosinophils in the development of asthma, they represent a promising target for the design of new therapeutic strategies that may block their activation. Currently asthma therapy is based on the use of anti-inflammatory steroids and sympathomimetic substances which mediate bronchodilatation. Although this represents a clear therapeutic benefit, novel causal

therapies targeted against key molecules of asthma pathogenesis may improve the current treatment options.

New therapeutic approaches could e.g. target directly IL-5 either by administration of blocking antibodies or by IL-5 antagonist proteins, peptides or small molecules. Such strategies have already been developed. For example, the anti-IL-5 antibody (Mepolizumab) has been shown to inhibit the eosinophil maturation and reduces the number of progenitor cells and the extent of tissue damage (Garrett et al., 2004). However, the anti-5 therapy did not deplete the eosinophils in the tissue (Oldhoff et al., 2006). In addition, peptides with antagonistic action on IL-5 have been tested as new therapies (England et al., 2000; Ishino et al., 2005; Ruchala et al., 2004). The peptides evaluated so far, mediate binding via the same contact residues as IL-5 and, therefore, might block the interaction with the receptor alpha chain. However, the antagonistic properties of these peptides and their possible use as a therapeutic option for asthma in humans must still be evaluated.

In 1996 Milburn and colleagues reported the X-ray crystallography structure of the human IL-5 expressed in *E. coli* (Milburn et al., 1993). Later on, the structure of the human IL-5 produced in an eukaryotic expression system, was also determined (Guisez et al., 1993; Johanson et al., 1995). Furthermore, the X-ray crystallography structure of the extracellular domain of the human IL-5R β was published (Carr et al., 2001). The IL-5R α is required for ligand-specific binding as first step of the IL-5 receptor activation. The analysis of the three dimensional structure of the IL-5R α /IL-5 complex by using the X-ray crystallography technique will help to understand the precise molecular basis of this interaction. This knowledge will lay the ground to identify or design novel antagonistic molecules for asthma treatment.

The X-ray structural analysis of the human IL-5/IL-5R α complex may become the most promising approach for rational drug design. On the other hand, antagonistic molecules, which may block the β_c could disrupt the IL-3 and GM-CSF functions such as the activation of immature myelomonocytic cells and the induction of differentiation of granulocyte and macrophage cells, respectively.

The first attempt to determine the human IL-5/IL-5R α complex structure by X-ray crystallography was done by Johanson and colleagues in 1995 (Johanson et al., 1995). They used deglycosylated human IL-5 and glycosylated human IL-5R α to prepare and cocrystallize the human IL-5/IL-5R α complex. Only needle crystals

were grown from this complex. But, the crystal structure of human IL-5/IL-5R α complex could not be determined successfully.

This work provides the first preliminary human IL-5R α /IL-5 complex structure at a resolution of 2.5 Å. The human IL-5R α /IL-5 complex structure demonstrates that the ligand-binding region of the human IL-5R α is dispersed all over three Fn-III domains of the extracellular part of human IL-5R α (Figure 5-2). The human IL-5R α recognizes its ligand through the first NH₂-terminal Fn-III domain and, additionally, by its cytokine recognition motif (CRM), which is formed by the second and third Fn-III domains (Figure 5-2).

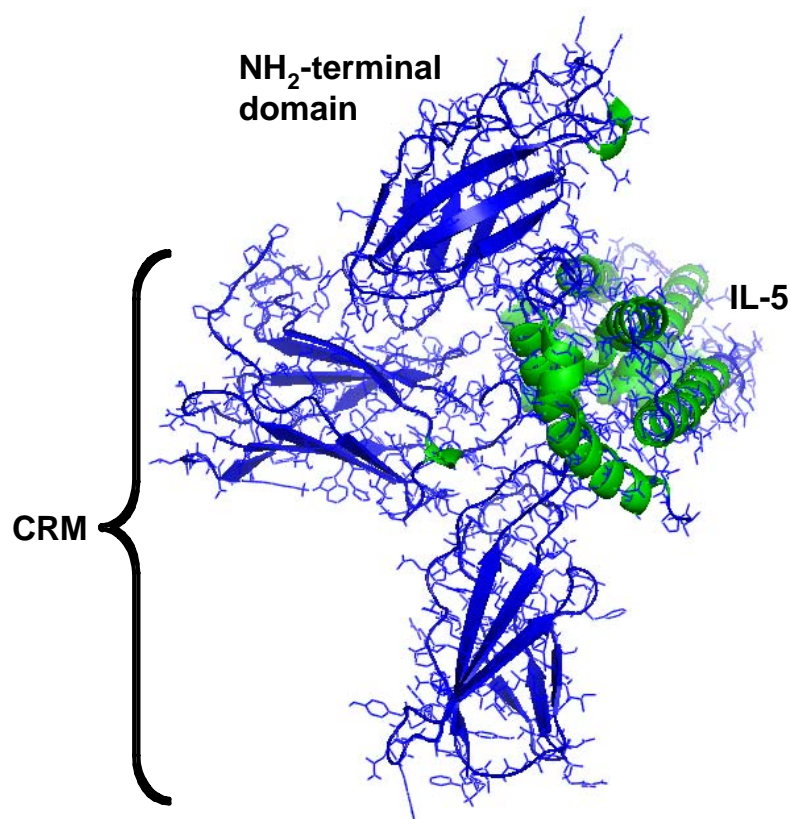


Figure 5-2. Structure of the human IL-5R α /IL-5 binary complex. Ribbon diagram of the complex structure shows the IL-5R α in blue and the IL-5 in green. The IL-5R α area participating in the CRM formation is indicated with the bracket.

The human IL-5R α /IL-5 complex structure shows a different binding topology compared to other members of the class I cytokine receptor family. A common feature of the class I receptors is the presence of two similar extracellular tandem domains which adopt a Fn-III like conformation (Bazan, 1990). These

receptors recognize the ligand through its cytokine recognition motifs (CRM) that is formed by these two Fn-III like extracellular domains (Figure 5-3).

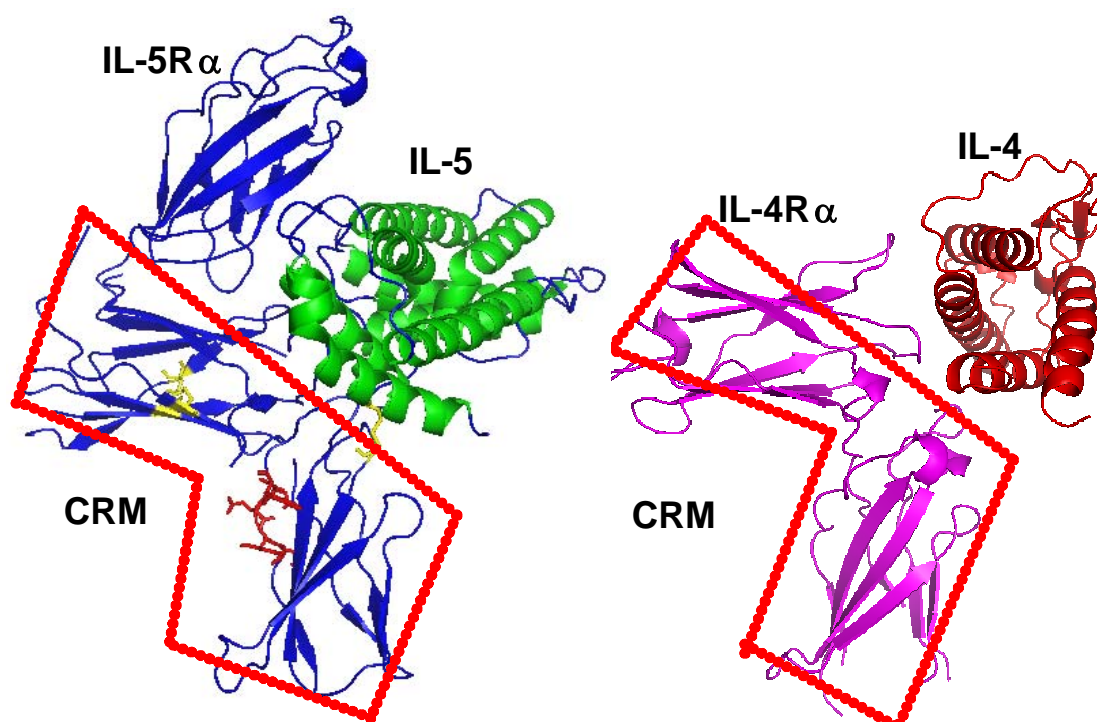


Figure 5-3. Representative structures of the class I cytokine family complexes. The CRM is defined as the region in which the ligand binds the specific receptor (red dotted lines) The IL-4R α /IL-4 (magenta and red) complex shows that the CRM is formed by two Fn-III like domains (right). The three dimensional structure of hIL-5R α /hIL-5 (blue and green) shows a new binding topology. Six cysteine residues are shown as yellow sticks. Two disulfide bridges are found in the second Fn-III domain between Cys114-Cys135 and Cys162-Cys176, respectively. The third disulfide bridge (Devos et al., 1994) is found in the third Fn-III domain between Cys249-Cys296. The WSXWS motif (red sticks) is also found in the third Fn-III domain.

There are four conserved cysteine residues in the first Fn-III like domain and a conserved WSXWS (Trp-SerX-Trp-Ser, where X is any residue) sequence in the second Fn-III like domain (Figure 5-3). Known structures of the IL-4R α /IL-4 and prolactin receptor/growth hormone (ProlR/GH) complexes have shown so far, that the two Fn-III like domains form an L shape. The ligand is bound to the elbow region, which is composed by several loops connecting the β -strands of each Fn-III type domain (de Vos et al., 1992; Hage et al., 1998; Hage et al., 1999; Somers et al., 1994). Similarly, the second/third tandem Fn-III domains of human IL-5R α form

cytokine recognition motifs (CRM), characteristic for the class I receptor family (Wells and de Vos, 1996). Although the human IL-5 also interacts with the elbow region formed by the CRM (Figure 5-3, see red dotted area), this complex adopts a binding topology in which the CRM needs the first Fn-III domain of the human IL-5R α to bind the ligand (Figure 5-3).

5.4 Cytokine recognition by human IL-5R α

In our work, we used *in vitro* interaction analysis of different human IL-5R α variants to determine the residues involved in IL-5 recognition. Our functional data confirm the binding topology of the preliminary structure, in which all three Fn-III domains of the human IL-5R α are involved in the direct interaction with IL-5.

BIAcore analysis shows that the first Fn-III like domain of the human IL-5R α plays a very crucial role in IL-5 binding (Figure 5-4). The human IL-5R α variants lacking this domain were not able to bind to IL-5 (4.1.4 see Del1 in table 4-4 and figure 4-9). Additionally, BIAcore analysis data demonstrate that the IL-5 binding properties of the first Fn-III domain also mainly depend on the Asp55 and Tyr57 residues (4.1.4 see table 4-4 and figure 4-9). The conservative replacement of D55E in human IL-5R α had a small effect on the binding properties with a 4-fold decreasing affinity. This D55E variant was found to increase the k_{off} (4.1.4 see table 4-4 and figure 4-9). Thus, these results suggest that the large size of the Glu side chain could generate a steric hindrance that could possibly be responsible for the decrease in ligand affinity. The negatively charged Asp55 residue was mutated for the neutral analogue Asn (D55N). This mutation showed less affinity because it possesses similar k_{on} and an increased k_{off} (unpublished data; (Ortmann, 2004)). However, the D55A mutation shows a dramatic decrease in the binding affinity, due to slow association rates and fast dissociation rates as shown by Ishino and Colleagues (Ishino et al., 2004). On the other hand, the receptor Y55F variant did not show any effect on receptor binding for IL-5 (4.1.4 see table 4-4). In contrast, the Y57A mutation resulted in a drastic reduction of ligand binding ($KD = 1.3 \mu\text{M}$) (unpublished data; (Ortmann, 2004)), possibly due to a different secondary structure of the receptor (4.1.2 see figure 4-7). These findings correlate with previous results that also showed no specific binding of the Y57A receptor variant (Cornelis et al., 1995). The Tyr57 residue in IL-5R α is highly conserved among all IL-5R α sequences found in Swiss-Prot (www.expasy.org). These results suggest that the

aromatic side chain of Tyr57 plays an important role in maintaining the oligomeric structure of the receptor.

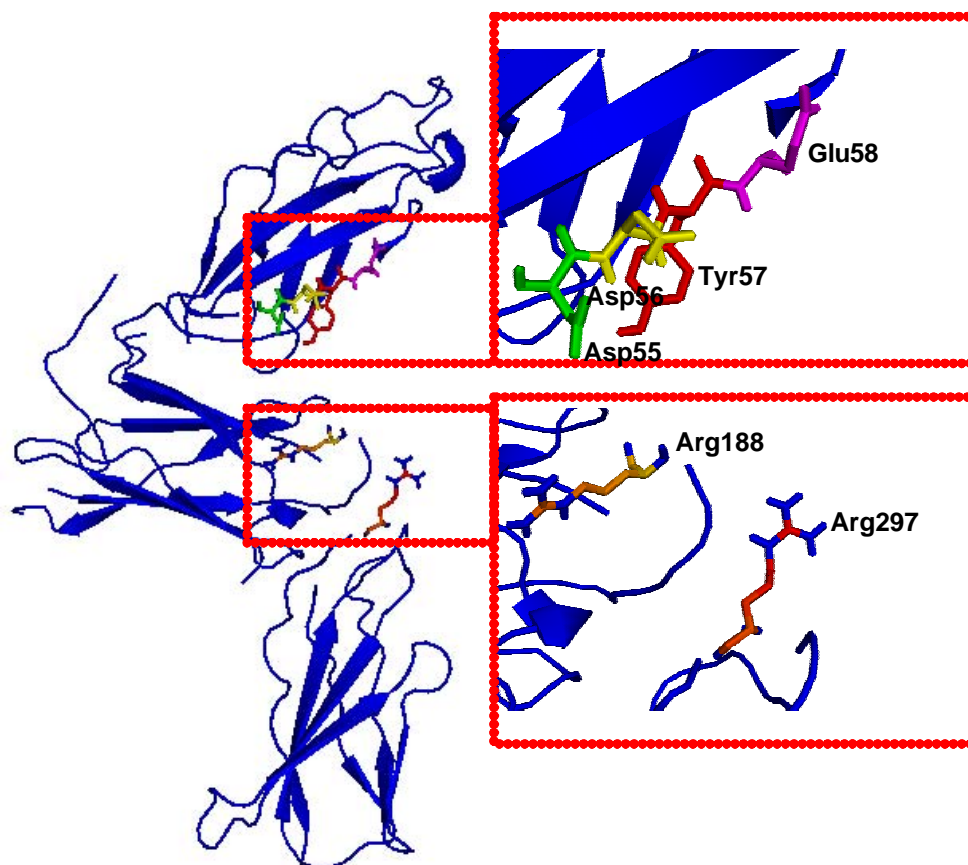


Figure 5-4. Schematic representation of the crucial hIL-5R α residues involved in IL-5 binding. The residues present in all three Fn-III like domains of hIL-5R α , which are responsible for association with the ligand are shown in the red squares. In the first domain Asp55 (green), Asp 56 (yellow), Tyr57 (red) and Glu58 magenta are shown. In the second and third domain the Arg 188 and Arg 297, are respectively shown.

In addition, Asp56 and Glu58 are crucial for the high affinity interaction of the receptor with IL-5 as shown by different groups (Cornelis et al., 1995; Ishino et al., 2004). These findings demonstrate the importance of the first Fn-III domain for human IL-5R α ligand binding (Figure 5-4).

The IL-5R α contains a free cysteine (Cys66) residue at the first Fn-III domain. Our data demonstrated that this Cys66 is modified by β -mercaptoethanol (β -ME) during receptor purification (4.1.2 see table 4-3). The mutation of the C66A avoids the interaction of β -ME with the free thiol group of the Cys residue, and the IL-5R α C66A variant still binds IL-5 with similar K_D as compared to the wild type

human IL-5R α (4.1.4 see table 4-4 and figure 4-9). However, BIAcore analysis shows that the C66A mutation increases the k_{on} ($5.2 \times 10^{-5} \text{ (s}^{-1}\text{M}^{-1}\text{)}$) and decreases the k_{off} ($1.4 \times 10^3 \text{ (s}^{-1}\text{)}$) leading to overall K_{D} value of 3.0 nM. The K_{D} determined in this work for the human IL-5R α C66A is in complete agreement with previous results (Johanson et al., 1995; Morton et al., 1994).

The ligand recognition mechanism was also dependent on the Arg188 residue present in the second Fn-III domain of the human IL-5R α . The mutation R188K resulted in a significant reduction of the binding activity (4.1.4 see table 4-4). These results suggest that the structural elements of the guanidinium group of the Arg are the major factors involved in binding, rather than just the positive charge of Arg188 (Figure 5-4). In addition, the R188A mutation was also shown to be crucial for the high affinity interaction with human IL-5 (Cornelis et al., 1995; Ishino et al., 2004). The position of Arg188 seems to be important in class I cytokine receptors. For example, in the growth hormone receptor there is a tryptophan residue (Trp104) instead of Arg (Arg188), as shown by CRM alignment of the two receptors (Cornelis, Plaetinck et al. 1995). This Trp104 residue plays a key role in ligand binding (Sundstrom et al., 1996).

Conservative mutation of F182A or I183A demonstrates that these residues are not required or involved in ligand binding (4.1.4 see table 4-4). It could be further shown that the deletion of the second and third Fn-III domains of the human IL-5R α had a dramatic effect on the binding activity of the receptor (4.1.4 see Del2 in table 4.4). Ishino and colleagues also demonstrated that the Arg297 residue in the third Fn-III domain of human IL-5R α is important for ligand binding (Ishino et al., 2004).

Our findings and those previously published (Cornelis et al., 1995; Ishino et al., 2004) demonstrated that, in contrast to other class I cytokine receptors, the CRM of human IL-5R α is not sufficient for the full binding activity.

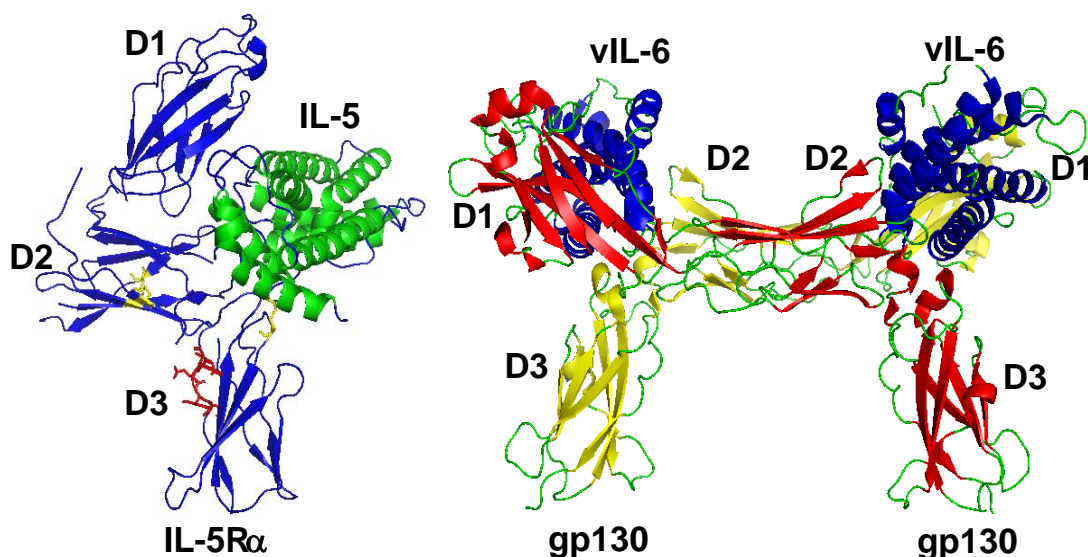


Figure 5-5. Comparison of the structures of class I complexes. The structures of the IL-5R α /IL-5 (left) and gp130/vIL-6 (right) complexes are shown in ribbon representation. The IL-5R α (blue) interacts with IL-5 (green) by using all three Fn-III domains (D1, and CRM (D2 and D3)). The two gp130 receptor molecules (red and yellow) interact with one vIL-6 molecule (blue) by using an interface between D1 from one gp130 molecule (red) and D2 and D3 from the other molecule (yellow), and vice versa.

The crystal structure of the complex formed by the human cytokine receptor gp130 and viral IL-6 (vIL-6) showed, that gp130 requires its N-terminal immunoglobulin (Ig)-like activation domain, in order to be functionally responsive to the cytokine (Chow et al., 2001). However, significant differences occur between these two cytokine class I receptor complexes (Figure 5-5): (i) The gp130/vIL-6 adopts a tetrameric arrangement consisting of two vIL-6 molecules and two gp130 receptors (Chow et al., 2001). In contrast, only one human IL-5 molecule binds to one human IL-5R α (Figure 5-5). (ii) In the binding interface, each vIL-6 molecule bridges two different gp130 receptors, and each gp130 receptor binds two vIL-6 (Chow et al., 2001). (iii) The gp130/vIL-6 complex is tethered through the interaction of one face of vIL-6 with gp130 (D2D3) and through a second vIL-6 epitope interacting with the N-terminal Ig-like domain of a different gp130 (D1) (Chow et al., 2001). In contrast, the human IL-5R α /IL-5 complex is formed through the interaction of the human IL-5 with the first Fn-III domain and CRM of the receptor (Figure 5-5). These data show that the IL-5R α /IL-5 complex adopts a totally novel binding topology.

5.5 Stoichiometrical interaction of human IL-5R α and human IL-5

Previous analysis using site-directed mutagenesis showed the importance of charged residues of human IL-5 for human hIL-5R α binding (Graber et al., 1995; Tavernier et al., 1995b).

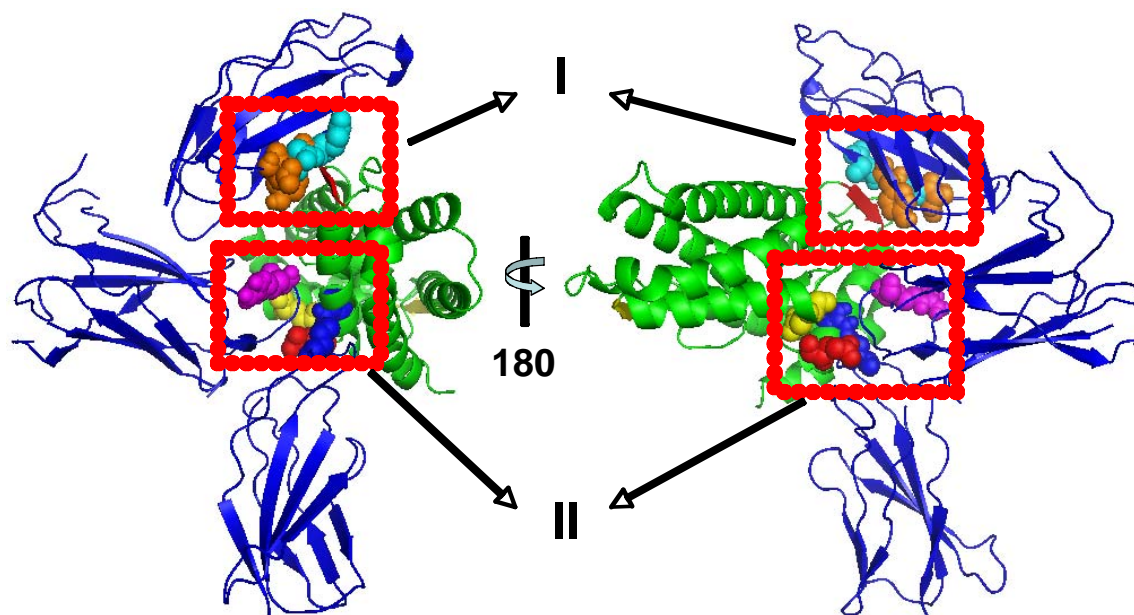


Figure 5-6. Regions involved in the interaction between hIL-5R α and hIL-5. Residues responsible for the interaction between hIL-5R α and hIL-5 are present in region I and II (red dotted squares). Region I shows the Asp55 (orange spheres), Asp56 (light blue spheres), Tyr 57 (orange spheres) and Glu58 (light blue spheres) of the IL-5R α (blue) and the β -sheet consisting of Glu89, Arg90, Arg91 and Arg 92 (red) of the IL-5 (green). Region II shows the Arg188 (magenta spheres) and Arg 297 (blue spheres) of the IL-5R α and Glu110 (red and yellow spheres) from both IL-5 monomers.

Our results for the preliminary human IL-5R α /IL-5 structure are consistent with these former human IL-5 mutagenesis data (Figure 5-6). The human IL-5R α /IL-5 complex structure suggests that the interaction between ligand and receptor could involve the negative patch in the first Fn-III domain of human IL-5R α (Asp55-Glu58) and the positively charged patch in IL-5 (Arg90 and Arg91 (β -sheet 2)) (see region I of the figure 5-6). Moreover, the positive patch of the CRM in the human IL-5R α (Arg188 and Arg297) (Figure 5-6) could interact with the negative charged Glu110 of the human IL-5 (Graber et al., 1995; Tavernier et al., 1995b) (see

region II of the figure 5-6). Since the human IL-5 has a dimeric structure (Milburn et al., 1993) binding of two human IL-5R α molecules appeared possible. The preliminary structure of the human IL-5R α /IL-5 complex clearly demonstrates that only one IL-5R α molecule binds one human IL-5 dimer molecule (molar stoichiometry of binding of 1:1) (Figure 5-7) (Devos et al., 1993; Johanson et al., 1995), consistent with functional data from our studies and other groups.

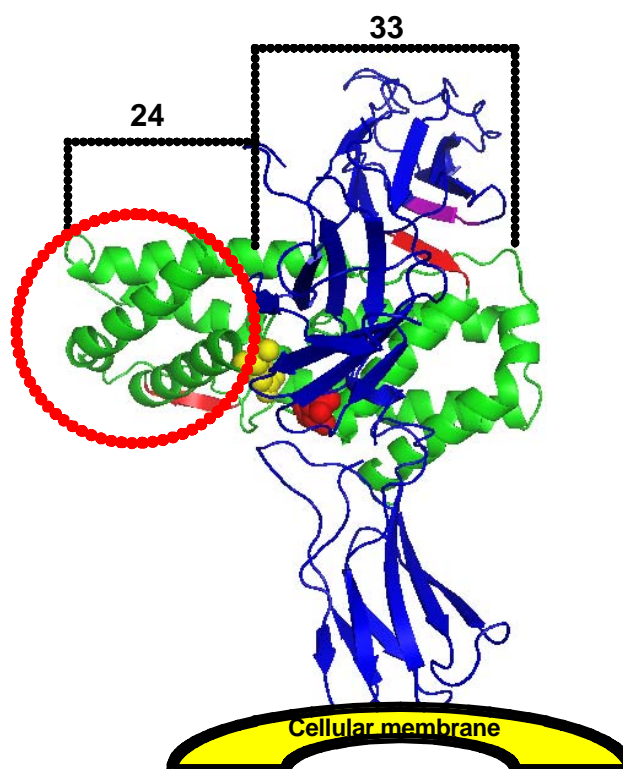


Figure 5-7. Stoichiometry of the IL-5R α and IL-5 complex. The structure of IL-5R α and IL-5 complex shows a 1:1 stoichiometry. Both IL-5R α (Asp55, Asp56, Tyr57 and Glu58) and IL-5 (Glu89, Arg90, Arg91 and Arg92) epitope residues are represented by magenta and red arrows, respectively. The Glu110 of IL-5 that interacts with IL-5R α is shown in red spheres. The Glu110 of the second monomer of IL-5 is depicted in yellow spheres. The red circle shows the second binding site in IL-5 (green). The black dotted lines show the free and occupied area for the IL-5R α on the IL-5 dimer.

Our data show that the steric hindrance of the first bound receptor prevents the binding of a second IL-5R α molecule to the IL-5R α /IL-5 complex (Figure 5-7). The first receptor binds in close proximity to the central symmetric axis of the IL-5 dimer in which the Glu110 is found (Figure 5-7). This 1:1 stoichiometry shown for our complex structure was anticipated by Devos and Johanson groups (Devos et al., 1993; Johanson et al., 1995).

How would then a biologically active receptor be formed? In order to address this central question, the group of Chaiken et al. showed in an elegant approach using asymmetric mutagenesis for IL-5 (Li et al., 1996), that the human IL-5R α binds to the single shared α chain site on IL-5. Most importantly, they demonstrated that the human IL-5R α /IL-5 only recruits one β_c (Fig 5-8).

Consequently, they proposed a step by step- model, in which the β_c is recruited to bind IL-5 once IL-5R α is bound. The favored β_c site is the “cis” site, namely the site involving the predominating Glu13 of the IL-5 (Li et al., 1996). In this model, the low affinity complex is formed by hIL-5R α /hIL-5 in a 1:1 ratio. Subsequently, this complex forms a trimeric complex by recruiting one IL-5R β (Fig 5-8). A similar assumption has also been made in the molecular models proposed by Johanson and colleagues in 1995 (Johanson et al., 1995).

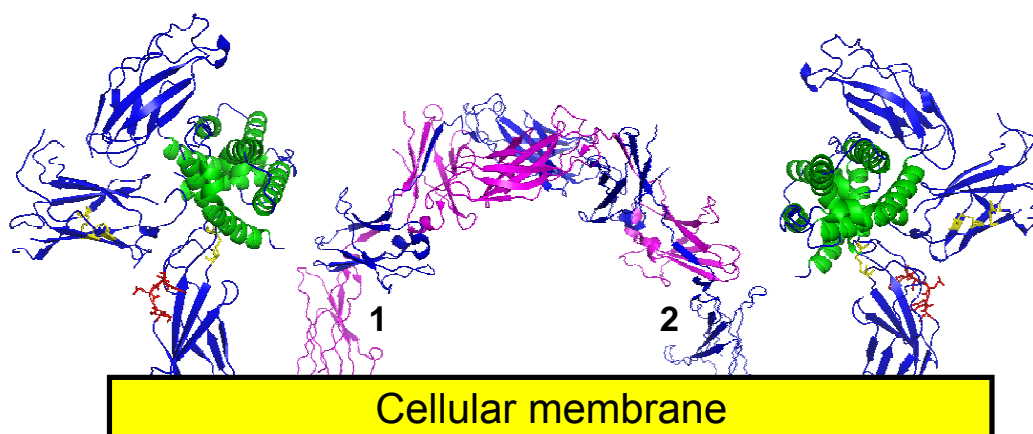


Figure 5-8. Model of the biologically active hIL-5 receptor complex. The structure of the low affinity and active IL-5R α /IL-5 (left) and modeled β_c (right) receptor complexes are shown. Two CRM of β_c are defined as the region in which the active IL-5R α /IL-5 binds the β_c (numbers 1 and 2).

The IL-5R α /IL-5 complex is different from other class-2 cytokine/receptor complexes, such as interleukin-10 and interferon- γ . Interleukin-10 and interferon- γ are symmetric homodimers with a similar topology (Walter and Nagabhushan, 1995). The crystal structure of the IL-10R1 and IL-10 shows that one IL-10 homodimer binds two IL-10R1 molecules (Figure 5-9) (Josephson et al., 2001). Equally, an interferon- γ dimer binds two high affinity interferon- γ receptor molecules (Walter et al., 1995). Our data, in contrast, provide evidence for a new topology interaction by the IL-5R α /IL-5 complex.

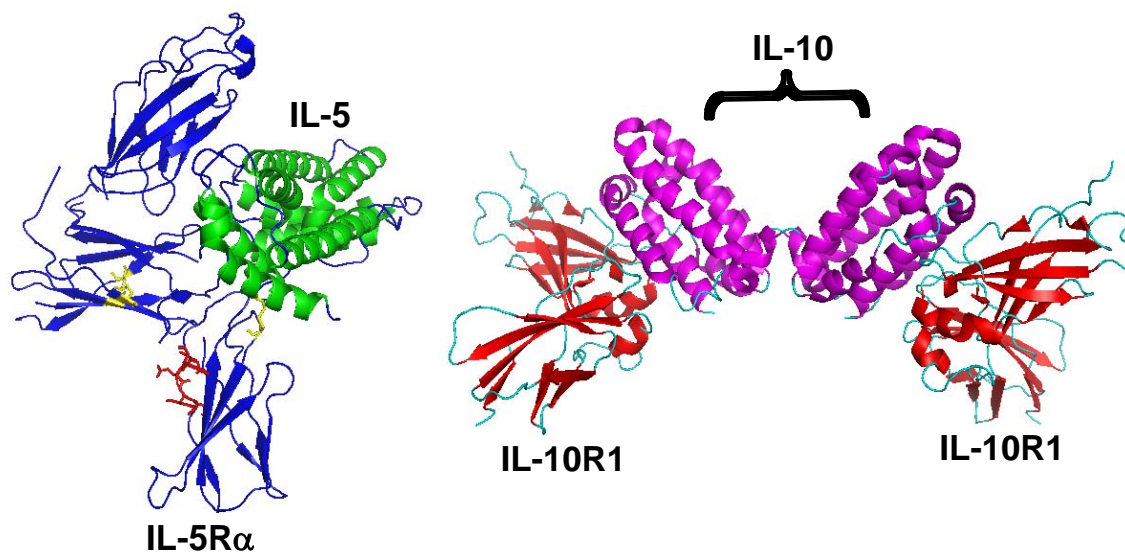


Figure 5-9. Differences between class I and class II cytokine complexes. In the class I cytokine complex shown one IL-5 dimer (green) binds only one molecule of the IL-5R α (blue). The class II cytokine complex shows one IL-10 dimer (magenta) interacting with two molecules of the IL-10R1 (red).

Taken together these results, this thesis provides for the first time insights into the IL-5R α /hIL-5 complex structure. It further confirms that the stoichiometrical interaction between IL-5R α and IL-5 follows a 1:1 ratio at the structural level. Finally, this thesis adds important knowledge to the central role the three Fn-III like domains play in ligand binding.

6 ABSTRACT

Interleukin-5 (IL-5) is a member of the hematopoietic class I cytokines and is specifically involved in eosinophil activation. IL-5 plays an important role in disease conditions such as allergic asthma and other hypereosinophilias, which are characterized by highly increased levels of eosinophils in peripheral blood and tissues. The IL-5 receptor is a heterodimer consisting of a binding alpha subunit (IL-5R α) and a common beta subunit (IL-5R β). This IL-5R β is shared with the IL-3 and GM-CSF receptors. The IL-5R α is required for ligand-specific binding, whereas the association of the IL-5R β subunit triggers intracellular signal transduction. Previous studies have described the crystallographic structure of human IL-5 (hIL-5), as well as that of the common IL-5R β chain (IL-5R β_c)

However, no experimental structural data are yet available for the interaction of the high-affinity IL-5 receptor IL-5R α with its ligand IL-5. Therefore, this thesis had the principle objective to gain new insights into the basis of this important agonist-receptor interaction. In particular, data on the recombinant expression, purification and preparation of the binary complex of hIL-5 bound to the receptor ectodomain of hIL-5R α are shown, as well as the subsequent crystal structure analysis of the binary ligand-receptor (hIL-5R α /hIL-5) complex.

Both proteins were expressed in an *Escherichia coli* expression system, purified to homogeneity, and crystallized. However, since the initial analysis of these crystals did not show any X-ray diffraction, each step of the preparation and crystallization procedure had to be stepwise optimized. Several improvements proved to be crucial for obtaining crystals suitable for structure analysis. A free cysteine residue in the N-terminal domain of the hIL-5R α ectodomain protein was mutated to alanine to remove protein heterogeneity. In addition, hIL-5 affinity chromatography of the receptor protein proved to be absolutely crucial for crystal quality. Additive screening using the initial crystallization condition finally yielded crystals of the binary complex, which diffracted to 2.5Å resolution and were suitable for structure analysis. The preliminary structure data demonstrate a new receptor architecture for the IL-5R α ligand-binding domain, which has no similarities to other cytokine class I receptor structures known so far. The complex structure demonstrates that the ligand-binding region of human IL-5R α is dispersed over all three extracellular domains, and adopts a binding topology in which the cytokine recognition motif (CRM) needs the first Fn-III domain of the human IL-5R α to bind

the ligand.

In a second project, a prokaryotic expression system for murine IL-5 (mIL-5) was established to allow the production of mIL-5 and mIL-5 antagonist that should facilitate functional studies in mice. Since the expression of mIL-5 in *E. coli* had never been successful so far, a fusion protein system was generated expressing high yields of mIL-5. Chemical cleavage with cyanogen bromide (CNBr) was used to release mIL-5 monomers, which were subsequently purified and refolded. This technique yielded an active murine IL-5 dimer as confirmed by TF-1 cell proliferation assays. The protein was crystallized and the structure of mIL-5 could be determined at 2.5Å resolution. The molecular structure revealed a symmetrical left-handed four helices bundle dimer similar to human IL-5. Analysis of the structure/function relationship allowed us to design specific mIL-5 antagonist molecules, which are still under examination. Taken together, these findings provide further insights in the IL-5 and IL-5R interaction which may help to further understand and depict this and other cytokine-receptor interactions of similar architecture, e.g. the IL-13 ligand-receptor system. Ultimately, this may represent another piece of puzzle in the attempts to rationally design and engineer novel IL-5-related pharmacological therapeutics.

7 ZUSAMMENFASSUNG

Interleukin-5 (IL-5) ist ein Mitglied der Gruppe der hematopoetischen Zytokine der Klasse I und spielt eine Schlüsselrolle bei der Aktivierung von eosinophilen Granulozyten. IL-5 hat damit eine wichtige pathophysiologische Funktion bei der Entstehung von Krankheiten wie allergischem Asthma und anderen Hypereosinophilien, die alle durch eine stark erhöhte Zahl von Eosinophilen in peripherem Blut und Geweben charakterisiert sind. Der IL-5 Rezeptor ist ein Heterodimer, der aus einer alpha-Untereinheit (IL-5R α) und einer mit den IL-3 und GM-CSF Rezeptoren gemeinsamen beta-Untereinheit (IL-5R β) besteht. Der IL-5R α ist für die spezifische Liganden-Bindung notwendig, während der mit der IL-5R β Untereinheit assoziierte Komplex die intrazelluläre Signaltransduktion einleitet.

In früheren Studien konnte bereits die Kristallstruktur des menschlichen IL-5 (hIL-5) und der gemeinsamen IL-5R β -Kette (IL-5R β_c) aufgeklärt werden. Allerdings liegen bisher noch keine experimentellen Strukturdaten für die Interaktionen des hochaffinen IL-5 Rezeptor IL-5R α mit seinem Ligand IL-5 vor. Deshalb war es die Hauptzielsetzung dieser Arbeit, neue Einblicke in die molekulare Basis der Interaktion von IL-5 Rezeptor und Agonisten zu gewinnen. Im Einzelnen beschreibe ich in dieser Arbeit die rekombinante Expression, Aufreinigung und Herstellung des binären Komplexes von der hIL-5 Bindung an die extrazellulären Domäne des Rezeptors hIL-5R α sowie die anschließende kristallographische Strukturanalyse dieses binären Ligand-Rezeptor-Komplexes (hIL-R α /hIL-5). Beide Proteine wurden in einem *Escherichia coli*-Expressionssystem rekombinant hergestellt, bis zur Homogenität gereinigt und anschließend kristallisiert. Die Analysen dieser ersten Kristalle zeigten nicht die gewünschte Beugung der Röntgenstrahlung, weshalb in allen anschließenden Schritten eine schrittweise Optimierung der Produktions- und Kristallisationsbedingungen durchgeführt wurde. Als Ergebnis dieser Optimierungsstrategie konnten schließlich Kristalle erhalten werden, die für eine Strukturanalyse geeignet waren. Ein ungepaartes Cystein in der N-terminalen Domäne des extrazellulären hIL-5R α -Protein wurde durch Alanin ersetzt, um so die

Protein-Heterogenität durch Cystein-Oxidationsprodukte zu verringern. Die Affinitätschromatographische Aufreinigung des Rezeptorproteins war ebenfalls entscheidend, um eine hohe Kristallqualität zu erreichen. Die Verwendung verschiedener Additivsubstanzen zusätzlich zu den initialen Kristallisationsbedingungen führte letztlich zur Bildung für die Strukturanalyse geeigneter Einzelkristalle des binären Komplexes (hIL-5R α /hIL-5). Ihre Messung ergab Beugungsdaten mit einer maximalen Auflösung von 2.5Å. Eine erste Strukturanalyse zeigt klar, dass die Liganden-bindende Domäne des IL-5R α Rezeptors eine bisher unbekannte, neuartige Rezeptor-Architektur aufweist, die keinerlei Ähnlichkeit zu bisher bekannten Zytokinrezeptor-Strukturen der Klasse I hat. Die Struktur des Komplexes zeigt zudem, dass das Liganden-bindende Epitop von IL-5R α über alle drei extrazellulären Domänen verteilt ist und eine Topologie aufweist, in der zusätzlich zu dem Zytokin-Erkennungsmotiv (CRM) die erste Fn-III Domäne von hIL-5R α benötigt wird, um den Liganden hochaffin binden zu können.

In einem zweiten Projekt wurde ein prokaryotisches Expressionssystem für murines Interleukin-5 (mIL-5) entwickelt, welches die Produktion von mIL-5 und eines mIL-5 Antagonisten für funktionelle Studien in einem Mausmodell ermöglichen sollte. Da eine rekombinante Produktion von mIL-5 in *E.coli* bisher nicht erfolgreich war, wurde ein Fusionsprotein-System entwickelt, welches die Produktion großer Mengen von mIL-5 Protein erlaubt. Es wurde eine chemische Spaltung mit Cyanbromid (CNBr) durchgeführt, um das Monomer aus dem Fusionsprotein freizusetzen. Das so erhaltene mIL-5 Monomer wurde gereinigt und renaturiert. Nach Rückfaltung zeigt das dimere Protein in TF-1 Zellen eine mit den Literaturwerten vergleichbare biologische Aktivität. Das so erhaltene mIL-5 Protein wurde kristallisiert und mittels Röntgenbeugung analysiert. Auf diese Weise konnten Beugungsdaten von mIL-5 Kristallen mit einer maximalen Auflösung von 2.5Å erhalten werden. Die Struktur weist ähnlich wie das humane IL-5 ein symmetrisches Vier-Helix Bündel auf. Die Struktur-/Funktionsanalyse ermöglichte daraufhin, definierte mIL-5-Antagonisten zu entwickeln, die sich derzeit noch in der Untersuchung befinden. Zusammengefasst tragen die hier präsentierten Ergebnisse

dazu bei, die molekularen Grundlagen der spezifischen IL-5 und IL-5R Bindung sowie Interaktionen ähnlichen Liganden-Rezeptor-Typen zu verstehen. Letztendlich besteht die Hoffnung, dass diese und ähnliche Arbeiten ein weiteres wichtiges Puzzlestück darstellen bei dem Versuch, neue und innovative pharmakologische Therapieansätze zu entwickeln, die bei dem für die Pathophysiologie von Asthma wichtigen Schlüssel-molekül IL-5 angreifen.

8 REFERENCES

- Amaki, Y., Nakano, H., and Yamane, T. (1994). Role of cysteine residues in esterase from *Bacillus stearothermophilus* and increasing its thermostability by the replacement of cysteines. *Appl Microbiol Biotechnol* *40*, 664-668.
- Azuma, C., Tanabe, T., Konishi, M., Kinashi, T., Noma, T., Matsuda, F., Yaoita, Y., Takatsu, K., Hammarstrom, L., Smith, C. I., and et al. (1986). Cloning of cDNA for human T-cell replacing factor (interleukin-5) and comparison with the murine homologue. *Nucleic Acids Res* *14*, 9149-9158.
- Bazan, J. F. (1990). Structural design and molecular evolution of a cytokine receptor superfamily. *Proc Natl Acad Sci U S A* *87*, 6934-6938.
- Brown, P. M., Tagari, P., Rowan, K. R., Yu, V. L., O'Neill, G. P., Middaugh, C. R., Sanyal, G., Ford-Hutchinson, A. W., and Nicholson, D. W. (1995). Epitope-labeled soluble human interleukin-5 (IL-5) receptors. Affinity cross-link labeling, IL-5 binding, and biological activity. *J Biol Chem* *270*, 29236-29243.
- Campbell, H. D., Tucker, W. Q., Hort, Y., Martinson, M. E., Mayo, G., Clutterbuck, E. J., Sanderson, C. J., and Young, I. G. (1987). Molecular cloning, nucleotide sequence, and expression of the gene encoding human eosinophil differentiation factor (interleukin 5). *Proc Natl Acad Sci U S A* *84*, 6629-6633.
- Carr, P. D., Gustin, S. E., Church, A. P., Murphy, J. M., Ford, S. C., Mann, D. A., Woltring, D. M., Walker, I., Ollis, D. L., and Young, I. G. (2001). Structure of the complete extracellular domain of the common beta subunit of the human GM-CSF, IL-3, and IL-5 receptors reveals a novel dimer configuration. *Cell* *104*, 291-300.
- Chen, J. C., Krucinski, J., Miercke, L. J., Finer-Moore, J. S., Tang, A. H., Leavitt, A. D., and Stroud, R. M. (2000). Crystal structure of the HIV-1 integrase catalytic core and C-terminal domains: a model for viral DNA binding. *Proc Natl Acad Sci U S A* *97*, 8233-8238.
- Cho, J. Y., Miller, M., Baek, K. J., Han, J. W., Nayar, J., Lee, S. Y., McElwain, K., McElwain, S., Friedman, S., and Broide, D. H. (2004). Inhibition of airway remodeling in IL-5-deficient mice. *J Clin Invest* *113*, 551-560.
- Chow, D., He, X., Snow, A. L., Rose-John, S., and Garcia, K. C. (2001). Structure of an extracellular gp130 cytokine receptor signaling complex. *Science* *291*, 2150-2155.

-
- Clamp, M., Cuff, J., Searle, S. M., and Barton, G. J. (2004). The Jalview Java alignment editor. *Bioinformatics* 20, 426-427.
- Cornelis, S., Plaetinck, G., Devos, R., Van der Heyden, J., Tavernier, J., Sanderson, C. J., Guisez, Y., and Fiers, W. (1995). Detailed analysis of the IL-5-IL-5R alpha interaction: characterization of crucial residues on the ligand and the receptor. *Embo J* 14, 3395-3402.
- Cudney, R., Patel, S., Weisgraber, K., Newhouse, Y., and McPherson, A. (1994). Screening and optimization strategies for macromolecular crystal growth. *Acta Crystallogr D Biol Crystallogr* 50, 414-423.
- de Groot, R. P., Coffey, P. J., and Koenderman, L. (1998). Regulation of proliferation, differentiation and survival by the IL-3/IL-5/GM-CSF receptor family. *Cell Signal* 10, 619-628.
- de Vos, A. M., Ultsch, M., and Kossiakoff, A. A. (1992). Human growth hormone and extracellular domain of its receptor: crystal structure of the complex. *Science* 255, 306-312.
- Devos, R., Guisez, Y., Cornelis, S., Verhee, A., Van der Heyden, J., Manneberg, M., Lahm, H. W., Fiers, W., Tavernier, J., and Plaetinck, G. (1993). Recombinant soluble human interleukin-5 (hIL-5) receptor molecules. Cross-linking and stoichiometry of binding to IL-5. *J Biol Chem* 268, 6581-6587.
- Devos, R., Guisez, Y., Plaetinck, G., Cornelis, S., Tavernier, J., van der Heyden, J., Foley, L. H., and Scheffler, J. E. (1994). Covalent modification of the interleukin-5 receptor by isothiazolones leads to inhibition of the binding of interleukin-5. *Eur J Biochem* 225, 635-640.
- Dickason, R. R., English, J. D., and Huston, D. P. (1996a). Engineering of a functional interleukin-5 monomer: a paradigm for redesigning helical bundle cytokines with therapeutic potential in allergy and asthma. *J Mol Med* 74, 535-546.
- Dickason, R. R., Huston, M. M., and Huston, D. P. (1996b). Delineation of IL-5 domains predicted to engage the IL-5 receptor complex. *J Immunol* 156, 1030-1037.
- Edgerton, M. D., Graber, P., Willard, D., Consler, T., McKinnon, M., Uings, I., Arod, C. Y., Borlat, F., Fish, R., Peitsch, M. C., *et al.* (1997). Spatial orientation of the alpha and beta receptor chain binding sites on monomeric human interleukin-5 constructs. *J Biol Chem* 272, 20611-20618.
- England, B. P., Balasubramanian, P., Uings, I., Bethell, S., Chen, M. J., Schatz, P. J., Yin, Q., Chen, Y. F., Whitehorn, E. A., Tsavaler, A., *et al.* (2000). A potent dimeric

- peptide antagonist of interleukin-5 that binds two interleukin-5 receptor alpha chains. *Proc Natl Acad Sci U S A* 97, 6862-6867.
- Enokihara, H., Kajitani, H., Nagashima, S., Tsunogake, S., Takano, N., Saito, K., Furusawa, S., Shishido, H., Hitoshi, Y., and Takatsu, K. (1990). Interleukin 5 activity in sera from patients with eosinophilia. *Br J Haematol* 75, 458-462.
- Feng, Y., Klein, B. K., and McWherter, C. A. (1996). Three-dimensional solution structure and backbone dynamics of a variant of human interleukin-3. *J Mol Biol* 259, 524-541.
- Flood-Page, P., Menzies-Gow, A., Phipps, S., Ying, S., Wangoo, A., Ludwig, M. S., Barnes, N., Robinson, D., and Kay, A. B. (2003a). Anti-IL-5 treatment reduces deposition of ECM proteins in the bronchial subepithelial basement membrane of mild atopic asthmatics. *J Clin Invest* 112, 1029-1036.
- Flood-Page, P. T., Menzies-Gow, A. N., Kay, A. B., and Robinson, D. S. (2003b). Eosinophil's role remains uncertain as anti-interleukin-5 only partially depletes numbers in asthmatic airway. *Am J Respir Crit Care Med* 167, 199-204.
- Gall, A. L., Ruff, M., and Moras, D. (2003). The dual role of CHAPS in the crystallization of stromelysin-3 catalytic domain. *Acta Crystallogr D Biol Crystallogr* 59, 603-606.
- Garman, S. C., Wurzburg, B. A., Tarchevskaya, S. S., Kinet, J. P., and Jardetzky, T. S. (2000). Structure of the Fc fragment of human IgE bound to its high-affinity receptor Fc epsilonRI alpha. *Nature* 406, 259-266.
- Garrett, J. K., Jameson, S. C., Thomson, B., Collins, M. H., Wagoner, L. E., Freese, D. K., Beck, L. A., Boyce, J. A., Filipovich, A. H., Villanueva, J. M., *et al.* (2004). Anti-interleukin-5 (mepolizumab) therapy for hypereosinophilic syndromes. *J Allergy Clin Immunol* 113, 115-119.
- Geijsen, N., Uings, I. J., Pals, C., Armstrong, J., McKinnon, M., Raaijmakers, J. A., Lammers, J. W., Koenderman, L., and Coffey, P. J. (2001). Cytokine-specific transcriptional regulation through an IL-5Ralpha interacting protein. *Science* 293, 1136-1138.
- Gillian E. Begg., a. D. W. S. (1999). Mass spectrometry detection and reduction of disulfide adducts between reducing agents and recombinant proteins with highly reactive cysteines. *Journal of Biomolecular Techniques* 10, 17-20.
- Gorman, D. M., Itoh, N., Kitamura, T., Schreurs, J., Yonehara, S., Yahara, I., Arai, K., and Miyajima, A. (1990). Cloning and expression of a gene encoding an

- interleukin 3 receptor-like protein: identification of another member of the cytokine receptor gene family. *Proc Natl Acad Sci U S A* *87*, 5459-5463.
- Gorska, M. M., Cen, O., Liang, Q., Stafford, S. J., and Alam, R. (2006). Differential regulation of interleukin 5-stimulated signaling pathways by dynamin. *J Biol Chem* *281*, 14429-14439.
- Graber, P., Bernard, A. R., Hassell, A. M., Milburn, M. V., Jordan, S. R., Proudfoot, A. E., Fattah, D., and Wells, T. N. (1993). Purification, characterisation and crystallisation of selenomethionyl recombinant human interleukin-5 from *Escherichia coli*. *Eur J Biochem* *212*, 751-755.
- Graber, P., Proudfoot, A. E., Talabot, F., Bernard, A., McKinnon, M., Banks, M., Fattah, D., Solari, R., Peitsch, M. C., and Wells, T. N. (1995). Identification of key charged residues of human interleukin-5 in receptor binding and cellular activation. *J Biol Chem* *270*, 15762-15769.
- Guisez, Y., Oefner, C., Winkler, F. K., Schlaeger, E. J., Zulauf, M., Van der Heyden, J., Plaetinck, G., Cornelis, S., Tavernier, J., Fiers, W., and et al. (1993). Expression, purification and crystallization of fully active, glycosylated human interleukin-5. *FEBS Lett* *331*, 49-52.
- Gustin, S. E., Church, A. P., Ford, S. C., Mann, D. A., Carr, P. D., Ollis, D. L., and Young, I. G. (2001). Expression, crystallization and derivatization of the complete extracellular domain of the beta(c) subunit of the human IL-5, IL-3 and GM-CSF receptors. *Eur J Biochem* *268*, 2905-2911.
- Guthridge, M. A., Stomski, F. C., Thomas, D., Woodcock, J. M., Bagley, C. J., Berndt, M. C., and Lopez, A. F. (1998). Mechanism of activation of the GM-CSF, IL-3, and IL-5 family of receptors. *Stem Cells* *16*, 301-313.
- Hage, T., Reinemer, P., and Sebald, W. (1998). Crystals of a 1:1 complex between human interleukin-4 and the extracellular domain of its receptor alpha chain. *Eur J Biochem* *258*, 831-836.
- Hage, T., Sebald, W., and Reinemer, P. (1999). Crystal structure of the interleukin-4/receptor alpha chain complex reveals a mosaic binding interface. *Cell* *97*, 271-281.
- Hara, T., and Miyajima, A. (1992). Two distinct functional high affinity receptors for mouse interleukin-3 (IL-3). *Embo J* *11*, 1875-1884.
- Harada, N., Kikuchi, Y., Tominaga, A., Takaki, S., and Takatsu, K. (1985). BCGFII activity on activated B cells of a purified murine T cell-replacing factor (TRF) from a T cell hybridoma (B151K12). *J Immunol* *134*, 3944-3951.

- Hassell, A. M., Wells, T. N., Graber, P., Proudfoot, A. E., Anderegg, R. J., Burkhart, W., Jordan, S. R., and Milburn, M. V. (1993). Crystallization and preliminary X-ray diffraction studies of recombinant human interleukin-5. *J Mol Biol* 229, 1150-1152.
- Hayashida, K., Kitamura, T., Gorman, D. M., Arai, K., Yokota, T., and Miyajima, A. (1990). Molecular cloning of a second subunit of the receptor for human granulocyte-macrophage colony-stimulating factor (GM-CSF): reconstitution of a high-affinity GM-CSF receptor. *Proc Natl Acad Sci U S A* 87, 9655-9659.
- Herbert, D. R., Lee, J. J., Lee, N. A., Nolan, T. J., Schad, G. A., and Abraham, D. (2000). Role of IL-5 in innate and adaptive immunity to larval *Strongyloides stercoralis* in mice. *J Immunol* 165, 4544-4551.
- Hogan, M. B., Weissman, D. N., Hubbs, A. F., Gibson, L. F., Piktel, D., and Landreth, K. S. (2003). Regulation of eosinophilopoiesis in a murine model of asthma. *J Immunol* 171, 2644-2651.
- Hoppe, J., Weich, H. A., and Eichner, W. (1989). Preparation of biologically active platelet-derived growth factor type BB from a fusion protein expressed in *Escherichia coli*. *Biochemistry* 28, 2956-2960.
- Hoppe, J., Weich, H. A., Eichner, W., and Tatje, D. (1990). Preparation of biologically active platelet-derived growth factor isoforms AA and AB. Preferential formation of AB heterodimers. *Eur J Biochem* 187, 207-214.
- Horikawa, K., and Takatsu, K. (2006). Interleukin-5 regulates genes involved in B-cell terminal maturation. *Immunology* 118, 497-508.
- Humbles, A. A., Lloyd, C. M., McMillan, S. J., Friend, D. S., Xanthou, G., McKenna, E. E., Ghiran, S., Gerard, N. P., Yu, C., Orkin, S. H., and Gerard, C. (2004). A critical role for eosinophils in allergic airways remodeling. *Science* 305, 1776-1779.
- Ingle, E., Cutler, R. L., Fung, M. C., Sanderson, C. J., and Young, I. G. (1991). Production and purification of recombinant human interleukin-5 from yeast and baculovirus expression systems. *Eur J Biochem* 196, 623-629.
- Ishino, T., Pasut, G., Scibek, J., and Chaiken, I. (2004). Kinetic interaction analysis of human interleukin 5 receptor alpha mutants reveals a unique binding topology and charge distribution for cytokine recognition. *J Biol Chem* 279, 9547-9556.
- Ishino, T., Pillalamarri, U., Panarello, D., Bhattacharya, M., Urbina, C., Horvat, S., Sarkhel, S., Jameson, B., and Chaiken, I. (2006). Asymmetric usage of antagonist

- charged residues drives interleukin-5 receptor recruitment but is insufficient for receptor activation. *Biochemistry* *45*, 1106-1115.
- Ishino, T., Urbina, C., Bhattacharya, M., Panarello, D., and Chaiken, I. (2005). Receptor epitope usage by an interleukin-5 mimetic peptide. *J Biol Chem* *280*, 22951-22961.
- Itou, H., Yao, M., Fujita, I., Watanabe, N., Suzuki, M., Nishihira, J., and Tanaka, I. (2002). The crystal structure of human MRP14 (S100A9), a Ca(2+)-dependent regulator protein in inflammatory process. *J Mol Biol* *316*, 265-276.
- Jana, S., and Deb, J. K. (2005). Strategies for efficient production of heterologous proteins in *Escherichia coli*. *Appl Microbiol Biotechnol* *67*, 289-298.
- Johanson, K., Appelbaum, E., Doyle, M., Hensley, P., Zhao, B., Abdel-Meguid, S. S., Young, P., Cook, R., Carr, S., Matico, R., and et al. (1995). Binding interactions of human interleukin 5 with its receptor alpha subunit. Large scale production, structural, and functional studies of *Drosophila*-expressed recombinant proteins. *J Biol Chem* *270*, 9459-9471.
- Josephson, K., Logsdon, N. J., and Walter, M. R. (2001). Crystal structure of the IL-10/IL-10R1 complex reveals a shared receptor binding site. *Immunity* *15*, 35-46.
- Kane, J. F. (1995). Effects of rare codon clusters on high-level expression of heterologous proteins in *Escherichia coli*. *Curr Opin Biotechnol* *6*, 494-500.
- Kay, A. B. (2005). The role of eosinophils in the pathogenesis of asthma. *Trends Mol Med* *11*, 148-152.
- Kinashi, T., Harada, N., Severinson, E., Tanabe, T., Sideras, P., Konishi, M., Azuma, C., Tominaga, A., Bergstedt-Lindqvist, S., Takahashi, M., and et al. (1986). Cloning of complementary DNA encoding T-cell replacing factor and identity with B-cell growth factor II. *Nature* *324*, 70-73.
- Kitamura, T., Sato, N., Arai, K., and Miyajima, A. (1991). Expression cloning of the human IL-3 receptor cDNA reveals a shared beta subunit for the human IL-3 and GM-CSF receptors. *Cell* *66*, 1165-1174.
- Kitamura, T., Tange, T., Terasawa, T., Chiba, S., Kuwaki, T., Miyagawa, K., Piao, Y. F., Miyazono, K., Urabe, A., and Takaku, F. (1989). Establishment and characterization of a unique human cell line that proliferates dependently on GM-CSF, IL-3, or erythropoietin. *J Cell Physiol* *140*, 323-334.

- Kodama, S., Tsuruoka, N., and Tsujimoto, M. (1991). Role of the C-terminus in the biological activity of human interleukin 5. *Biochem Biophys Res Commun* *178*, 514-519.
- Kopf, M., Brombacher, F., Hodgkin, P. D., Ramsay, A. J., Milbourne, E. A., Dai, W. J., Ovington, K. S., Behm, C. A., Kohler, G., Young, I. G., and Matthaei, K. I. (1996). IL-5-deficient mice have a developmental defect in CD5+ B-1 cells and lack eosinophilia but have normal antibody and cytotoxic T cell responses. *Immunity* *4*, 15-24.
- Kouro, T., Kikuchi, Y., Kanazawa, H., Hirokawa, K., Harada, N., Shiiba, M., Wakao, H., Takaki, S., and Takatsu, K. (1996). Critical proline residues of the cytoplasmic domain of the IL-5 receptor alpha chain and its function in IL-5-mediated activation of JAK kinase and STAT5. *Int Immunol* *8*, 237-245.
- LaVallie, E. R., DiBlasio, E. A., Kovacic, S., Grant, K. L., Schendel, P. F., and McCoy, J. M. (1993). A thioredoxin gene fusion expression system that circumvents inclusion body formation in the E. coli cytoplasm. *Biotechnology (N Y)* *11*, 187-193.
- Lee, J. J., Dimina, D., Macias, M. P., Ochkur, S. I., McGarry, M. P., O'Neill, K. R., Protheroe, C., Pero, R., Nguyen, T., Cormier, S. A., *et al.* (2004). Defining a link with asthma in mice congenitally deficient in eosinophils. *Science* *305*, 1773-1776.
- Li, J., Cook, R., and Chaiken, I. (1996). Mutants of single chain interleukin 5 show asymmetric recruitment of receptor alpha and beta subunits. *J Biol Chem* *271*, 31729-31734.
- Li, J., Cook, R., Doyle, M. L., Hensley, P., McNulty, D. E., and Chaiken, I. (1997). Monomeric isomers of human interleukin 5 show that 1:1 receptor recruitment is sufficient for function. *Proc Natl Acad Sci U S A* *94*, 6694-6699.
- Loughnan, M. S., Takatsu, K., Harada, N., and Nossal, G. J. (1987). T-cell-replacing factor (interleukin 5) induces expression of interleukin 2 receptors on murine splenic B cells. *Proc Natl Acad Sci U S A* *84*, 5399-5403.
- Magnan, A., and Vervloet, D. (1998). [Role of eosinophilia in atopic pathology]. *Med Trop (Mars)* *58*, 444-446.
- Martinez-Moczygamba, M., and Huston, D. P. (2001). Proteasomal regulation of beta signaling reveals a novel mechanism for cytokine receptor heterotypic desensitization. *J Clin Invest* *108*, 1797-1806.

- Martinez-Moczygamba, M., and Huston, D. P. (2003). Biology of common beta receptor-signaling cytokines: IL-3, IL-5, and GM-CSF. *J Allergy Clin Immunol* *112*, 653-665; quiz 666.
- McKenzie, A. N., Barry, S. C., Strath, M., and Sanderson, C. J. (1991a). Structure-function analysis of interleukin-5 utilizing mouse/human chimeric molecules. *Embo J* *10*, 1193-1199.
- McKenzie, A. N., Ely, B., and Sanderson, C. J. (1991b). Mutated interleukin-5 monomers are biologically inactive. *Mol Immunol* *28*, 155-158.
- McKinnon, M., Page, K., Uings, I. J., Banks, M., Fattah, D., Proudfoot, A. E., Graber, P., Arod, C., Fish, R., Wells, T. N., and Solari, R. (1997). An interleukin 5 mutant distinguishes between two functional responses in human eosinophils. *J Exp Med* *186*, 121-129.
- Menzies-Gow, A., Flood-Page, P., Sehmi, R., Burman, J., Hamid, Q., Robinson, D. S., Kay, A. B., and Denburg, J. (2003). Anti-IL-5 (mepolizumab) therapy induces bone marrow eosinophil maturational arrest and decreases eosinophil progenitors in the bronchial mucosa of atopic asthmatics. *J Allergy Clin Immunol* *111*, 714-719.
- Milburn, M. V., Hassell, A. M., Lambert, M. H., Jordan, S. R., Proudfoot, A. E., Graber, P., and Wells, T. N. (1993). A novel dimer configuration revealed by the crystal structure at 2.4 Å resolution of human interleukin-5. *Nature* *363*, 172-176.
- Mita, S., Harada, N., Naomi, S., Hitoshi, Y., Sakamoto, K., Akagi, M., Tominaga, A., and Takatsu, K. (1988). Receptors for T cell-replacing factor/interleukin 5. Specificity, quantitation, and its implication. *J Exp Med* *168*, 863-878.
- Mita, S., Takaki, S., Hitoshi, Y., Rolink, A. G., Tominaga, A., Yamaguchi, N., and Takatsu, K. (1991). Molecular characterization of the beta chain of the murine interleukin 5 receptor. *Int Immunol* *3*, 665-672.
- Mita, S., Tominaga, A., Hitoshi, Y., Sakamoto, K., Honjo, T., Akagi, M., Kikuchi, Y., Yamaguchi, N., and Takatsu, K. (1989). Characterization of high-affinity receptors for interleukin 5 on interleukin 5-dependent cell lines. *Proc Natl Acad Sci U S A* *86*, 2311-2315.
- Miyazaki, Y., Matsufuji, S., Murakami, Y., and Hayashi, S. (1993). Single amino-acid replacement is responsible for the stabilization of ornithine decarboxylase in HMOA cells. *Eur J Biochem* *214*, 837-844.
- Monahan, J., Siegel, N., Keith, R., Caparon, M., Christine, L., Compton, R., Cusik, S., Hirsch, J., Huynh, M., Devine, C., *et al.* (1997). Attenuation of IL-5-mediated

- signal transduction, eosinophil survival, and inflammatory mediator release by a soluble human IL-5 receptor. *J Immunol* 159, 4024-4034.
- Morton, T., Li, J., Cook, R., and Chaiken, I. (1995). Mutagenesis in the C-terminal region of human interleukin 5 reveals a central patch for receptor alpha chain recognition. *Proc Natl Acad Sci U S A* 92, 10879-10883.
- Morton, T. A., Bennett, D. B., Appelbaum, E. R., Cusimano, D. M., Johanson, K. O., Matico, R. E., Young, P. R., Doyle, M., and Chaiken, I. M. (1994). Analysis of the interaction between human interleukin-5 and the soluble domain of its receptor using a surface plasmon resonance biosensor. *J Mol Recognit* 7, 47-55.
- Murata, Y., Takaki, S., Migita, M., Kikuchi, Y., Tominaga, A., and Takatsu, K. (1992). Molecular cloning and expression of the human interleukin 5 receptor. *J Exp Med* 175, 341-351.
- Murphy, J. M., Ford, S. C., Wiedemann, U. M., Carr, P. D., Ollis, D. L., and Young, I. G. (2003). A novel functional epitope formed by domains 1 and 4 of the human common beta-subunit is involved in receptor activation by granulocyte macrophage colony-stimulating factor and interleukin 5. *J Biol Chem* 278, 10572-10577.
- Muto, A., Watanabe, S., Miyajima, A., Yokota, T., and Arai, K. (1996). The beta subunit of human granulocyte-macrophage colony-stimulating factor receptor forms a homodimer and is activated via association with the alpha subunit. *J Exp Med* 183, 1911-1916.
- Nakamura, T., Ouchida, R., Kodama, T., Kawashima, T., Makino, Y., Yoshikawa, N., Watanabe, S., Morimoto, C., Kitamura, T., and Tanaka, H. (2002). Cytokine receptor common beta subunit-mediated STAT5 activation confers NF-kappa B activation in murine proB cell line Ba/F3 cells. *J Biol Chem* 277, 6254-6265.
- Nakanishi, K., Yoshimoto, T., Katoh, Y., Ono, S., Matsui, K., Hiroishi, K., Noma, T., Honjo, T., Takatsu, K., Higashino, K., and et al. (1988). Both B151-T cell replacing factor 1 and IL-5 regulate Ig secretion and IL-2 receptor expression on a cloned B lymphoma line. *J Immunol* 140, 1168-1174.
- Ogata, N., Kouro, T., Yamada, A., Koike, M., Hanai, N., Ishikawa, T., and Takatsu, K. (1998). JAK2 and JAK1 constitutively associate with an interleukin-5 (IL-5) receptor alpha and beta subunit, respectively, and are activated upon IL-5 stimulation. *Blood* 91, 2264-2271.
- Oldhoff, J. M., Darsow, U., Werfel, T., Bihari, I. C., Katzer, K., Laifaoui, J., Plotz, S., Kapp, A., Knol, E. F., Bruijnzeel-Koomen, C. A., et al. (2006). No effect of anti-

- interleukin-5 therapy (mepolizumab) on the atopy patch test in atopic dermatitis patients. *Int Arch Allergy Immunol* 141, 290-294.
- Ortmann, S. (2004) Mutagenesis and Binding studies of human Interleukin-5 receptor alpha, Julius-Maximilian Universität Würzburg, Würzburg.
- Owen, W. F., Rothenberg, M. E., Petersen, J., Weller, P. F., Silberstein, D., Sheffer, A. L., Stevens, R. L., Soberman, R. J., and Austen, K. F. (1989). Interleukin 5 and phenotypically altered eosinophils in the blood of patients with the idiopathic hypereosinophilic syndrome. *J Exp Med* 170, 343-348.
- Plaetinck, G., Van der Heyden, J., Tavernier, J., Fache, I., Tuypens, T., Fischkoff, S., Fiers, W., and Devos, R. (1990). Characterization of interleukin 5 receptors on eosinophilic sublines from human promyelocytic leukemia (HL-60) cells. *J Exp Med* 172, 683-691.
- Plotz, S. G., Simon, H. U., Darsow, U., Simon, D., Vassina, E., Yousefi, S., Hein, R., Smith, T., Behrendt, H., and Ring, J. (2003). Use of an anti-interleukin-5 antibody in the hypereosinophilic syndrome with eosinophilic dermatitis. *N Engl J Med* 349, 2334-2339.
- Proudfoot, A. E., Fattah, D., Kawashima, E. H., Bernard, A., and Wingfield, P. T. (1990). Preparation and characterization of human interleukin-5 expressed in recombinant *Escherichia coli*. *Biochem J* 270, 357-361.
- Ruchala, P., Varadi, G., Ishino, T., Scibek, J., Bhattacharya, M., Urbina, C., Ryk, D. V., Uings, I., and Chaiken, I. (2004). Cyclic peptide interleukin 5 antagonists mimic CD turn recognition epitope for receptor alpha. *Biopolymers* 73, 556-568.
- Sanderson, C. J., O'Garra, A., Warren, D. J., and Klaus, G. G. (1986). Eosinophil differentiation factor also has B-cell growth factor activity: proposed name interleukin 4. *Proc Natl Acad Sci U S A* 83, 437-440.
- Sanderson, C. J., Warren, D. J., and Strath, M. (1985). Identification of a lymphokine that stimulates eosinophil differentiation in vitro. Its relationship to interleukin 3, and functional properties of eosinophils produced in cultures. *J Exp Med* 162, 60-74.
- Schlx, P. J., and Worhunsky, D. J. (2003). Translational repression mechanisms in prokaryotes. *Mol Microbiol* 48, 1157-1169.
- Shanafelt, A. B., Miyajima, A., Kitamura, T., and Kastelein, R. A. (1991). The amino-terminal helix of GM-CSF and IL-5 governs high affinity binding to their receptors. *Embo J* 10, 4105-4112.

- Somers, W., Ultsch, M., De Vos, A. M., and Kossiakoff, A. A. (1994). The X-ray structure of a growth hormone-prolactin receptor complex. *Nature* *372*, 478-481.
- Straumann, A., Bauer, M., Fischer, B., Blaser, K., and Simon, H. U. (2001). Idiopathic eosinophilic esophagitis is associated with a T(H)2-type allergic inflammatory response. *J Allergy Clin Immunol* *108*, 954-961.
- Sundstrom, M., Lundqvist, T., Rodin, J., Giebel, L. B., Milligan, D., and Norstedt, G. (1996). Crystal structure of an antagonist mutant of human growth hormone, G120R, in complex with its receptor at 2.9 Å resolution. *J Biol Chem* *271*, 32197-32203.
- Swain, S. L., Howard, M., Kappler, J., Marrack, P., Watson, J., Booth, R., Wetzel, G. D., and Dutton, R. W. (1983). Evidence for two distinct classes of murine B cell growth factors with activities in different functional assays. *J Exp Med* *158*, 822-835.
- Takaki, S., Mita, S., Kitamura, T., Yonehara, S., Yamaguchi, N., Tominaga, A., Miyajima, A., and Takatsu, K. (1991). Identification of the second subunit of the murine interleukin-5 receptor: interleukin-3 receptor-like protein, AIC2B is a component of the high affinity interleukin-5 receptor. *Embo J* *10*, 2833-2838.
- Takaki, S., and Takatsu, K. (1994). Reconstitution of the functional interleukin-5 receptor: the cytoplasmic domain of alpha-subunit plays an important role in growth signal transduction. *Int Arch Allergy Immunol* *104 Suppl 1*, 36-38.
- Takaki, S., Tominaga, A., Hitoshi, Y., Mita, S., Sonoda, E., Yamaguchi, N., and Takatsu, K. (1990). Molecular cloning and expression of the murine interleukin-5 receptor. *Embo J* *9*, 4367-4374.
- Takatsu, K., Kikuchi, Y., Takahashi, T., Honjo, T., Matsumoto, M., Harada, N., Yamaguchi, N., and Tominaga, A. (1987). Interleukin 5, a T-cell-derived B-cell differentiation factor also induces cytotoxic T lymphocytes. *Proc Natl Acad Sci U S A* *84*, 4234-4238.
- Takatsu, K., Tominaga, A., and Hamaoka, T. (1980). Antigen-induced T cell-replacing factor (TRF). I. Functional characterization of a TRF-producing helper T cell subset and genetic studies on TRF production. *J Immunol* *124*, 2414-2422.
- Tanabe, T., Konishi, M., Mizuta, T., Noma, T., and Honjo, T. (1987). Molecular cloning and structure of the human interleukin-5 gene. *J Biol Chem* *262*, 16580-16584.

-
- Tavernier, J., Cornelis, S., Devos, R., Guisez, Y., Plaetinck, G., and Van der Heyden, J. (1995a). Structure/function analysis of human interleukin 5 and its receptor. *Agents Actions Suppl* 46, 23-34.
- Tavernier, J., Devos, R., Cornelis, S., Tuypens, T., Van der Heyden, J., Fiers, W., and Plaetinck, G. (1991). A human high affinity interleukin-5 receptor (IL5R) is composed of an IL5-specific alpha chain and a beta chain shared with the receptor for GM-CSF. *Cell* 66, 1175-1184.
- Tavernier, J., Devos, R., Van der Heyden, J., Hauquier, G., Bauden, R., Fache, I., Kawashima, E., Vandekerckhove, J., Contreras, R., and Fiers, W. (1989). Expression of human and murine interleukin-5 in eukaryotic systems. *Dna* 8, 491-501.
- Tavernier, J., Tuypens, T., Plaetinck, G., Verhee, A., Fiers, W., and Devos, R. (1992). Molecular basis of the membrane-anchored and two soluble isoforms of the human interleukin 5 receptor alpha subunit. *Proc Natl Acad Sci U S A* 89, 7041-7045.
- Tavernier, J., Tuypens, T., Verhee, A., Plaetinck, G., Devos, R., Van der Heyden, J., Guisez, Y., and Oefner, C. (1995b). Identification of receptor-binding domains on human interleukin 5 and design of an interleukin 5-derived receptor antagonist. *Proc Natl Acad Sci U S A* 92, 5194-5198.
- van Leeuwen, B. H., Martinson, M. E., Webb, G. C., and Young, I. G. (1989). Molecular organization of the cytokine gene cluster, involving the human IL-3, IL-4, IL-5, and GM-CSF genes, on human chromosome 5. *Blood* 73, 1142-1148.
- Walter, M. R., Cook, W. J., Ealick, S. E., Nagabhushan, T. L., Trotta, P. P., and Bugg, C. E. (1992). Three-dimensional structure of recombinant human granulocyte-macrophage colony-stimulating factor. *J Mol Biol* 224, 1075-1085.
- Walter, M. R., and Nagabhushan, T. L. (1995). Crystal structure of interleukin 10 reveals an interferon gamma-like fold. *Biochemistry* 34, 12118-12125.
- Walter, M. R., Windsor, W. T., Nagabhushan, T. L., Lundell, D. J., Lunn, C. A., Zauodny, P. J., and Narula, S. K. (1995). Crystal structure of a complex between interferon-gamma and its soluble high-affinity receptor. *Nature* 376, 230-235.
- Wells, J. A., and de Vos, A. M. (1996). Hematopoietic receptor complexes. *Annu Rev Biochem* 65, 609-634.
- Wills-Karp, M., and Karp, C. L. (2004). Biomedicine. Eosinophils in asthma: remodeling a tangled tale. *Science* 305, 1726-1729.

- Wilmanns, O. M. a. M. (1999). X-ray analysis of protein crystals with thin-plate morphology *J Synchrotron Rad* *6*, 1016-1020.
- Woodcock, J. M., Bagley, C. J., Zacharakis, B., and Lopez, A. F. (1996). A single tyrosine residue in the membrane-proximal domain of the granulocyte-macrophage colony-stimulating factor, interleukin (IL)-3, and IL-5 receptor common beta-chain is necessary and sufficient for high affinity binding and signaling by all three ligands. *J Biol Chem* *271*, 25999-26006.
- Woodcock, J. M., McClure, B. J., Stomski, F. C., Elliott, M. J., Bagley, C. J., and Lopez, A. F. (1997). The human granulocyte-macrophage colony-stimulating factor (GM-CSF) receptor exists as a preformed receptor complex that can be activated by GM-CSF, interleukin-3, or interleukin-5. *Blood* *90*, 3005-3017.
- Yamada, T., Sun, Q., Zeibecoglou, K., Bungre, J., North, J., Kay, A. B., Lopez, A. F., and Robinson, D. S. (1998). IL-3, IL-5, granulocyte-macrophage colony-stimulating factor receptor alpha-subunit, and common beta-subunit expression by peripheral leukocytes and blood dendritic cells. *J Allergy Clin Immunol* *101*, 677-682.

9 APPENDIX

ABBREVIATIONS

The standard one-letter code is used for amino acids. i.e. Point mutations are labelled like C66A, in which cystein 66 is mutated to alanine.

aa	amino acid
ACN	Acetonitril
AE	anion exchange chromatography
AHR	Airway hyperresponsiveness
AIC2B	Mouse beta chain
Aid	Activation-induced cytidine deaminase
Amp	Ampicillin
APS	Amonium-persulphate
ATP	Atopic path test
β_c	Beta common chain
BCDF	B-cell differentiation factor
BCGF	B-cell growth factor
BCL ₁	B leukaemia cells line
BIAcore	Biomolecular interaction analysis
Blimp-1	B lymphocyte-induced maturation protein-1
β -ME	β -Mercaptoethanol
BNPS-Skatole	3-bromo-3-methyl-2 (2-notrophenylmercapto)-3H-indole
bp	Base pair
CD	Circular dicroism
CIS	Cytokine-inducible SH2-containing proteins
CHAPS	3-[(3-Cholamidopropyl)dimethylammonio]-1-propanesulfonate
CHES	2-(N-Cyclohexylamino) ethane Sulfonic Acid
cDNA	Complementary DNA
CM5	Carboxymethyl dextran-5
CNBr	Cyanogen bromide
cpm	Counts per minute
CRH	Cytokine receptor homology
CRM	Cytokine recognition motif
Da	Dalton
DC	Dendritic cell
deg	degrades
DTT	Dithiothreitol
EC ₅₀	Fifty maximal inducer concentration
dH ₂ O	Distilled water
ECD	Extracellular binding domain
ECM	Extra cellular matrix
<i>E. coli</i>	<i>Escherichia coli</i>
ECP	Eosinophils cationic protein
EDF	Eosinophil differentiation factor
EDN	Eosinophil-derived neurotoxin

EDTA	Ethylenediaminetetraacetic acid
EG	Ethylene glycol
EPO	Eosinophil peroxidase
ERK	Extracellular receptor-activated kinase
ESI	Electro-spray mass spectrometry
EtBr	Etidium bromide
Fn-III-like	Fibronectin type III-like domain
GH	Growth hormone
GHR	Growth hormone receptor
GM-CSF	Granulocyte macrophage colony-stimulating factor
GM-CSFR	Granulocyte macrophage colony-stimulating factor receptor
Grb2	Growth factor receptor-bound adaptor protein
GSH	Reduced glutathione
GSSH	Oxidized glutathione
GuHCl	Guanidinium hydrochloride
FPLC	Fast pressure liquid chromatography
HEPES	N-2-Hydroxyethylpiperazin-N'-2-ethanesulpho acid
HES	Hypereosinophilic syndrome
hIL-5	Human interleukin-5
hIL-5R α	Human interleukin-5 receptor alpha
IB	Inclusion bodies
IC ₅₀	Half maximal inhibition concentration
IgE	Immunoglobulin-E
IL	Interleukin
IPTG	Isopropyl-beta-D-thiogalactopyranoside
IR	Immune response
JAK	Janus kinase
K	Kelvin degrees
K _D	Affinity constant
kDa	Kilodaltons
K _{off}	Dissociation constant
K _{on}	Association constant
KSI	Ketosteroid isomerase
λ	Wavelength
LB	Luria Bertani medium
MAPK	Mitogen-activated protein kinase
MBP	Major basic protein
M-CSF	Macrophage colony-stimulating factor
Mepolizumad	Antibody against hIL-5
MES	2-Morpholinoethanesulfonic acid
mg	miligram
mIL-5	mouse IL-5
ml	mililiter
MOPS	3-(N-morpholino) propanesulfonic acid
MPD	2-Methyl-2,4-pentanediol
mRNA	messenger ribonucleic acid
MW	Molecular weight
MWCO	Molecular weight cut off
m/z	mass/charge
NaAc	Sodium acetate

NFκβ	Nuclear factor kappa beta
nm	nanometers
nM	nanomolar
NTCB	2-Nitro-5 thiocyanobenzoic acid
OD ₆₀₀	Optical density at 600 nm
ON	Over night
ORF	Open reading frame
PAGE	Polycrylamide gel electrophoresis
PCR	Polymerase chain reaction
PDB	Protein data bank
PEG	Polyethylen glycol
pfu pol	<i>Pyrococcus furiosus</i> polymerase
PI3K	Phosphatidyl inositol 3-kinase
PIAs	Protein inhibitors STAT
RP-HPLC	Reverse phase-HPLC
ProLR	Prolactin receptor
rms	root mean square
rpm	revolutions per minute
RT	Room temperature
RU	Resonance units
SDS	Sodium dodecyl sulphate
SOCS	Suppressor of cytokine signalling
SPR	Surface plasmon resonance
STAT	Signal transducer and activator of transcription
TB	Terrific medium
TCA	Trichloroacetic acid
TEMED	N,N,N',N'-Tetramethylethylenediamine
TFA	Tri-fluoro acetic acid
Tris	Tris (-hydroxymethyl)-aminoethan
TRF	T-cell replacing factor
U	International units
VCAM-1	Vascular cell adhesion molecule-1
VLA-4	Vascular ligand adhesion-4
v/v	volumen/volumen
w/v	weight/volumen
wt	Wild type

Lebenslauf

Persönliche Daten:

Name: Edwin Bairon Patiño Gonzalez

Geburtsdatum: 20.05.1967

Geburtsort: Medellín, Kolumbien

Staatsangehörigkeit: kolumbianisch

Studium:

11/2002-heute	Julius-Maximilians-Universität Würzburg Lehrstuhl für Physiologische Chemie II, Prof. Dr. Walter Sebald Promotion.
1997-2000	Universidad de Antioquia, Medellin, Kolumbien: Magister (Immunologie)
1989-1995	Universidad de Antioquia, Medellin, Kolumbien: Studium der Biologie

Publikationen

2006	Michael Kraich, Markus Klein, <u>Edwin Patiño</u> , Henning Harrer, Joachim Nickel, Walter Sebald, and Thomas D. Mueller. A modular interface of IL-4 allows for scalable affinity without affecting specificity for the IL-4 receptor. BMC Biology 4:13 (2006).
2007	<u>Edwin Patiño</u> , Michael Kraich, Alexander Kotsch, Walter Sebald, and Thomas D. Mueller. PROTEIN STRUCTURE OF MOUSE INTERLEUKIN-5 (mIL-5). Inter. Journal. Molec. Science. (Summited)

Symposien

9/2006	3 rd International PhD Student Symposium, Horizons in Molecular Biology. Göttingen/Germany, Max Planck Institute. Poster: Crystallization and preliminary X-ray diffraction analysis of murine interleukin-5 (mIL-5).
--------	---

10/2006 2nd International Symposium, From Bench To Bedside.
Würzburg/Germany. Rudolf-Virchow-Center. **Talk:**
Molecular Mechanism of Interleukin-5 Receptor
Activation.

Curriculum Vitae

Personal data:

Name: Edwin Bairon Patiño Gonzalez

Date of birth: May 20th, 1967

Place of birth: Medellín, Colombia, South America.

Citizenship: Colombian

Education:

- | | |
|---------------|---|
| 11.2002-Today | Julius-Maximilians-Universität Würzburg
Institute for Physiological Chemistry-II, Prof. Dr. Walter Sebald
PhD-Studies |
| 1997-2000 | Universidad de Antioquia, Medellin, Colombia:
Master of Science (Immunology) |
| 1989-1995 | Universidad de Antioquia, Medellin, Colombia:
Study in Biology |

Publications (Papers):

- | | |
|------|---|
| 2006 | Michael Kraich, Markus Klein, <u>Edwin Patiño</u> , Henning Harrer, Joachim Nickel, Walter Sebald, and Thomas D. Mueller. A modular interface of IL-4 allows for scalable affinity without affecting specificity for the IL-4 receptor. BMC Biology 4:13 (2006). |
| 2007 | <u>Edwin Patiño</u> , Michael Kraich, Alexander Kotzsch, Walter Sebald, and Thomas D. Mueller. PROTEIN STRUCTURE OF MOUSE INTERLUEKIN-5 (mIL-5). Inter. Journal. Molec. Science. (Summited) |

Symposiums:

- | | |
|---------|---|
| 9. 2006 | 3 rd International PhD Student Symposium, Horizons in Molecular Biology. Göttingen/Germany, Max Planck Institute. Poster: Crystallization and preliminary X-ray diffraction analysis of murine interleukin-5 (mIL-5). |
|---------|---|

10. 2006 2nd International Symposium, From Bench To Bedside.
Würzburg/Germany. Rudolf-Virchow-Center. **Talk:**
Molecular Mechanism of Interleukin-5 Receptor
Activation.

ACKNOWLEDGEMENTS

I am pleased to acknowledge and thank many people who helped me to reach this point. First of all, I am very thankful to my PhD mentor Prof. Dr. Walter Sebald for giving me an opportunity to start my scientific career in the field of protein biochemistry. Many thanks to Dr. Thomas Müller for the fruitful supervision and coordination of my work.

I thank Alexander Kotzsch for introduction into protein crystallography. Thanks to Michael Kraich for the execution of BIAcore and cell assay analysis. I thank Werner Schmitz for excellent mass spectrometry analysis. Many thanks to Alicia Pontesucré, Marcela Fajardo, Laura van Geersdaele, Axel Seher, Joachim Nickel and Christof Berberich for their critical readings and advises throughout this work. In addition, thanks Marcela Fajardo, Claudia Serna and Christof Berberich for their efforts in the translation of Summary into Deutsch version.

Thanks for Christian Söder and Maike Gottermeier for excellent technical assistance. I'm very grateful for Ulrike Borst for her assistance in administrative tasks. I thank the secretary of our department Bettina Lakeit. I would also like to express my thanks to my colleagues: Markus Klein, Stefan Saremba, Stella Keiper and Anne Paschke.

I thank my colleagues of the GK 520 "Immunmodulation" for strong scientific guidance in immunology during my studies.

Erklärung

Hiermit erkläre ich, dass ich die Dissertation

„Functional Studies and X-Ray Structure Analysis of Human
Interleukin-5 Receptor Alpha and Human Interleukin-5 Complex“

in allen Teilen selbstständig angefertigt und keine anderen als die genannten Quellen und Hilfsmittel verwendet habe.

Weiterhin versichere ich, dass diese Dissertation weder in gleicher noch in ähnlicher Form in einem anderen Prüfungsverfahren vorgelegen hat.

Ich habe bisher außer den mit dem Zulassungsgesuch urkundlich vorgelegten Graden keine weiteren akademischen Grade erworben oder zu erwerben versucht.

Würzburg, Juli 2007

Edwin Bairon Patiño Gonzalez